code 1 cat. 7

SACRAMENTO PLANT

97p.

HIGH CHAMBER PRESSURE OPERATION FOR LAUNCH VEHICLE ENGINE PROGRAM

FINAL REPORT

Contract NAS 8-4008,
Supplemental Agreement No. 4

Report 4008-SA4-F

1 June 1964

FACILITY FORM 602

N64-29706 (ACCESSION NUMBER)

(THRU)

97 (PAGES)

1 (CODE)

CR 56672 (NASA CR OR TMX OR AD NUMBER)

27 (CATEGORY)

OTS PRICE

XEROX $ 8.60 ph

MICROFILM $

AEROJET GENERAL TIRE GENERAL

1 June 1964

Report 4008-SA4-F

HIGH CHAMBER PRESSURE OPERATION
FOR
LAUNCH VEHICLE ENGINES PROGRAM

FINAL REPORT

Prepared under
Contract NAS 8-4008, Supplemental Agreement No. 4

Prepared for

GEORGE C. MARSHALL SPACE FLIGHT CENTER
National Aeronautics and Space Administration
Huntsville, Alabama

AEROJET-GENERAL CORPORATION 773T
A SUBSIDIARY OF THE GENERAL TIRE & RUBBER COMPANY

FOREWORD

This final report presents a summary of all technical progress and accomplishments in the course of fulfilling Contract NAS 8-4008, Supplemental Agreement No. 4, "High Chamber Pressure Operation for Launch Vehicle Engines Program."

Work was conducted by the Research and Advanced Technology Division at the Liquid Rocket Plant, Sacramento, California, for the contract period of performance from 1 April 1963 to 31 March 1964, and was under the direction of R. Beichel, Division Manager; D. J. Iddins, Project Manager; W. S. Howard, Project Engineer; and Dr. F. H. Reardon, Combustion Stability Analyst.

TABLE OF CONTENTS

		Page
I.	Introduction	1
II.	Summary	2
III.	Conclusions	3
IV.	Accomplishments	5
	A. Design	5
	B. Test Setup	8
	C. Shock-Wave Generator (Pulse Gun)	9
	D. Instrumentation	11
	E. Test Results	13
	F. Stability Parameters	22
	G. Experimental Test Performance	25
	H. Problem Areas	26
V.	Nonlinear Extension of Sensitive Time Lag Theory	27
VI.	Recommendations	41

APPENDIX

Distribution List

TABLE LIST

	Table
Summary of Test Results	1
High-Frequency Stability Data	2
Summary of Pulse Characteristics	3
Summary of Stability Behavior	4

FIGURE LIST

	Figure
Thrust Chamber Assembly	1
26-in. Length Thrust Chamber Assembly on Test Stand	2
6-in. Length Thrust Chamber Assembly on Test Stand	3
Hardware Configuration and Instrumentation Location	4
LO_2/LH_2 Pentad Injector	5
4-5K lb Thrust Pentad Injector	6
Pentad Injector Flow Pattern	7

FIGURE LIST (cont.)

	Figure
LO_2/LH_2 Coaxial Injector	8
Coaxial Injector, 18-Element	9
Coaxial Injector Flow Pattern	10
LO_2/LH_2 Conventional Injector	11
Conventional Injector	12
Conventional Injector Flow Pattern	13
LO_2/LH_2 High Pressure Test Facilities	14
Shock Wave Generator, Model V	15
Shock Wave Generator, Exploded View	16
Typical Pulse Charge	17
Recessed Photocon Installation	18
EMF Graph for Thermocouple	19
Oscillogram - D521-LM-14, Stable Run, Conventional Injector	20
Oscillogram - D521-LM-23, Stable Run, Coaxial Injector	21
Oscillogram - D521-LM-22, Stable Run, Pentad Injector	22
Oscillogram - D521-LM-19, Stable Run, Pentad Injector	23
Oscillogram - D521-LM-15, Unstable Run, Conventional Injector (1T)	24
Oscillogram - D521-LM-25, Unstable Run, Conventional Injector (1T)	25
Oscillogram - D521-LM-18, Unstable Run, Coaxial Injector (1L)	26
Oscillogram - D521-LM-13, Unstable Run, Pentad Injector(LF)	27
Conventional Injector after Test D521-LM-14	28
Damage to Conventional Injector After Test D521-LM-15	29
Damage to Conventional Injector After Test D521-LM-5	30
Damage to Conventional Injector After Test D521-LM-10	31
Damage to Conventional Injector After Test D521-LM-25	32
Coaxial Injector After Test D521-LM-17	33
Damage to Coaxial Injector After Test D521-LM-8	34
Damage to Coaxial Injector After Test D521-LM-8	35
Pentad Injector After Test D521-LM-13	36
Damage to Pentad Injector After Test D521-LM-22	37
"Cold Pulse" Calibrations	38

FIGURE LIST (cont.)

	Figure
Typical Instability Zone for a Given Mode and Combustor Configuration	39
Instability Zones and Estimated Operating Point of Conventional Injector	40
Instability Zones and Estimated Operating Point of Coaxial Injector	41
Instability Zones and Estimated Operating Point of Pentad Injector	42
Correlation of Stability Parameters	43
Reduced Oscillograph for Test D521-LM-12	44
Pentad Injector Damage After Test D521-LM-4	45
Computer Program Flow Diagram	46

I. INTRODUCTION

The purpose of this investigation was to continue the study of the suitability of high chamber pressure operation for launch vehicle engines. An experimental program was conducted to investigate the effects of chamber pressure, injector type, and chamber length on combustion dynamics. Parallel analytical studies were conducted to improve and apply current theories of combustion stability. The experimental phase was performed using a single-stage unit of 20,000 lb thrust at nominal engine mixture ratios and at chamber pressures of 1000, 1500, and 2500 psia, with liquid oxygen/liquid hydrogen as propellants.

The program was a one-year effort, completed on 31 March 1964. All previous work has been documented in Aerojet-General Report 4008-F-1, of the same title, dated 15 April 1963.

II. SUMMARY

ABS 4

29706

The effects of chamber pressure, injector type and size, and thrust chamber length on combustion stability have been experimentally and theoretically studied. A series of 21 valid tests was conducted using LO_2/LH_2 as propellants. The Sensitive Time Lag theory, developed at Princeton University, was used for evaluation and correlation of experimental test results.

The test program included tests with 6-, 12.5-, and 26-in length chambers using pentad (5000 lb thrust per element), coaxial (1100 lb thrust per element), and conventional (220 lb thrust per element) types of injectors, in an 8-in. dia chamber. The conventional injector was observed to be marginally unstable in the first tangential mode over the range of pressures (1000 to 2500 psia) and chamber lengths employed. The coaxial injector also showed instability; but it was found to be in the first longitudinal mode, and only with the 26-in. length chamber at 2500 psia. The pentad injector was stable over the entire ranges of pressure and length.

Values of the stability parameters, n and τ, were deduced by comparing the test results with the theoretically predicted instability zones (on the n,τ-plane). The resulting values agreed generally with previously observed trends with chamber pressure and thrust per element, but in addition, indicated that the type of injector has a significant influence on stability behavior.

Author

III. CONCLUSIONS

The experimental effort on this program constituted an exploration of the combustion dynamic behavior of the liquid oxygen/liquid hydrogen propellant system at high operating chamber pressures. The pressure range investigated extended from 1000 psia (corresponding to current technology) to 2500 psia, which is in the range of proposed high chamber pressure applications. Mixture ratio was not taken into account as a parameter in these studies, but was maintained in the vicinity of 6.0, which is considered desirable for thrust chamber applications. Three basic injector types were considered: conventional (multiple-orifice showerhead), coaxial, and pentad (four oxidizer streams impinging on one fuel stream). Since each test injector provided practical element size, the same injectors were used to study the effect of the amount of thrust per element on stability. As a result, the program yielded data over a wide range of design parameters, but these parameters could not be considered in depth.

According to the Sensitive Time Lag Theory, and confirmed by experimental research, high-frequency combustion instability is strongly affected by the geometry of the combustion chamber. Because the diameter of the thrust chamber used on this program was fixed, some control of the stability behavior (particularly relating to longitudinal modes) was achieved by operating at three chamber lengths: 6, 12.5, and 26 in. The subsonic length of the exhaust nozzle was kept as short as possible to promote wave reflection in order to enhance the possibility of the occurrence of instability.

No instances of spontaneous instability were observed on the present program. However, it is of interest to note that three different types of instability: tangential mode, longitudinal mode, and low frequency ("chugging") were triggered by the Aerojet tangential pulse generator. This result indicates that the instabilities which can be studied by use of this technique are not limited to the tangential modes of high frequency instability. Pulse charges ranging from 20 to 160 grains of powder were fired, resulting in pressure disturbances from 100 to 3400 psia (maximum, peak-to-peak), or 8 to 153% of mean chamber pressure.

III, Conclusions (cont.)

The experimental results were correlated by means of the Sensitive Time Lag theory. From the comparison of the test data with theoretical calculations of the requirements for spontaneous instability, values of the combustion stability parameters were estimated. Because of the lack of a nonlinear theory, rather large uncertainties are associated with the parameter values obtained. However, the results show general agreement with previous data, which indicates that increasing the chamber pressure tends to produce a somewhat greater susceptibility to high-frequency instability, and to higher frequency, more complex modes. This effect was shown to be countered by increasing the injector element size, which had exactly the opposite effects. Superimposed on these general trends is the influence of the injector type. The coaxial injector had a longer sensitive time lag (and therefore a tendency to lower frequency modes) than would be expected on the basis of conventional injector experience. On the other hand, the time lag for the pentad was shorter than expected from conventional injector experience. A definitive trend of the interaction index with injector type could not be formulated. However, all of the data studied to date indicate that a small interaction index is associated with a large sensitive time lag, and vice versa.

The difficulty of obtaining definitive stability parameter values from pulse-triggered instabilities is a result of the lack of a nonlinear time lag theory. For this reason, efforts were made on the present program to extend the Sensitive Time Lag Theory to include nonlinear combustion effects. The technique used was that of equivalent linearization of the combustion response by means of a describing function. The resultant analysis is limited to moderate oscillation amplitudes, but is a first step in the solution of the nonlinear problem. A complete exploration of this approach was not achieved on this program. However, the basic analysis and computer program outline were set up. The extended theory will predict zones of instability in terms of the stability parameters of the linear theory, with the oscillation amplitude level as a parameter. The instability zones can then be linked to the pulses which trigger instability by means of the experimental observation of disturbance amplitude. Remaining work on the theory extension includes the completion of the computer program, and investigation of the nature of the nonlinear combustion response as related to the injector pattern, propellant combination, and operation conditions.

IV. ACCOMPLISHMENTS

A. DESIGN

1. Pulse Chamber

All hardware used during this program was designed to operate at 20,000 lb thrust and was of the "workhorse" type. The pulse combustion chamber (Figures 1, 2 and 3) was fabricated from carbon steel and had a Rokide "Z" inside coating designed to protect the chamber for test durations of 1 sec or less. The chamber was comprised of several sections to provide flexibility in chamber length. The chamber lengths used in this program were 6, 12.5, and 26 in. For improved joint sealing, all joints were serrated for the application of thin Durabla gaskets. The chamber nozzle was replaceable with three different sizes to accommodate chamber pressures of 1000, 1500, and 2500 psia. To promote longitudinal instability, the nozzles were designed with a short convergent section with an angle of 50°. The four shock-wave generators("pulse guns")were located 2.95 in. from the injector and were set at an angle to the center line of the chamber as shown in Figure 4. Three Photocon high-frequency pickups were located between the pulse guns. The fourth Photocon pickup was located near the nozzle directly down the chamber from one of the pickups at the injector. The four pulse guns were used to set off a disturbance in the combustion chamber during the test. The pulse sizes were 20, 40, 80, and 160 gr. The pulse gun is further described in Section IV,C.

2. Injectors

Three injector designs: pentad, coaxial, and conventional were evaluated during this program. The injection velocities were calculated by assuming the following propellant densities: $\rho_o = 72$ lb/ft^3, $\rho_f = 4.0$ lb/ft^3.

IV, A, Design (cont.)

a. Four-Element Pentad Injector

This design incorporates four, 5000-lb thrust, pentad elements. Each element consists of four oxidizer streams impinging on a central fuel stream. The injector design and water flow pattern as shown in Figures 5, 6, and 7. The injector design parameters are listed below.

Propellant flow rate, lb/sec	$\dot{w}_o = 52$
	$\dot{w}_f = 8.7$
Velocity at injector orifice, ft/sec	$V_o = 140$
	$V_f = 550$
Momentum ratio	$\frac{\dot{w}_o V_o}{\dot{w}_f V_f} = 1.52$

b. Coaxial Injector

The coaxial injector is an 18-element concentric tube design. In each element, liquid hydrogen is injected through the annulus around the liquid oxygen tube that is provided by the concentric fuel tube. For this type of injector, the initial propellant mixing is attained by the shearing action provided by the differential velocity of the propellants. To facilitate breakup and mixing of the propellants, each element is constructed so that the annular fuel stream will converge on the central oxidizer stream. The injector design and water flow pattern are shown in Figures 8, 9, and 10. The design parameters are listed below:

Propellant flow rate, lb/sec	$\dot{w}_o = 52$
	$\dot{w}_f = 8.7$
Velocity at injector orifice, ft/sec	$V_o = 120$
	$V_f = 350$
Momentum ratio	$\frac{\dot{w}_f V_f}{\dot{w}_o V_o} = 0.49$

IV, A, Design (cont.)

c. Conventional Showerhead Injector

This design incorporates 12 rows of alternate fuel fan elements and showerhead oxidizer orifices. Two outer rows of fuel showerhead orifices provide cooling for the chamber wall. This injector is manifolded from the rear so that a minimum length of line will be required for connection to the thrust chamber valves. The design and water flow pattern are shown in Figures 11, 12, and 13. The injector design parameters are listed below:

Propellant flow rate, lb/sec	$\dot{w}_o = 52$
	$\dot{w}_f = 8.7$
Velocity at injector orifice, ft/sec	$V_o = 140$
	$V_f = 560$

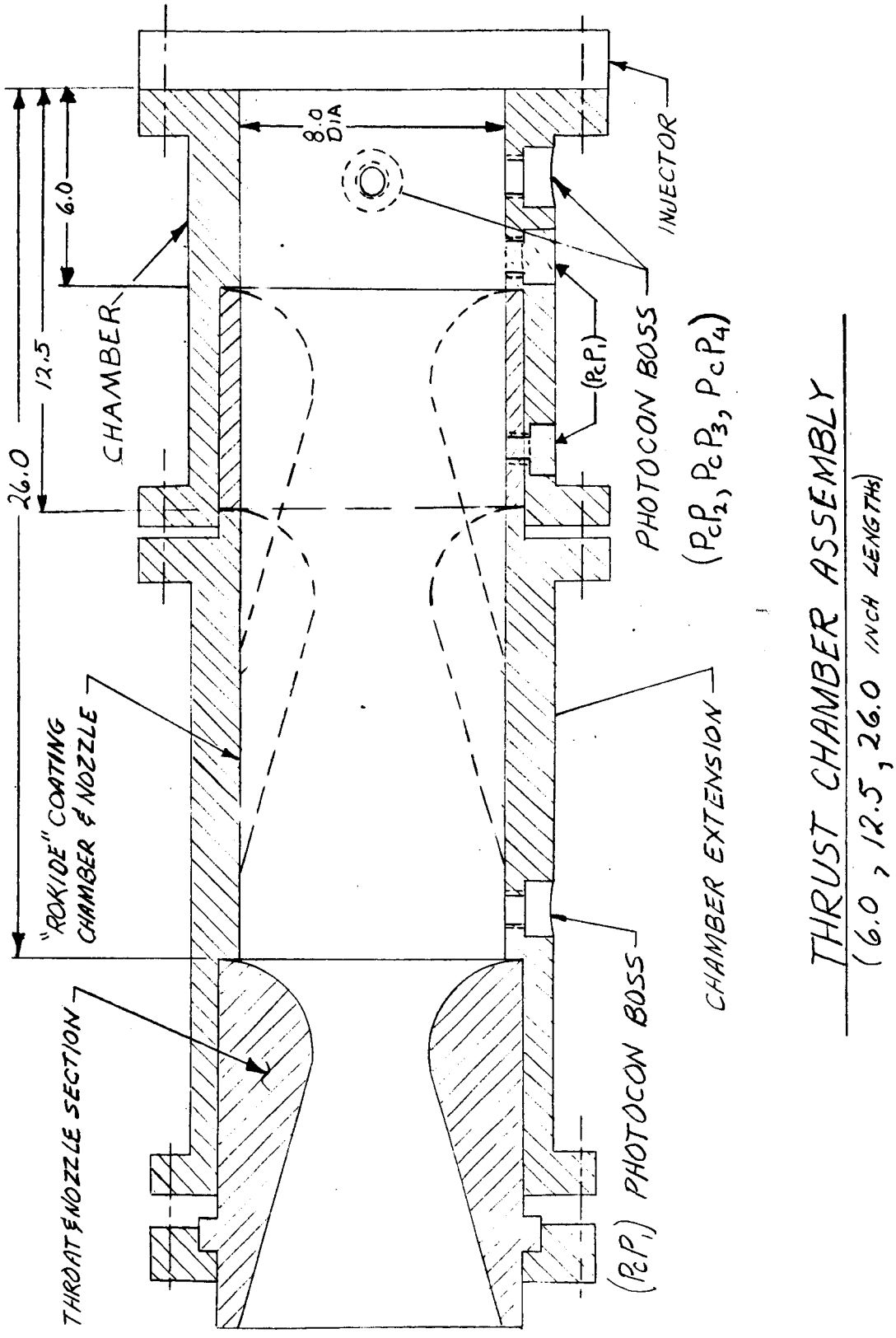

Thrust Chamber Assembly

Figure 1

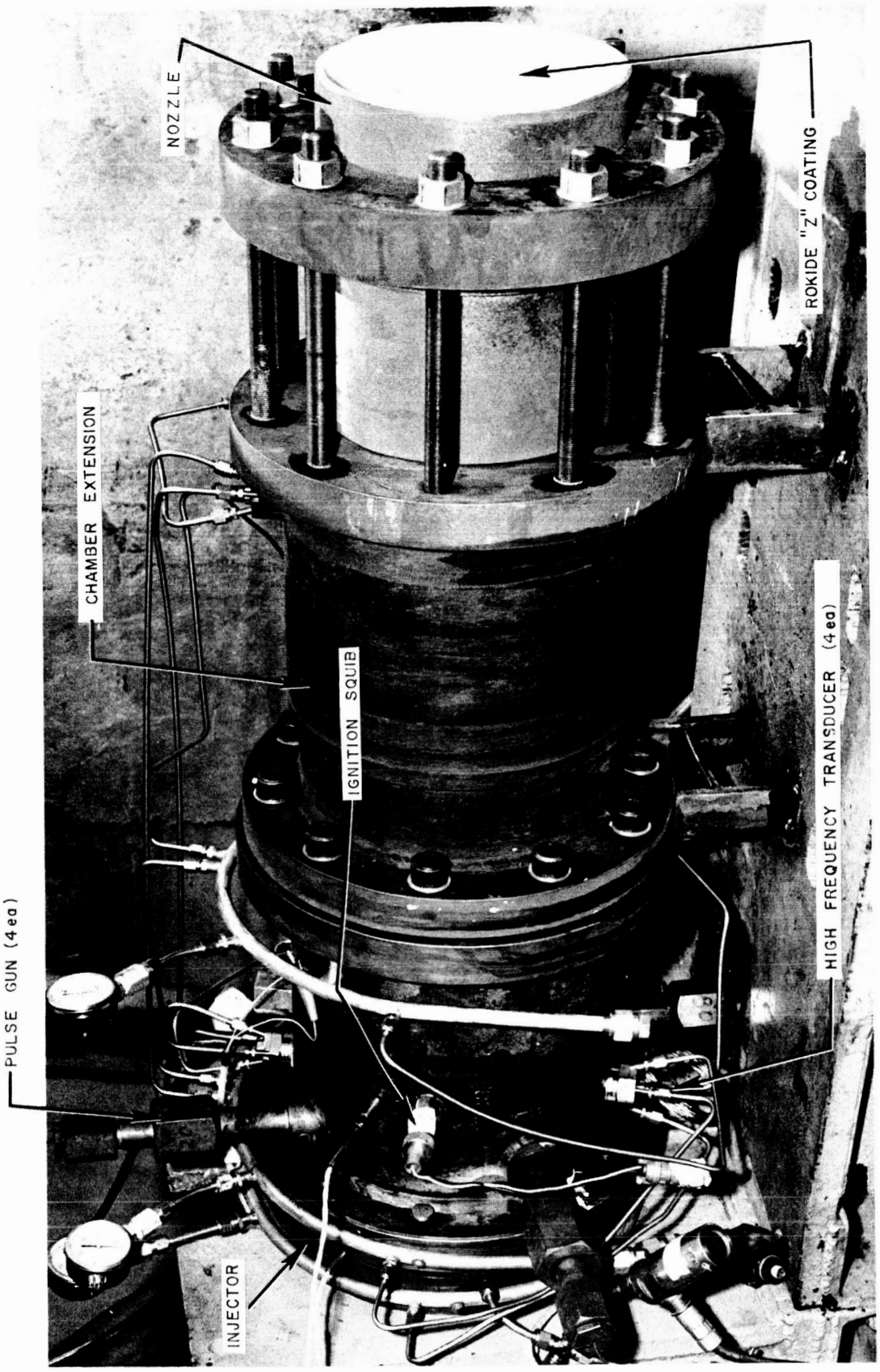

26-in. Length Thrust Chamber Assembly on Test Stand

Figure 2

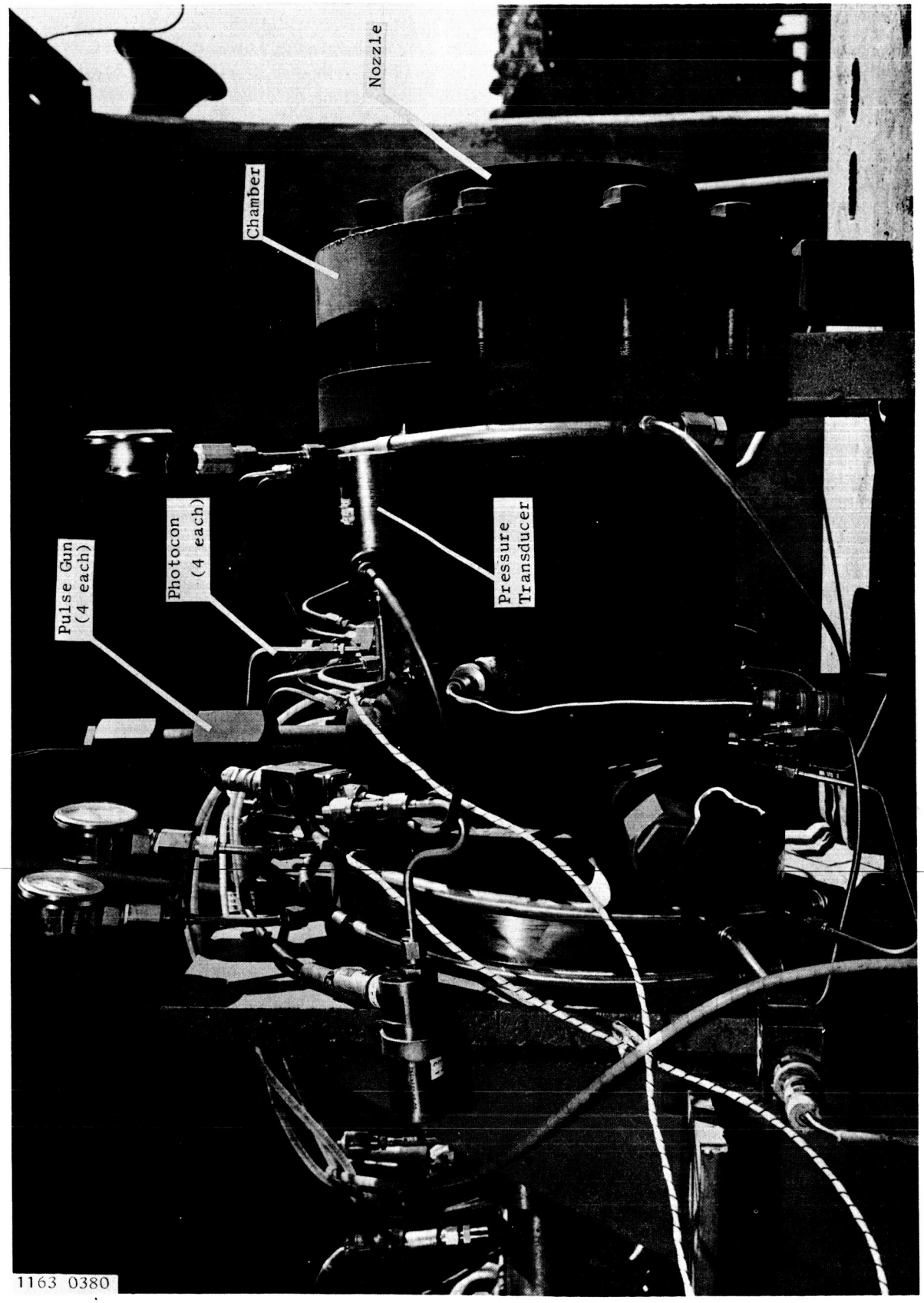

6-in. Length Thrust Chamber Assembly on Test Stand

Figure 3

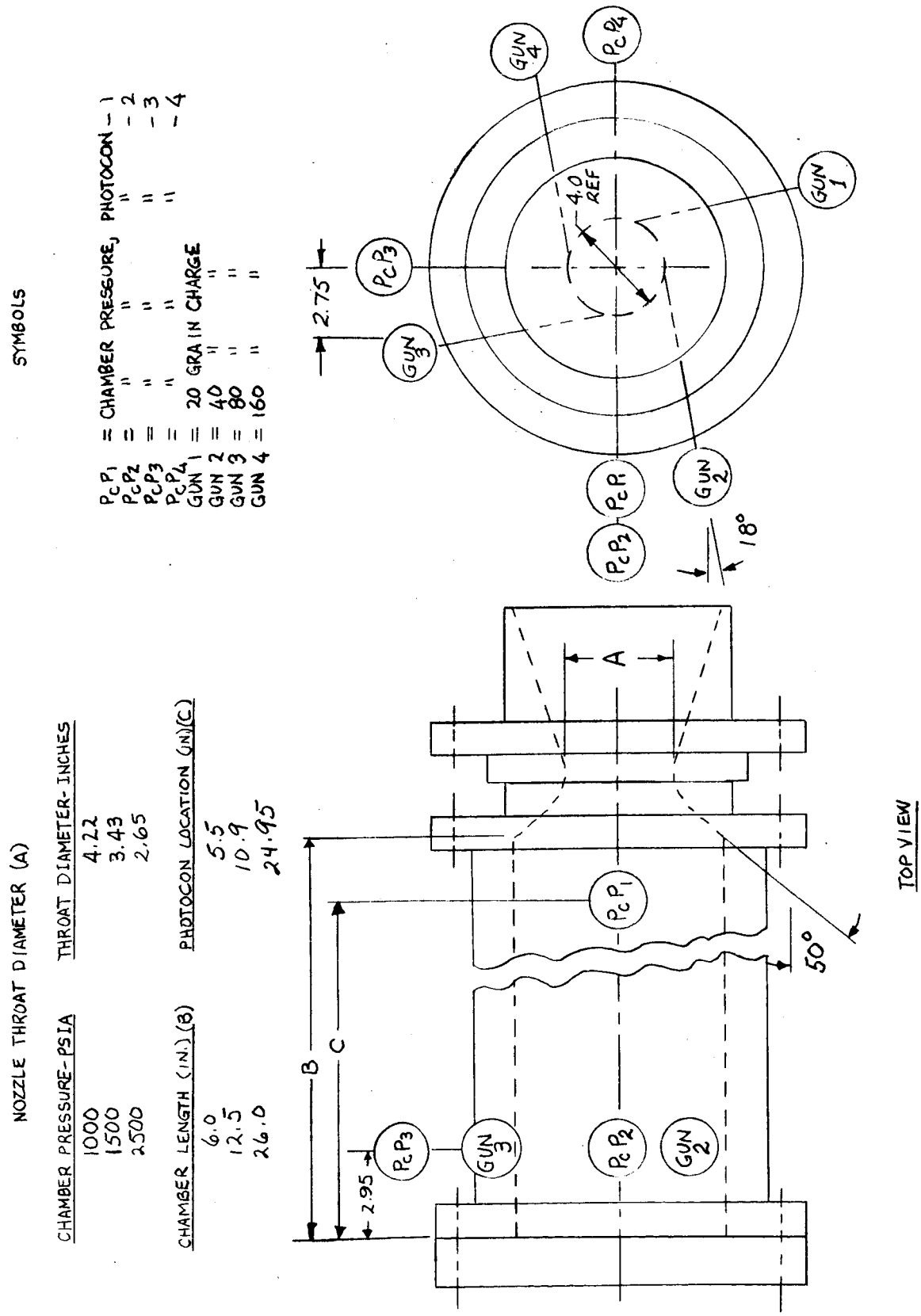

Hardware Configuration and Instrumentation Location

Figure 4

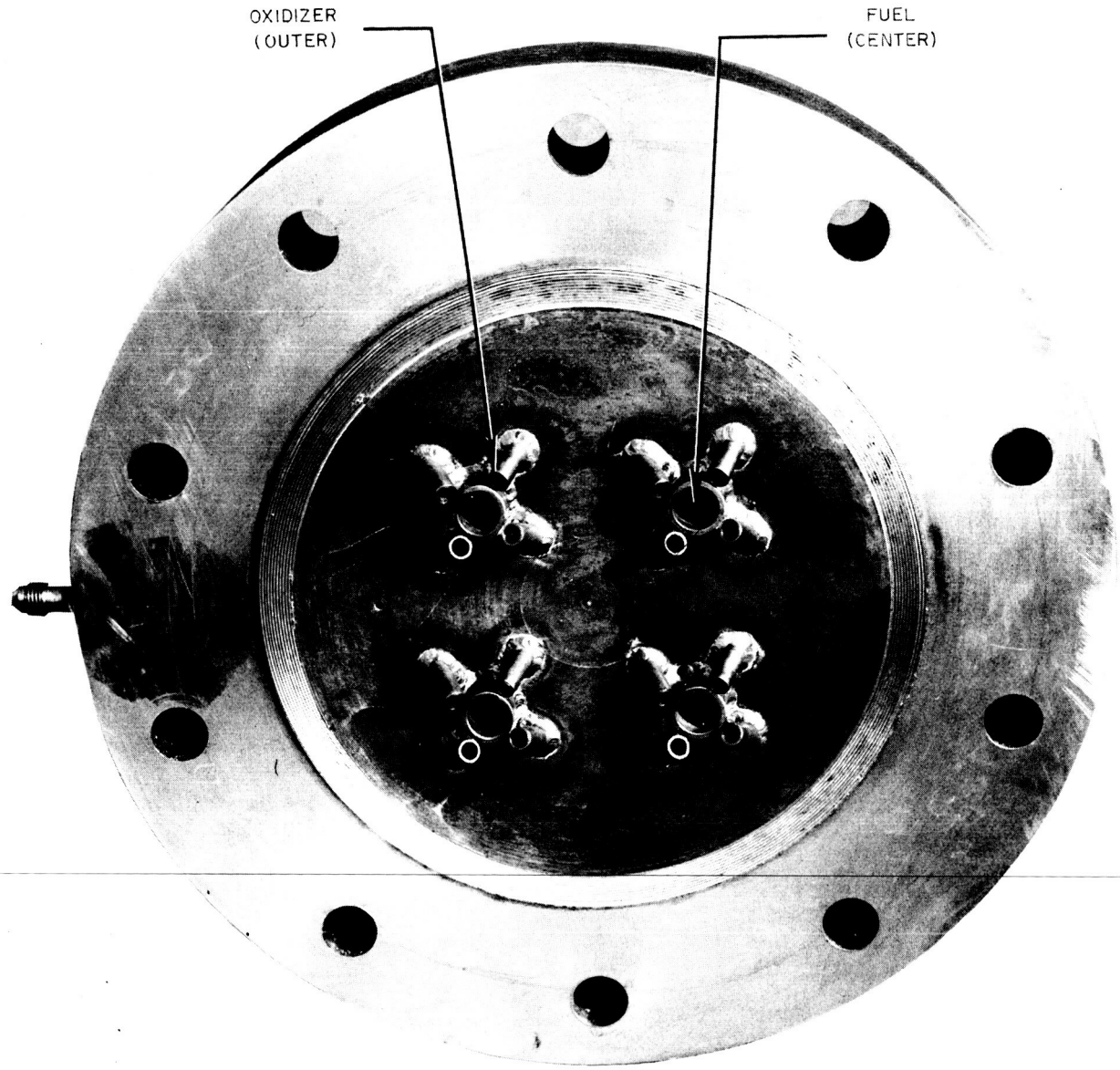

LO_2/LH_2 Pentad Injector

Figure 5

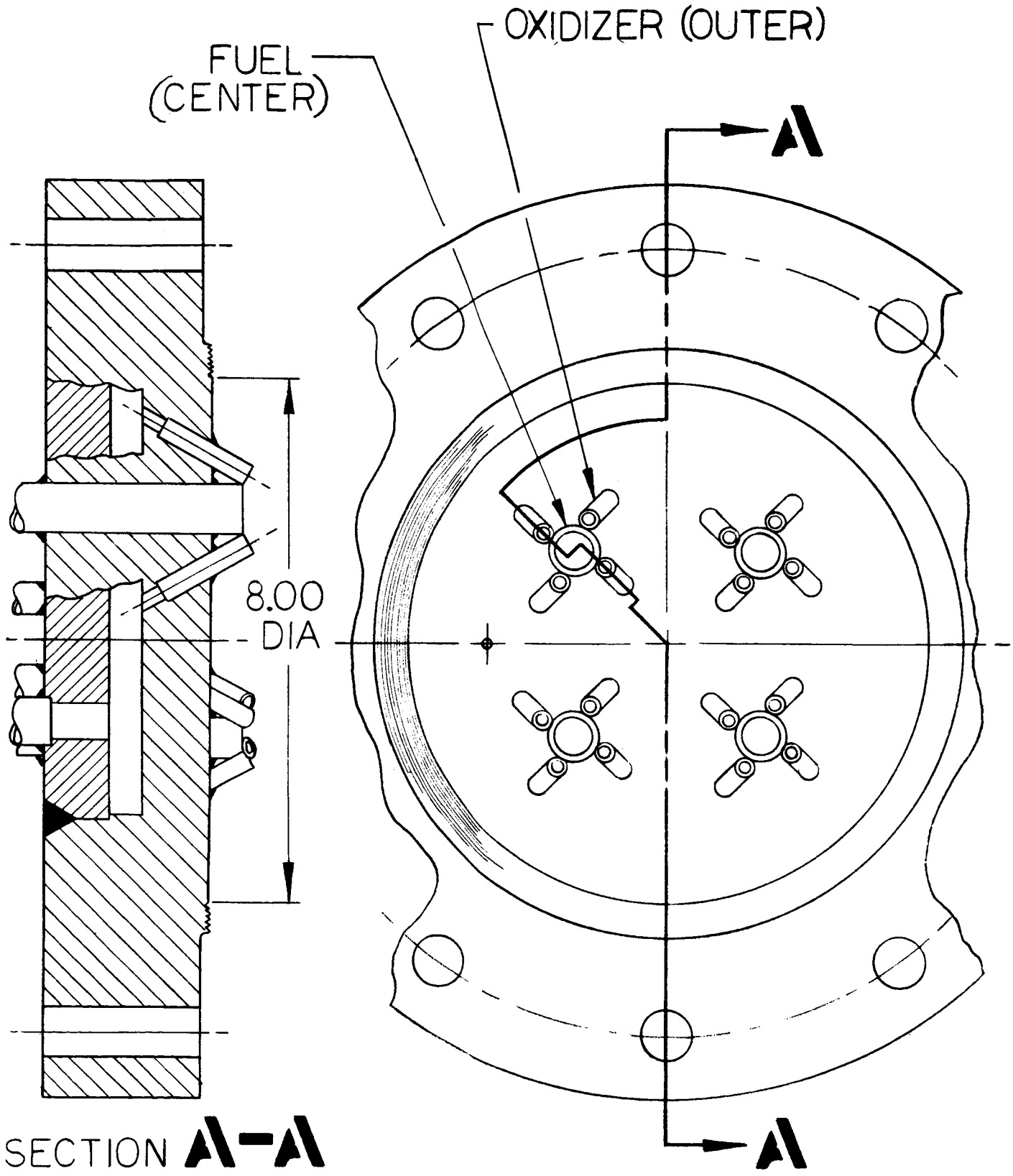

4-5K lb Thrust Pentad Injector

Figure 6

Pentad Injector Flow Pattern

Figure 7

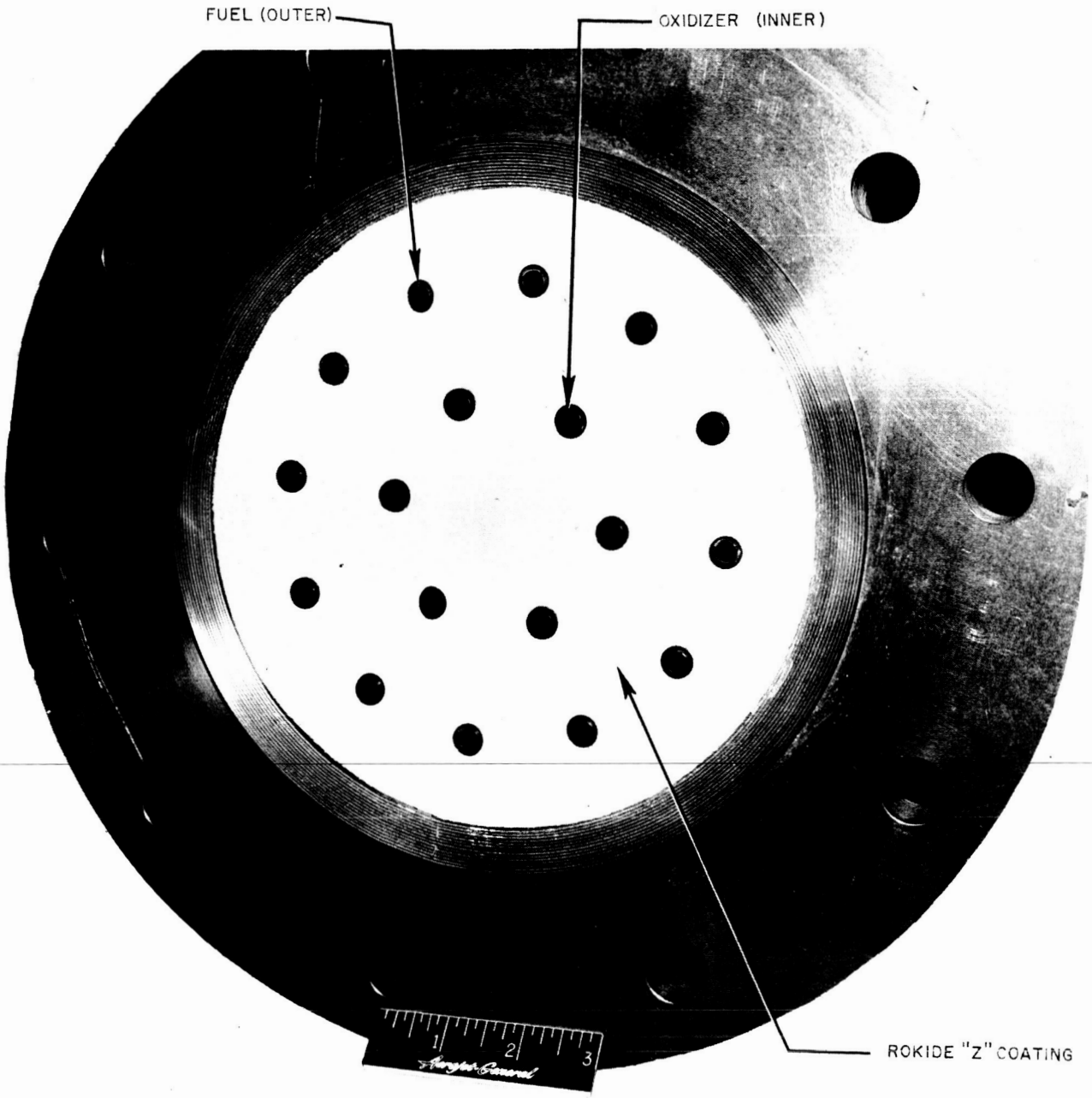

LO_2/LH_2 Coaxial Injector

Figure 8

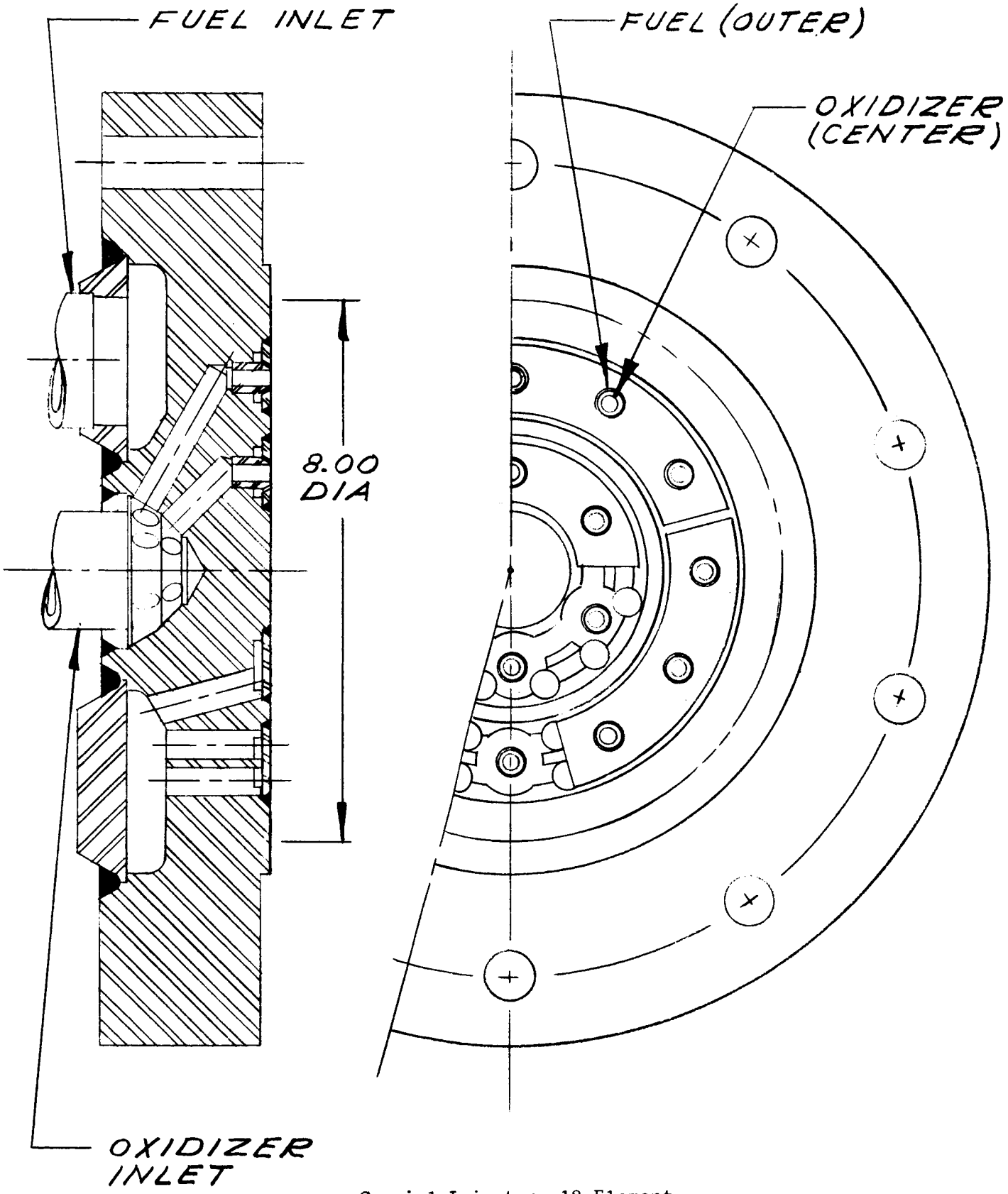

Coaxial Injector, 18-Element

Figure 9

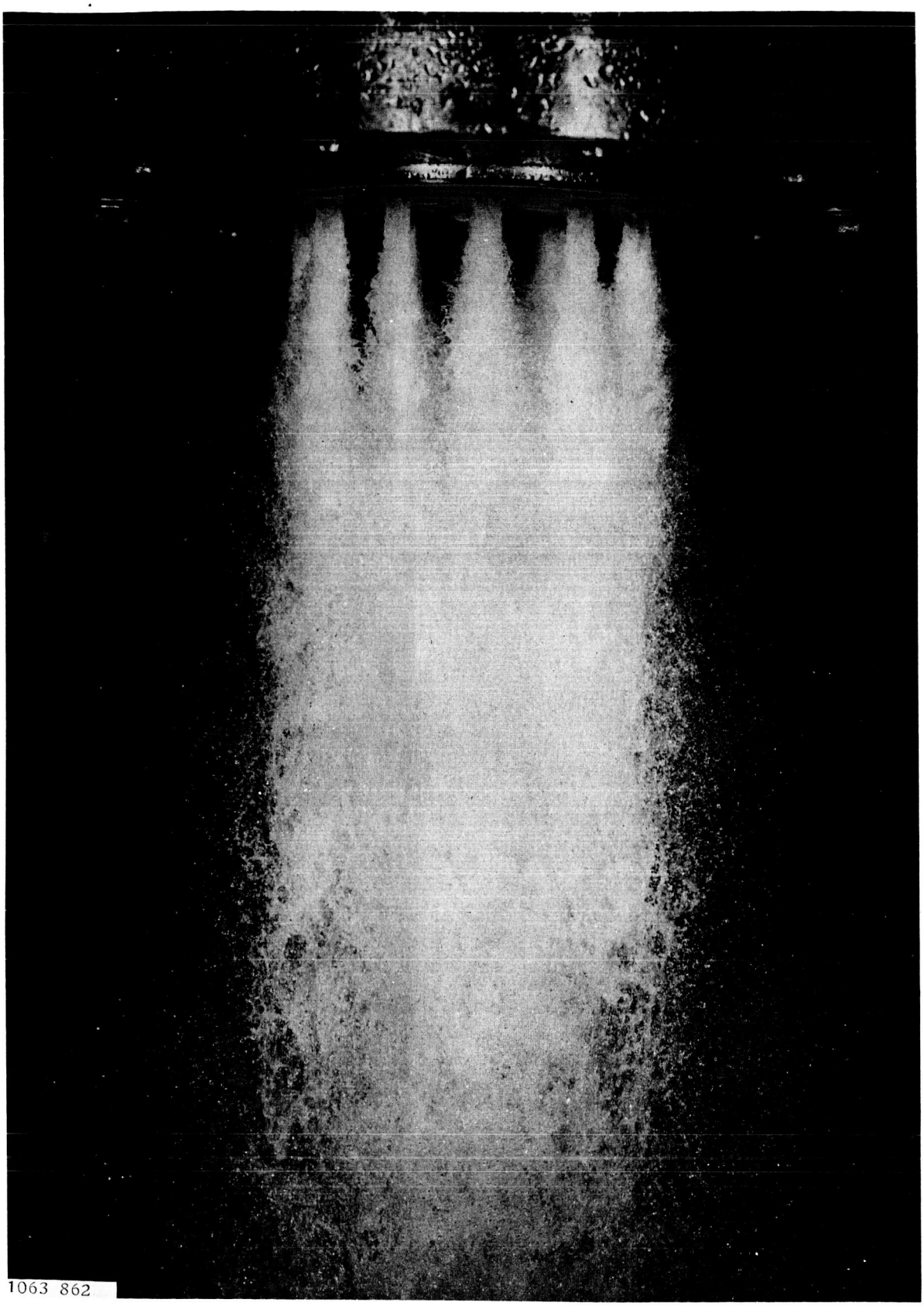

Coaxial Injector Flow Pattern

Figure 10

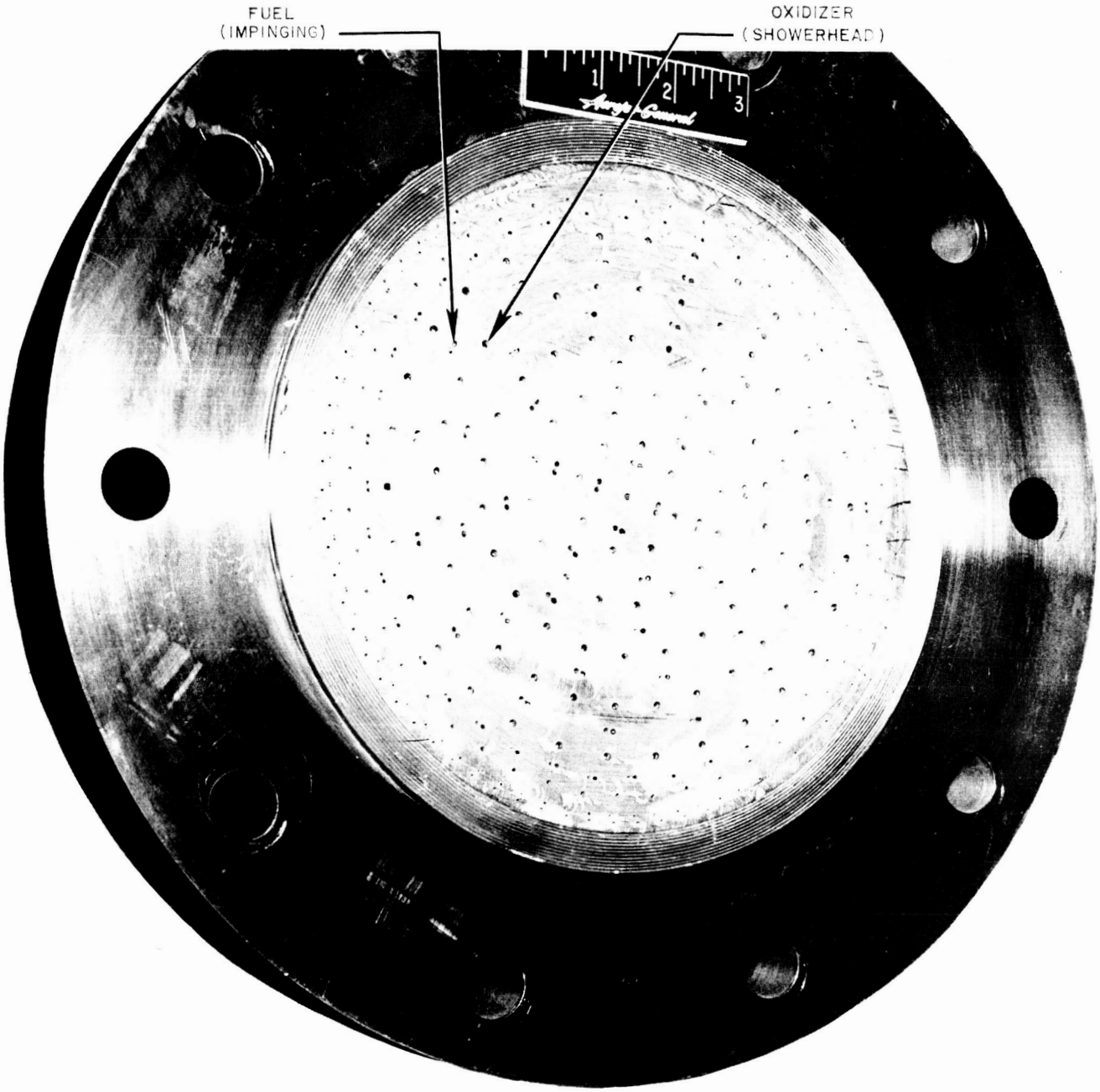

LO_2/LH_2 Conventional Injector

Figure 11

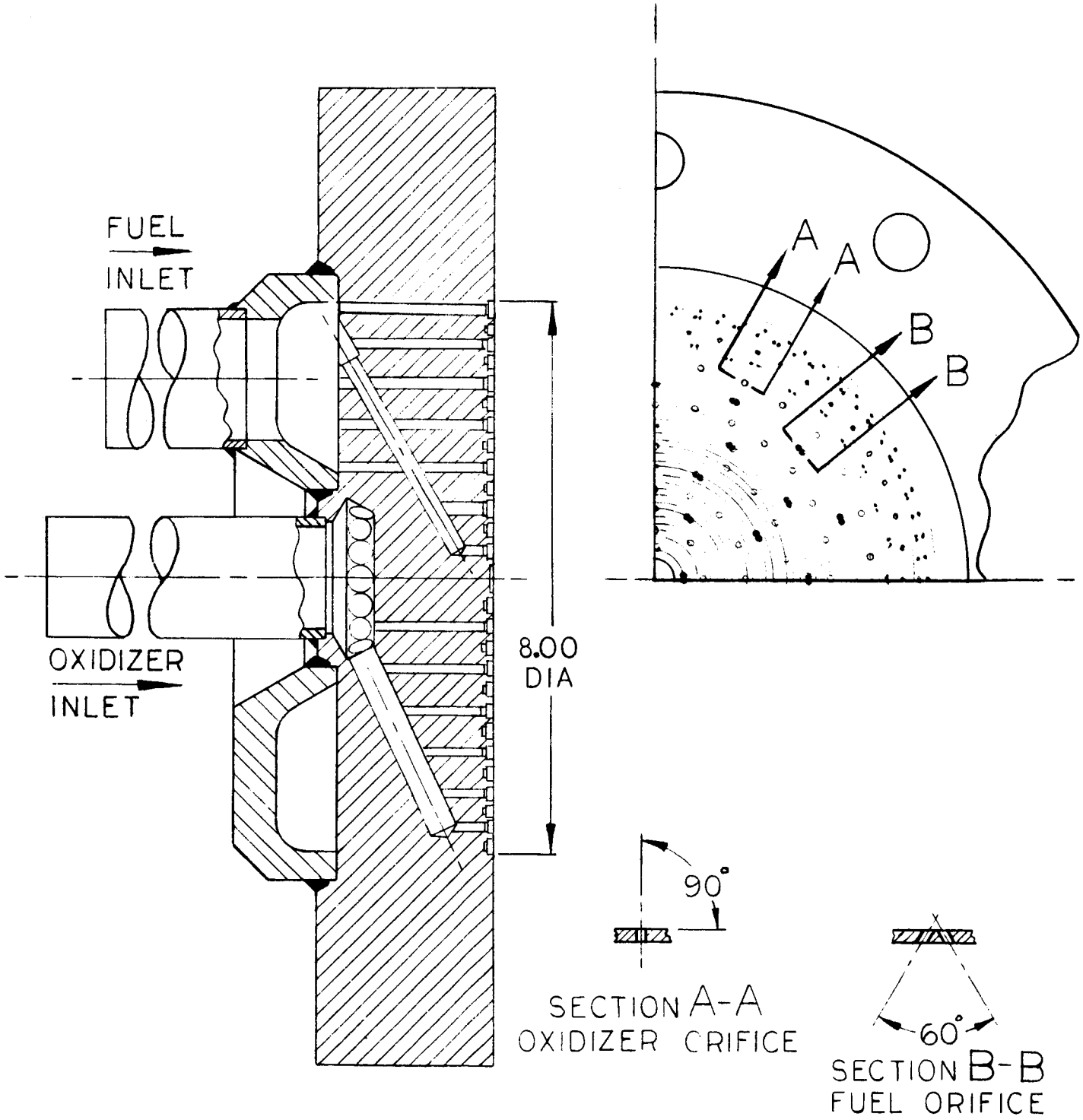

Conventional Injector

Figure 12

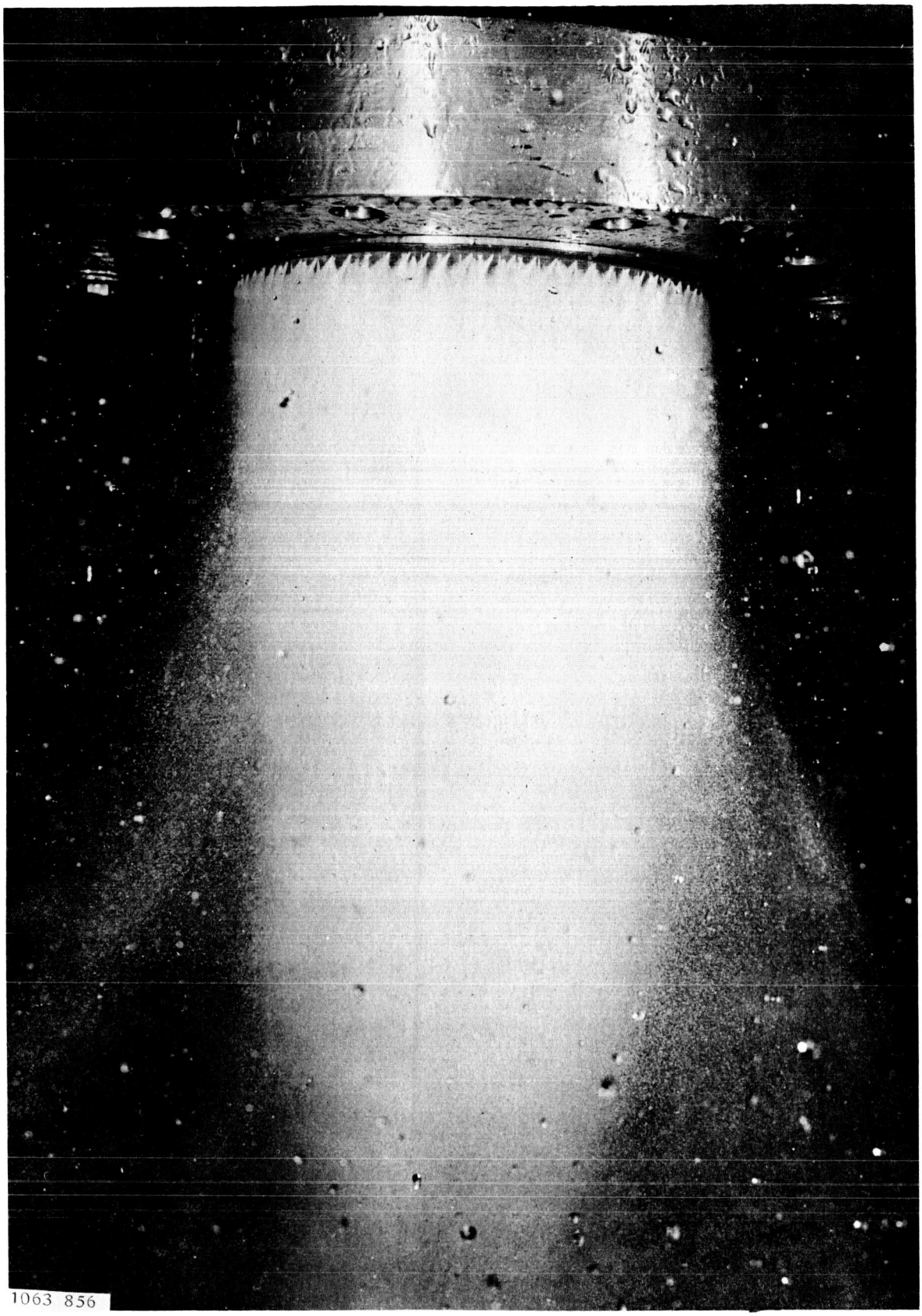

Conventional Injector Flow Pattern

Figure 13

IV, Accomplishments (cont.)

B. TEST SETUP

All propellant lines were insulated from the tank to the valves; the length of the uninsulated line behind the injector was reduced to the minimum. A high-pressure liquid nitrogen line was attached just downstream of the fuel thrust chamber valve to allow prechilling of the injector manifold and chamber before each test. This procedure allowed the tests to be conducted with liquid hydrogen at the injector. A redundant ignition system was used which allowed sequencing and firing of two igniters through two completely separate circuits. The igniters were mounted through the sides of the chamber.

The propellant flow rate was measured with Potter flow meters. The fuel flow meter was designed for high-pressure LH_2 service by using a ball-bearing suspension for the turbine. The flow meter was sized to permit linear flow measurements from 3 to 12 lb/sec of LH_2. It was calibrated with liquid hydrogen at Wyle Laboratories to determine their operational capabilities and the degree of deviation from a standard calibration with water. The unit operated satisfactorily with LH_2; moreover, the LH_2 calibration showed close agreement with the water calibration.

Fuel temperature measurements were made in the tank, fuel Potter flow meter, and injector manifold with Rosemount platinum resistance wire probes. Calibration tests indicated a somewhat slower response time than is desirable for accurate measurements in the fuel injector manifold for the test durations involved. Therefore, faster-responding gold-cobalt thermocouples were used for the last four tests in the injector manifold. Since the fuel temperature probes at the tank and fuel Potter flow meter are immersed in the fuel prior to a test, there was no temperature response lag when testing was begun. The temperature measurements for the oxidizer lines were made with standard copper-constantan thermocouples.

The test stand and related propellant tankage located at the Von Karman Center, Azusa, California, is shown in Figure 14.

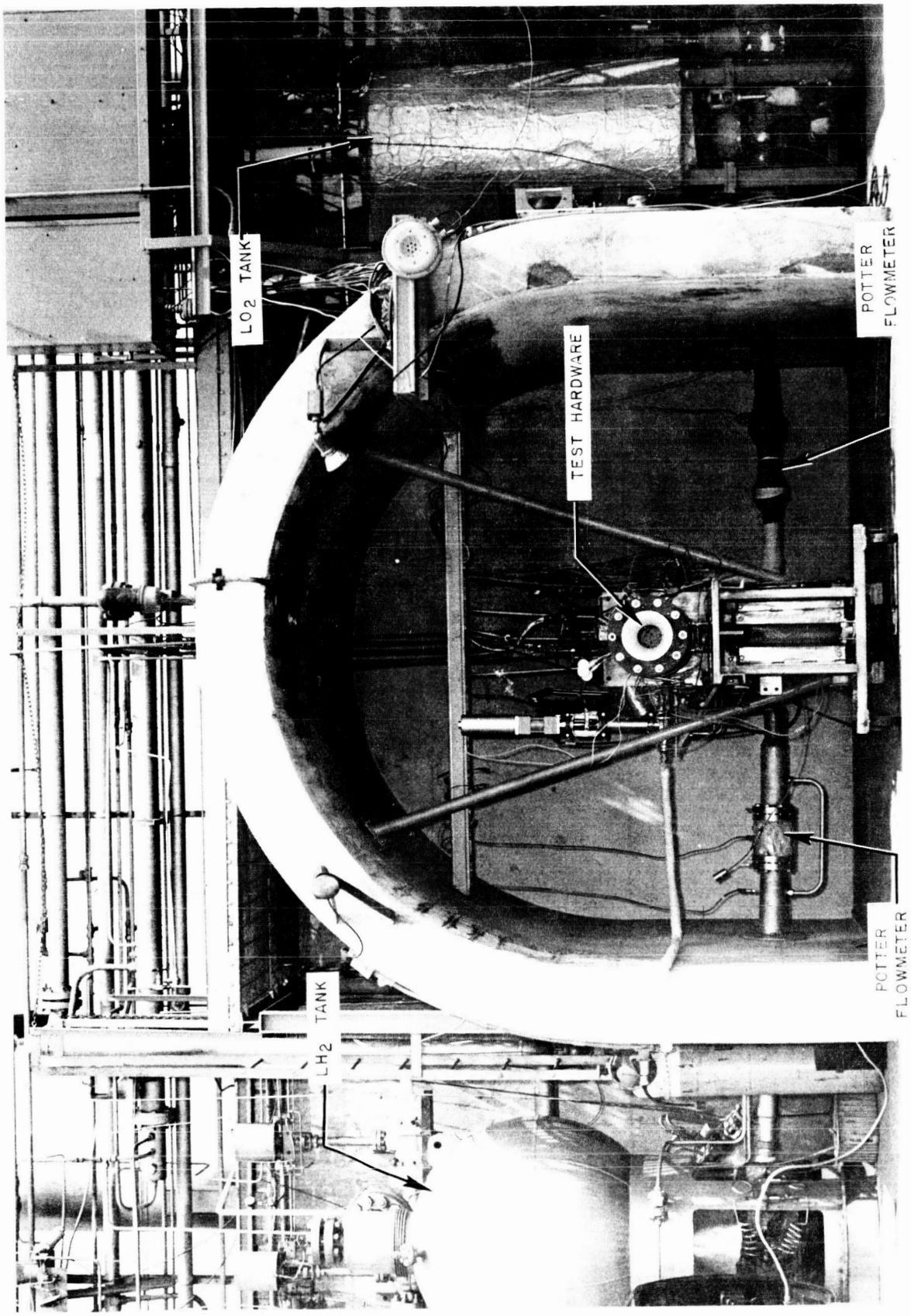

LO_2/LH_2 High Pressure Test Facilities

Figure 14

IV, Accomplishments (cont.)

C. SHOCK-WAVE GENERATOR

The following paragraphs describe the Shock Wave Generator, Model V, PN 0-049425, manufactured by Aerojet-General Corporation, Azusa, California.

The shock wave generator, or pulse gun (Figure 15), is used to test the combustion stability of rocket engines. The generator produces a shock wave that is introduced into an operating thrust chamber, interrupting the dynamic stability of the combustion process. Shock waves of different amplitudes can be produced by varying the pulse charge in the generator. This variation permits experimental creation of known or suspected transients in the combustion process to test the ability of the engine to return to stable operation, and/or to acquire data on the general characteristics of the engine during the period of instability.

Principal specifications are tabulated below.

Physical Dimensions	
Length, in.	9 (nominal)
Diameter, in.	2-5/16 (maximum)
Weight, lb	4.5 (nominal)
Utility Data	
Primer	Electrically Initiated Squib
Firing voltage, vdc	1.8 (minimum)
Firing current, amp	0.4 (minimum)
Thread size required for mount	1.500-12UNF3B (MIL-S-7742)
Performance Data	
Shock Wave Amplitude	Dependent upon pulse charge used

IV, C, Shock-Wave Generator (cont.)

The variety of pulse charges available for test purposes makes the performance of the shock generator assembly virtually unlimited. An exploded view of the shock wave generator is shown in Figure 16.

The shock wave generator is, in effect, a gun that fires blank cartridges. It contains a primer (1)* held in a split retainer (2) behind a firing pin (4). The firing pin is guided by the obdurator disc (5) against the primer in the cartridge (7, 8). The diaphragm holddown (9, 10) serves as a breech, with the obdurator disc acting as a breech block. The diaphragm holddown is pressed down over the diaphragm (11, 12) by the coupling nut (6) to ensure a gas-tight seal. The diaphragm holder ring (13) backs up the diaphragm against the holddown, and contains a hollow center through which the diaphragm bursts when the generator is fired. The burst diaphragm holder (15) contains mating threads for the coupling nut (6) and for mounting the shock wave generator in the equipment during testing. The face of the holder (15) is serrated to form a gas-tight seal when torqued down on the gasket (16) during installation of the shock wave generator.

The pulse charge is the primer (1), cartridge (7 or 8), and burst diaphragm (11 or 12) which are expended in each firing of the shock wave generator. The primer is the same for each pulse charge. Cartridges and diaphragms vary according to the performance requirements for specific tests and are not interchangeable. A typical pulse charge is shown in Figure 17.

---

* Numbers in parentheses correspond to the components called out in Figure 16.

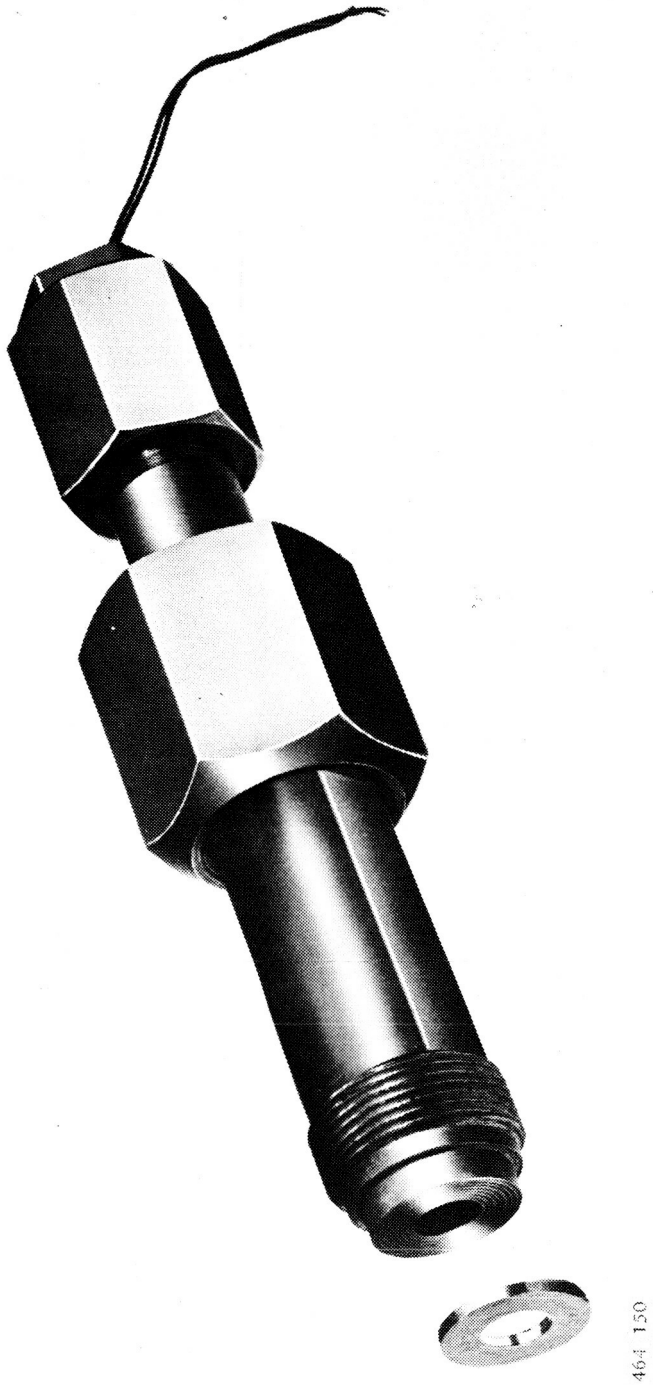

Shock Wave Generator, Model V

Figure 15

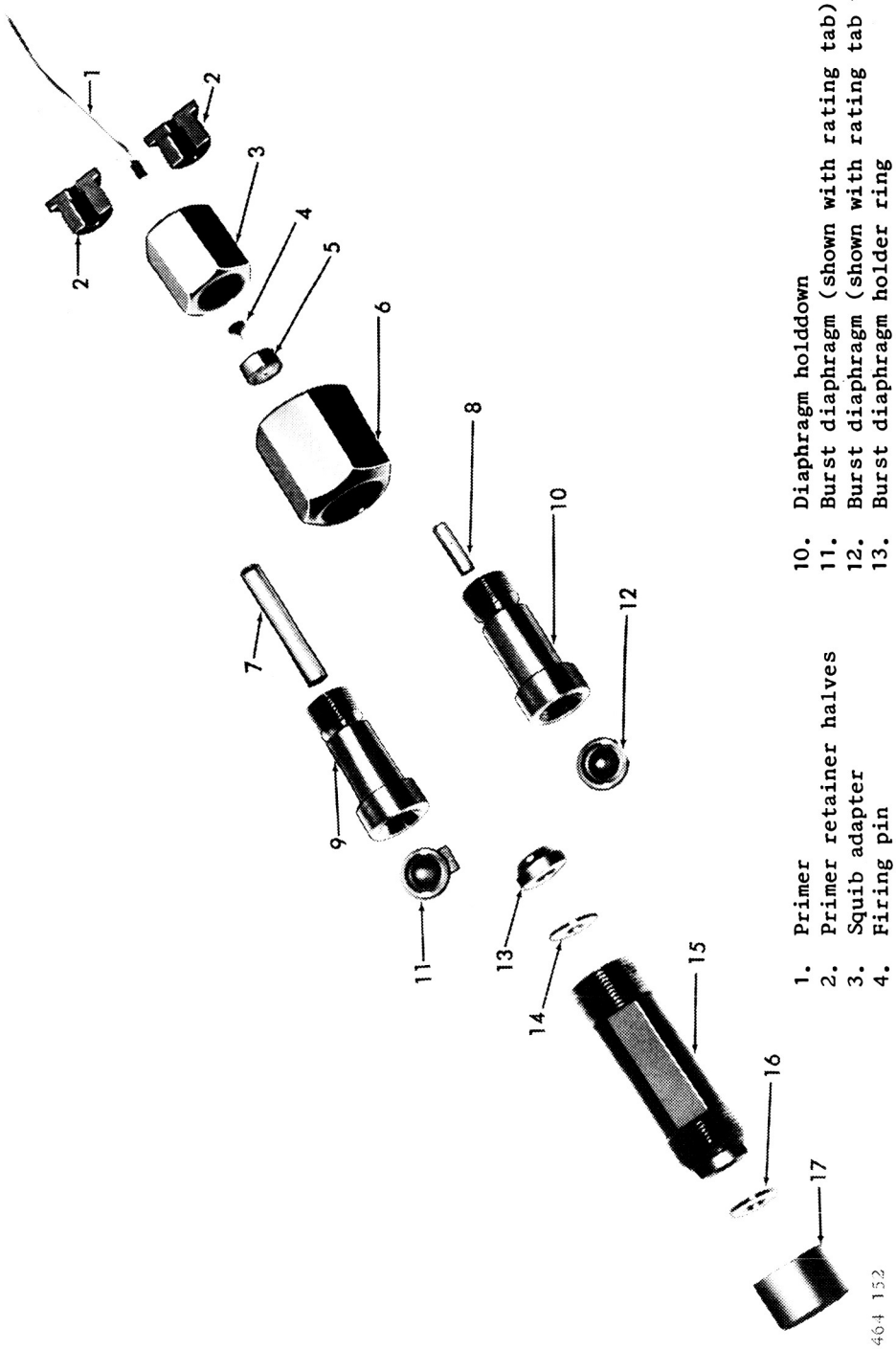

1. Primer
2. Primer retainer halves
3. Squib adapter
4. Firing pin
5. Obdurator disc
6. Coupling nut
7. Magnum cartridge
8. .38 special cartridge
9. Diaphragm holddown
10. Diaphragm holddown
11. Burst diaphragm (shown with rating tab)
12. Burst diaphragm (shown with rating tab trimmed off)
13. Burst diaphragm holder ring
14. Gasket
15. Burst diaphragm holder
16. Gasket
17. Protective cap

Shock Wave Generator, Exploded View

Figure 16

Typical Pulse Charge

Figure 17

IV, Accomplishments (cont.)

D. INSTRUMENTATION

1. Photocon

High-frequency pressure oscillations were measured with water-cooled Photocon pressure transducers mounted in adapters to provide a recessed heat-shield installation. This adapter, (Figure 18) was developed during the testing of the past year, and has worked very satisfactorily. The frequency response of this adapter is flat within 25% for frequencies up to 4500 cps, which is approximately the frequency of the first tangential mode of the 8-in. combustion chamber.

2. Gold-Cobalt vs Copper Thermocouples

A survey of available thermocouple materials indicates that an alloy of gold and cobalt (2.1 atom% of cobalt) vs copper gives the greatest output and has the greatest change of output per degree in the temperature range near the boiling point of liquid hydrogen. Figure 19 is a plot in which the outputs of gold-cobalt vs copper, copper vs constantan, and chromel vs alumel are compared.

Several precautions must be observed when using the gold-cobalt vs copper thermocouple. The gold-cobalt alloy is mechanically weak and requires careful handling. The alloy is an unstable composition below 1080°F, and the alloy must not be heated above 160°F or the cobalt will migrate or precipitate to the grain boundaries, which would change the electrical characteristics. Also, samples of wire from different lots show slightly different EMF values.

To cope with these special characteristics, each thermocouple was fabricated individually, handled with care, and calibrated separately.

IV, D, Instrumentation (cont.)

The first gold-cobalt vs copper thermocouple used in the test program was employed in Test D521-LM-22. Upon calibration of this thermocouple, it was found that the EMF values varies slightly from the design values. However, the addition of a constant numerical connection factor to the observed data made the converted data correspond with the values in the design table. During the test, the response time of the gold-cobalt vs copper thermocouple was shorter than the Rosemount (platinum resistant wire) temperature probe used on the previous tests. The new gold-cobalt vs copper thermocouple was used in the remaining tests.

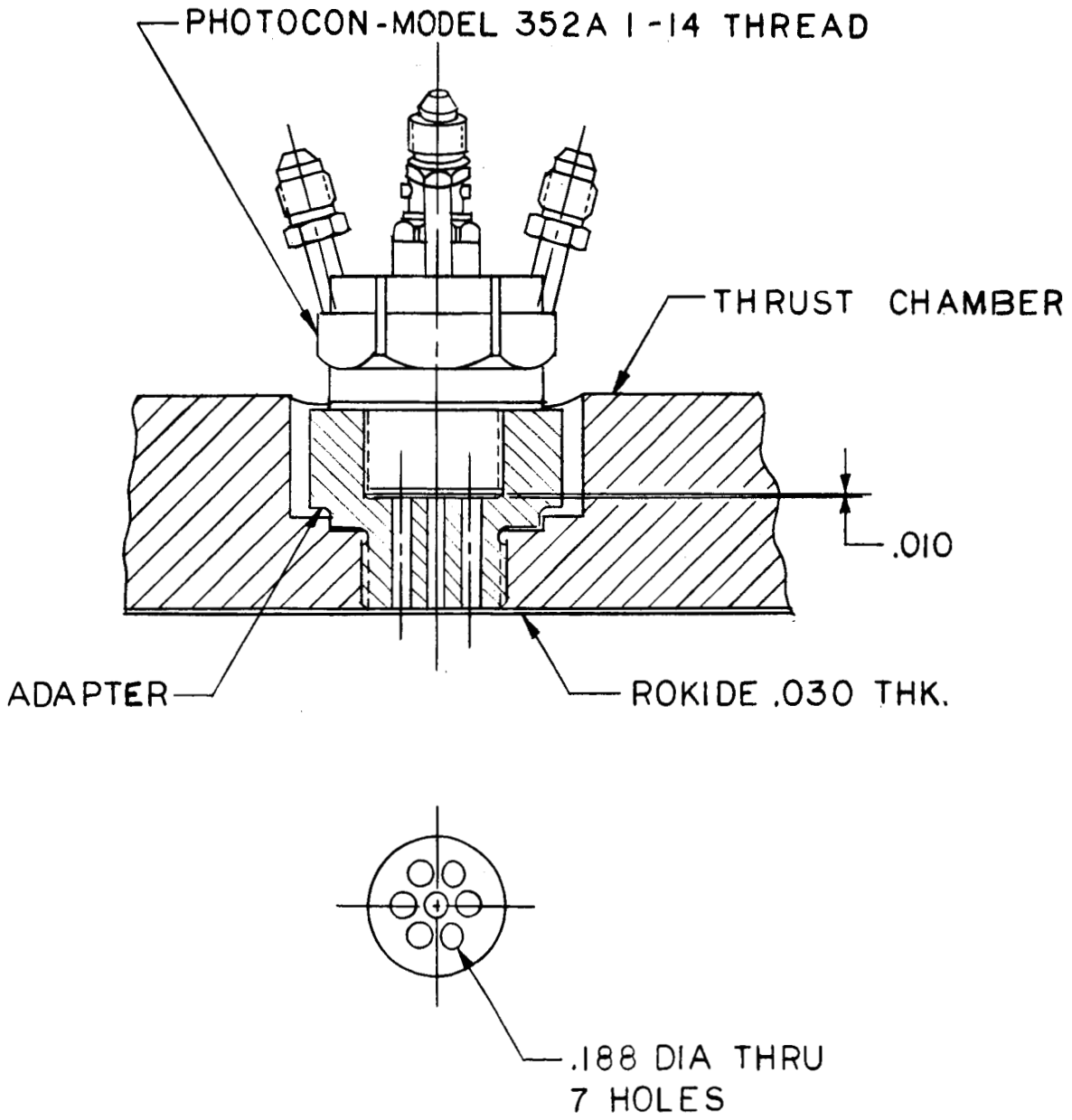

Recessed Photocon Installation

Figure 18

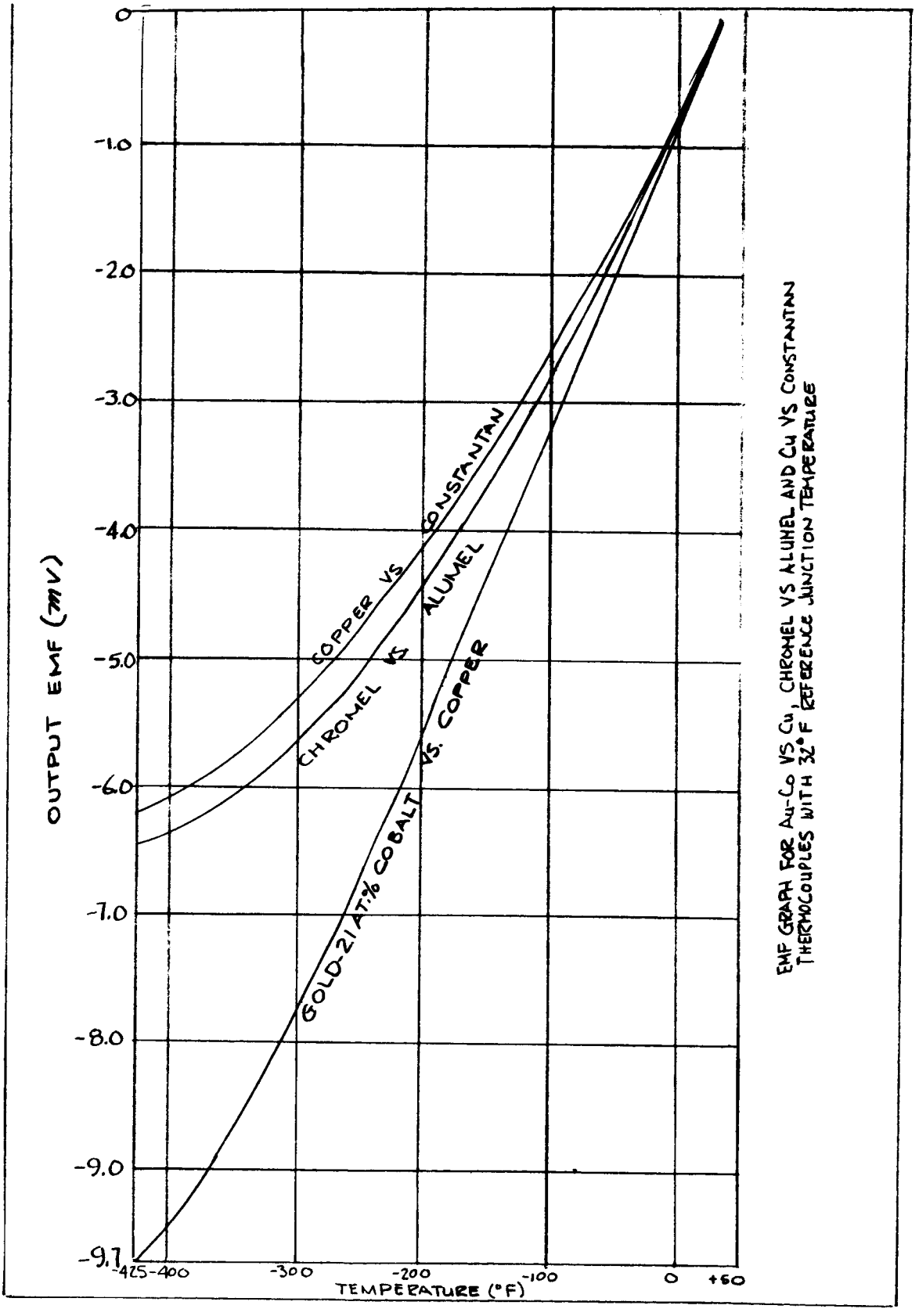

EMF Graph for Thermocouple

Figure 19

IV, Accomplishments (cont.)

E. TEST RESULTS

The test conditions are summarized in Table 1. Stability behavior with respect to high-frequency modes is presented in Table 2. The frequency amplitude and decay characteristics of the disturbances produced by the tangential pulse generator are listed in Table 3. Finally, the stability data are grouped in Table 4 to show the effects of chamber length and chamber pressure on stability behavior. Figures 20 through 27 show oscillograms of typical pulses from both stable and unstable tests.

The following paragraphs discuss in detail the tests performed on the program, and are organized according to injector type and chamber length.

1. Conventional Injector (220 lb Thrust/Element)

a. 6-in. Length Chamber

Tests D-521-LM-14 and -15 were performed with the 6-in.-length chamber at chamber pressures of 735 and 2315 psia, respectively. Test D-521-LM-14 was stable when pulsed with charges up to 80-gr (no 160-gr charge was fired). The initial peak-to-peak amplitude of the 20-gr pulse was 35% of the chamber pressure for a pulse duration of 10 msec; the pressure oscillations were at 3500 cps (1T mode). The subsequent 40- and 80-gr pulses damped to 5% of P_c within 11 sec. Test D-521-LM-15 resulted in an instability of the first tangential mode at the 20-gr pulse. Peak-to-peak initial amplitude at this pulse was approximately 380 psi (16% of P_c) compared with 260 psi for the corresponding instant in Test D-521-LM-14. The pressure perturbation increased to 1460 psi at 20 msec, then converged to 1000 psi at shutdown. Severe erosion occurred on the injector face, but no other damage was sustained. Figures 28 and 29 show little injector damage from Test D-521-LM-14 compared with Test D-521-LM-15.

IV, E, Test Results (cont.)

b. 12.5-in.-Length Chamber

Test D-521-LM-24 was performed at 2555 psia with the 12.5-in. length chamber. This test was driven unstable in the first tangential mode (4000 cps) at the 40-gr pulse. The 20-gr pulse damped within 22 msec. The peak-to-peak initial pressure amplitude for the 40-gr pulse was 1900 psi. This perturbation amplitude increased to a maximum value of 3400 psi within 45 msec. The amplitude then was modulating ("footballing") until fire switch two (FS_2) at 120 msec where it was 1700 psi and more clearly definable as the first tangential mode. Damage to the injector face was severe, similar to Test D-521-LM-5.

c. 26-in.-Length Chamber

Tests D-521-LM-5, -10 and -25 were performed with the 26-in.-length combustion chamber at 1110, 870, and 2218 psia, respectively. All three tests were driven unstable in the first tangential mode by a moderately small (20-gr) pulse charge. Conditions of Tests D-521-LM-5 and -10 differed in the temperature of the fuel. The test results from Tests D-521-LM-5 and -10 showed that the change in fuel temperature had no significant effect on the initiation of stability. These results indicated that the conventional showerhead injector, at a chamber pressure of 1000 to 2500 psia and with a chamber length of 26-in., is marginally unstable in the first tangential mode. With a fuel inlet temperature of -406°F, Test D-521-LM-5 showed no damping tendency at FS_2. With the fuel inlet temperature of -336°F, (Test D-521-LM-10) the oscillations were damping immediately before FS_2. This damping was accompanied by a slight increase in performance, indicative of a change in the combustion characteristics. Tests D-521-LM-5 and -10 had initial peak-to-peak amplitudes of 1400 and 900 psi, respectively for the 20-gr pulse. Both of these tests showed similar characteristics: the first tangential mode, 4000 to 4300 cps, had a wave pattern which appeared to be an irregularly drifting-standing pattern. The resultant amplitudes of these tests, after 60 msec, were 1400 psi and 800 psi, respectively for Tests D-521-LM-5 and -10. Following each of these two tests the injector was found to be eroded; Test D-521-LM-10 damage was the more severe (Figures 30 and 31).

IV, E, Test Results (cont.)

Test D-521-LM-25 was performed at 2218 psia with the 26-in.-length chamber. This test was also driven unstable in the first tangential mode (4400 cps) at the 20-gr pulse. The initial peak-to-peak pressure amplitude was 1900 psi. Within 13 msec, the amplitude had reached 3000 psi. The amplitude was modulating during shutdown (1100 psi at 52 msec). At 190 msec, just prior to complete closure of the oxidizer thrust chamber valve, the amplitude was 2000 psi. The instability resulted in severe injector face erosion as shown in Figure 32.

2. Coaxial Injector (1100 lb Thrust/Element)

a. 6-in.-Length Chamber

Test D-521-LM-16 was performed at 913 psia with the 6-in.-length chamber. A malfunction occurred in the pulse gun circuit; none of the pulses fired. Cleaning the contacts in the firing switch and increasing the electrical current prevented a similar malfunction in subsequent tests. Combustion was stable throughout the test. No injector or chamber damage occurred but the nozzle throat was eroded in one area.

Test D-521-LM-17 was performed with the 6-in.-length combustion chamber at a chamber pressure of 2345 psia. This test was stable when pulsed up to a charge size of 160 gr. Some high-frequency (first tangential mode) instability was detected; however, with an initial pressure amplitude of 13% of P_c, this mode damped within 7 msec at the 20-gr pulse. A high-amplitude, low-frequency (180 cps) oscillation dominated upon each pulse firing. The most severe perturbation occurred during the 80-gr pulse; the initial amplitude was 153% of P_c (3600 psi peak-to-peak) which damped in 46 msec. No evidence of longitudinal mode instability was found with the shorter chamber. Figure 33 shows the no-damage condition of this injector after Test D-521-LM-17.

IV, E, Test Results (cont.)

b. 12.5 in.-Length Chamber

Test D-521-LM-23 was performed at a chamber pressure of 2345 psia. Using the intermediate chamber length (12.5-in.), this test was stable when pulsed with charge sizes up to 160 gr. The first tangential mode was present (the initial peak-to-peak amplitude, P_o was 15% of P_c) and decayed within 8 msec at the 20-gr pulse. Subsequent pulses decayed within 22 msec. No longitudinal mode instability was present at the intermediate chamber length. Low-frequency oscillations were present, and ranged from 37 to 72% of P_c for the pulses fired; however, all low-frequency oscillations decayed to 5% of P_c within 41 msec. There was no injector damage.

c. 26-in.-Length Chamber

Tests D-521-LM-6, -7, -8, and -18 were performed with the 26-in.-length combustion chamber at 1020, 1360, 2325, and 2495 psia, respectively.

The first two tests were stable when pulsed up to a charge size of 160 gr. Amplitudes of the pressure disturbances were higher for the pulse test at 1500 psia than for the test at 1000 psia. Initial peak-to-peak amplitude for the 20-gr pulse was approximately 980 psi for the test at 1360 psia chamber pressure compared with that of 570 psi for the test at 1000 psia. Pulse durations were approximately 10 msec for the first two tests at the 20-gr pulse. Pulse durations were shorter than those corresponding to the 26-in.-length chamber pulse tests with the 4-5K lb thrust/element pentad injector. Pulse frequencies were 4000 to 4200 cps (1T mode). There was no injector damage during Tests D-521-LM-6 and -7.

Test D-521-LM-8 (2325 psia) was driven unstable by the 20-gr pulse. A first longitudinal mode oscillation (1280 cps) occurred immediately upon

IV, E, Test Results (cont.)

pulse initiation and lasted until shutdown. These results agreed with previous observations of decreased stability at the higher chamber pressures. The injector face was damaged during the test (Figures 34 and 35).

Test D-521-LM-18 was performed to repeat Test D-521-LM-8. The 26-in.-length combustion chamber was used at a chamber pressure of 2495 psia. This test developed a first longitudinal instability of 1100 cps, with an initial amplitude of 24% of P_c upon firing the 20-gr pulse; the amplitude of this pressure perturbation continued to diverge until shutdown. The near-design mixture ratio of 6.3 compared with 3.2 for Test D-521-LM-8 still resulted in a longitudinal instability as in Test D-521-LM-8. Minor high frequency oscillations (initial amplitude 14% of P_c at the 20-gr pulse) were present, but a neutral (constant) amplitude dominated until shutdown. These high-frequency oscillations (9000 to 11,000 cps) correspond to the resonant frequency of the Photocon adapter. There was no injector damage this test.

3. Pentad Injector (5000 lb Thrust/Element)

a. 6-in.-Length Chamber

Tests D-521-LM-12, -13, and -20 were performed with the 6-in-length combustion chamber at 910, 2255, and 1935 psia, respectively. Test D-521-LM-12 was stable with pulse charges up to 160 gr. These pulse perturbations were highly attentuated compared with Test D-521-LM-1 in which the 26-in.-length chamber was used. Pulse initial amplitudes were 100 to 175 psi for Test D-521-LM-12, compared with 380 to 630 psi for Test D-521-LM-1. Pulse durations for Test D-521-LM-12 were less than 8 msec. Both tests, (D-521-LM-12 and -13) indicated a damped high-frequency of 4000 cps, corresponding to the first tangential mode. Tests D-521-LM-12, -13, and -20 sustained no injector damage.

IV, E, Test Results (cont.)

Test D-521-LM-13 developed a low-frequency instability, 375 cps, during the 80-gr pulse. The first two pulses fired (20- and 40-gr charges) caused initial pressure perturbations which were less than 500 psi peak-to-peak amplitude. Although the low-frequency perturbation was evident in the starting transient and during the first two pulses, these pulses decayed to 5% of P_c within 50 msec. The 80-gr charge, however, generated a low-frequency perturbation having an initial amplitude of 1100 psi, peak-to-peak. This perturbation decayed to 540 psi in 15 msec and was sustained at this level for a few milliseconds, then increased to a value of 860 psi within 70 msec. This oscillation continued to diverge until interrupted by the 160-gr pulse. This last pulse showed an initial amplitude of 1000 psi which decayed to approximately 800 psi, then rose again and continued to diverge until shutdown. It was noted that the fuel injector pressure drop was less than 13% of P_c with a mixture ratio of 8.0. The low-frequency perturbation was undoubtedly caused by the feed system interacting with the higher temperature combustion process at the stoichiometric mixture ratio. Figure 36 shows that no injector face damage was incurred as a result of the chugging mode.

Test D-521-LM-20, also performed with the 6-in.-length combustion chamber was operated at 1935 psia as a rerun of Test D-521-LM-13. This test was similar to that of D-521-LM-13 except for the mixture ratio of 5.9 compared with the mixture ratio of 8.0 for Test D-521-LM-13. Test D-521-LM-20 was stable with respect to pulsing up to a charge size of 160 gr. High-frequency oscillations showed an initial amplitude of 12.9% of P_c and damped rapidly (within 3 msec) to 5% of P_c at the 20-gr pulse. Subsequent pulses were attenuated within 5 msec. In contract to Test D-521-LM-13, no low-frequency oscillations occurred during Test D-521-LM-20 which was conducted at the design mixture ratio of 5.9. There was no injector damage during Test D-521-LM-20.

IV, E, Test Results (cont.)

b. 12.5 in.-Length Chamber

Test D-521-LM-22 was performed with the 12.5-in.-length combustion chamber at a pressure of 2141 psia. This test was stable when pulsed up to a charge size of 160 gr. High-frequency oscillations at 4100 cps (first tangential mode) were observed to damp rapidly. The initial peak-to-peak amplitude, P_o, for the 20-gr pulse was 37% of P_c; this perturbation damped to 5% of P_c within 8 msec. Subsequent pulses were attenuated within 8 msec also. There was no evidence of low-frequency oscillations as in Test D-521-LM-13, although both tests were performed at high mixture ratios, with Test D-521-LM-13 having the 6-in.-length chamber. Figure 37 shows that minor injector damage was sustained.

c. 26-in.-Length Chamber

Tests D-521-LM-1, -2, and -19 were performed with the 26-in.-length combustion chamber at 1036 psia, 1515 psia, and 2415 psia pressure, respectively. Tests D-521-LM-1 and -2 were stable when pulsed to a charge size of 80-gr; Test D-521-LM-19 was stable up to 160 gr. The 10-gr pulse charge had no perceptible effect in either Test D-521-LM-1 or -2; therefore, this charge size was replaced with a 160-gr size during subsequent testing. Initial peak-to-peak amplitude of the pressure perturbations increased with pulse size as well as with the threshold of operating pressure. Pulse frequencies were dominantly of the first tangential mode of 4000 cps. The pulse durations for the 20-gr pulses were 14 to 12 msec over the pressure range from 1036 to 2415 psia. Minor first longitudinal oscillations were present during the 2415 psia test (Test D-521-LM-19), but damped within 8 msec. There was no injector damage during these tests with a chamber length of 26 in.

IV, E, Test Results (cont.)

4. Pulse Calibration Tests

a. 12.5-in.-Length Chamber

Tests D-521-LM-21A and -21B were performed in a manner similar to Tests D-521-LM-11A and -11B. Test D-521-LM-21A was performed by plugging the throat and pressurizing the intermediate (12.5-in.) length chamber with 1000 psia nitrogen. Analyses of Test D-521-LM-21A showed a high-frequency of 3000 cps which corresponded to inherent transducer resonance. Pressure perturbations were irregular and matched no calculated modes of instability apart from some 1200 cps oscillations detected during the 160-gr pulse. These oscillations were near the first tangential mode of 1100 cps.

Test D-521-LM-12B showed irregular, non-oscillatory pressure perturbations for the chamber pressurized to 2500 psia with nitrogen gas. Filtered tape playbacks showed some 1150 to 1200 cps oscillations which were detected during all pulses with peak-to-peak amplitudes from 6 to 16% of chamber pressure for charge sizes from 20 to 160 gr. These oscillations appeared to be near the first tangential mode, 1120 cps, and decayed within 28 msec. No evidence of any longitudinal modes was present.

b. 26-in.-Length Chamber

Tests D-521-LM-11A and -11B consisted of detonating four pulse charges of 20, 40, 80, and 160 gr in the 26-in. chamber without combustion. The injector inlet valves were closed and the throat was plugged on the 1000 psia nozzle. The chamber was pressurized with nitrogen gas at 1000 and 2500 psia, respectively for Tests D-521-LM-11A and -11B.

IV, E, Test Results (cont.)

Test D-521-LM-11A at 1000 psia showed irregularly mixed high-frequency pressure oscillations. First and second tangential modes, 1020 and 1700 cps respectively, occurred intermittently after each pulse charge. Initial peak-to-peak amplitude of these transverse perturbations was approximately 500 psi (50% of P_c) at the 20-gr pulse with a decay time (to 5% of P_c) of 60 msec. The first longitudinal mode (250 cps) occurred strongly during each pulse and had an initial amplitude of 200 psi with a duration of 10 msec. Test D-521-LM-11B at 2500 psia resulted in pressure perturbations similar to those in Test D-521-LM-11A. Initial peak-to-peak amplitude of Test D-521-LM-11B transverse oscillations was approximately 1000 psi (40% of P_c) at the 20-gr pulse, with a decay time (to 5% of P_c) of 60 msec. The first longitudinal mode, at 300 cps, had an initial amplitude of 210 psi, with a duration of 50 msec. Cold-pulse durations were three- to four-times as long as those in the corresponding hot pulse tests. Pulse characteristics are shown in Figure 38.

TABLE 1

Test No.	Date	Injector Type	Chamber Length, in.	L*, in.	A_C/A_T	P_c psia	M.R. W_o/W_f	Wt, lb/sec	W_f lb/sec	W_o lb/sec	T_f, °F	T_o °F	F lb	c*	%Theo c*	Pulse Charges, grain	Duration, sec	Remarks
D-521-LM-1	7-23-63	4-5K Pentad	26	97	3.6	1036	5.2	61.4	9.8	51.6	-399	-275	20,454	7522	96	10,20,40,80	0.74	Stable test.
D-521-LM-2	7-29-63	4-5K Pentad	26	145	5.4	1515	5.7	59.5	8.9	50.6	-399	-270	20,232	7462	97	10,20,40,80	0.47	Stable test.
D-521-LM-3	8-19-63	4-5K Pentad	26	245	9.1	---	--	--	--	--	--	--	--	--	--	10,20,40,80	--	No combustion: oxidizer valve failed to open.
D-521-LM-4	8-19-63	4-5K Pentad	26	245	9.1	2500	--	--	--	--	--	--	--	--	--	--	0.12	Bolts failed at injector chamber joint due to hot gas leakage.
D-521-LM-5	9-10-63	Conventional	26	97	3.6	1110	6.3	67.5	9.2	58.2	-406	-294	20,368	7346	97	20,40	0.45	High-frequency instability following 20-gr pulse. Injector face severely damaged.
D-521-LM-6	9-16-63	Coaxial	26	97	3.6	1020	4.3	57.2	10.7	48.5	-407	-296	19,656	7850	98	20,40,80,160	0.46	Stable test.
D-521-LM-7	9-20-63	Coaxial	26	145	5.4	1360	4.3	54.8	10.3	44.5	-407	-206	18,720	7250	92	20,80,160	0.6	Stable test.
D-521-LM-8	9-27-63	Coaxial	26	245	9.1	2325	3.2	54.0	12.9	41.1	-412	-297	18,560	7200	90	20	0.45	High-frequency instability following 20-gr pulse. Injector face damaged.
D-521-LM-9	10-9-63	4-5K Pentad	26	245	9.1	2105	2.1	49.4	14.9	34.5	-405	-298	15,480	7123	91	--	0.20	High-frequency instability shutdown initiated during start sequence. No pulse charges fired.
D-521-LM-10	10-29-63	Conventional	26	97	3.6	870	6.8	53.9	6.9	47.0	-336	-285	7,280	7296	93	20,40	0.34	High-frequency instability following 20-gr pulse. Severe injector damage.

SUMMARY OF TEST RESULTS

TABLE 1 (cont.)

Test No.	Date	Injector Type	Chamber Length, in.	L*, in.	A_C/A_T	P_c psia	M.R. W_o/W_f	Wt, lb/sec	W_f lb/sec	W_o lb/sec	T_f, °F	T_o °F	F lb	c*	%Theo c*	Pulse Charges, grain	Duration, sec	Remarks
D-521-LM-11	11-4-63	Calibration of Photocons at chamber pressure of 1000 and 2500 psia. Chamber length of 26 in.																
D-521-LM-12	11-8-63	4-5K Pentad	6	24	3.6	910	5.4	62.7	9.8	52.8	-409	-289	18,680	6390	83	20,40,80,160	0.5	Stable test. No injector damage.
D-521-LM-13	11-18-63	4-5K Pentad	6	61	9.1	2255	8.0	60.1	6.6	53.5	-393	-289	19,880	6330	89	20,40,80,160	0.46	Low-frequency instability (approx 375 cps) following 80-gr pulse.
D-521-LM-14	11-26-63	Conventional	6	24	3.6	735	5.6	67.8	10.2	57.6	-368	-290	14,400	4720	62	20,40,80	0.44	Stable test.
D-521-LM-15	12-5-63	Conventional	6	61	9.1	2315	6.8	57.9	7.4	50.6	-396	-291	20,000	6440	86	20	0.39	High-frequency instability following 20-gr pulse. Injector face damage.
D-521-LM-16	12-12-63	Coaxial	6	24	3.6	913	7.6	78.2	9.1	69.1	-407	-283	17,600	5210	72	--	0.52	Stable test. No pulse charges fired.
D-521-LM-17	12-19-63	Coaxial	6	61	9.1	2345	4.4	60.5	11.3	49.2	-403	-274	19,760	6680	85	20,40,80,160	0.50	Stable test.
D-521-LM-18	12-27-63	Coaxial	26	245	9.1	2495	6.6	63.7	8.4	55.3	-402	-287	22,240	6760	89	20	0.43	High-frequency instability following 20-gr pulse. Repeat of Test -8.
D-521-LM-19	1-7-64	Pentad	26	245	9.1	2415	5.4	55.8	8.7	47.1	-403	-276	20,320	7210	93	20,40,80,160	0.53	Stable test. P_{C1} line failed. Repeat of Test -9.
D-521-LM-20	2-6-64	Pentad	6	61	9.1	1935	5.9	56.7	8.2	48.5	-360	-267	15,640	5840	77	20,40,80,160	0.51	Stable test. Repeat of Test -13.
D-521-LM-21	2-17-64	Calibration of Photocons at chamber pressure of 1000 and 2500 psia. Chamber length of 12.5 in.																
D-521-LM-22	2-24-64	Pentad	12.5	124	9.1	2141	8.3	63.0	6.7	56.3	-369	-287	19,352	6029	97	20,40,80,160	0.49	Stable test. Severe erosion at nozzle-to-chamber joint due to hot gas leak.
D-521-LM-23	3-5-64	Coaxial	12.5	124	9.1	2345	5.7	58.7	8.7	50.0	-384	-287	20,000	6720	87	20,40,80,160	0.67	Stable test.
D-521-LM-24	3-13-64	Conventional	12.5	124	9.1	2558	6.2	62.2	8.7	53.5	-390	-268	21,592	7303	95	20,40	0.46	High-frequency instability following 40-gr pulse. Injector face damage.
D-521-LM-25	3-24-64	Conventional	26	245	9.1	2218	4.2	51.3	9.9	41.4	-388	-268	19,520	7673	96	20	0.39	High-frequency instability following 20-gr pulse. Injector face damage.

TABLE 2

HIGH-FREQUENCY STABILITY DATA

Injector Type	Chamber Length, in.	Chamber Pressure, psia	Test Number D-521-LM-	Mixture Ratio o/f	Amplitude of Largest Pulse, % of P_c	Stability	
						Frequency cps	Mode
Conventional	6	735	14	4.9	109	3500	Stable
	6	2135	15	6.4	16	4000	First tangential
	12.5	2555	24	6.5	74	4000	First tangential
	26	870 (1)	10	6.8	103	4000	First tangential
	26	1110	5	6.3	126	4300	First tangential
	26	2218	25	4.2	85	4400	First tangential
Coaxial	6	2345 (2)	17	4.4	36	4500	Stable
	12.5	2345	23	5.7	34	4000	Stable
	26	1020	6	4.3	94	4100	Stable
	26	1360	7	4.3	75	4200	Stable
	26	2325	8	3.2	---	1280	First longitudinal
	26	2495	18	6.3	24	1100	First longitudinal
Pentad	6	910	12	5.4	12	4000	Stable
	6	1935	20	5.9	33	3600	Stable
	6	2255 (3)	13	8.0	44	4000	Stable
	12.5	2141	22	8.3	65	4100	Stable
	26	1036	1	5.2	46	4000	Stable
	26	1515	2	5.7	55	4100	Stable
	26	2415	19	5.4	61	4000	Stable

Notes: (1) Hydrogen temperature 124°R, approximately 70° higher than normal.
(2) Marginal low-frequency stability, 180 cps
(3) Low-frequency instability, 375 cps.

TABLE 3

Injector Type	Chamber Length, in.	Chamber Pressure, psia	Test Number D-521-LM-	Pulse Size, gr	Dominant Frequencies, cps	Initial Amplitude psi	Decay Time (1), msec	Remarks
Conventional	6	735	14	20	3500	260	10	
	6	735	14	40	3500	320	10	
	6	735	14	80	3500	800	11	
	6	2315	15	20	4000	380	--	Diverged to 1460 psi in 20 msec, then decreased to 1000 psi at FS_2.
	12.5	2555	24	20	4000	950	22	
	12.5	2555	24	40	4000	1900	--	Diverged to 3400 psi in 45 msec, then decreased to 1700 psi at FS_2.
	26	1020	10	20	4000	900	--	Diverged to 1060 psi in 35 msec, then decreased to 800 psi at FS_2.
	26	1110	5	20	4300	1400	--	Diverged to 1460 psi in 35 msec, then decreased to 1400 psi at FS_2.
	26	2218	25	20	4400	1900	--	Diverged to 3000 psi in 13 msec, then decreased to 1100 psi at FS_2.
Coaxial	6	2345	17	20	4500 180	300 1800	7 40	
	6	2345	17	40	4500 180	440 2300	10 41	
	6	2345	17	80	4500 180	850 3600	13 46	
	6	2345	17	160	4500 180	850 3400	13 80	
	12.5	2345	23	20	4000 142	340 860	8 10	
	12.5	2345	23	40	4000 142	540 1450	9 19	
	12.5	2345	23	80	4000 142	750 2000	22 41	
	12.5	2345	23	160	4000 142	800 1700	18 41	
	26	1020	6	20	4100	570	10	
	26	1020	6	40	4100	790	11	
	26	1020	6	80	4100	970	11	
	26	1020	6	160	4100	780	12	Pulse gun pressure leakage at 160 gr.
	26	1360	7	20	4200	980	10	
	26	1360	7	80	4200	1020	11	
	26	1360	7	160	4200	1020	8	

(1) Time for pulse to decay to 5% of P_c.

SUMMARY OF PULSE CHARACTERISTICS

TABLE 3 (cont.)

Injector Type	Chamber Length, in.	Chamber Pressure, psia	Test Number D-521-LM-	Pulse Size, gr	Dominant Frequencies, cps	Initial Amplitude psi	Decay Time (1), msec	Remarks
Coaxial	26	2325	8	20	1280	---	--	Diverging oscillation, amplitude unknown due to instrumentation malfunction.
	26	2495	18	20	8000	350	--	Neutral oscillations at 350 psi.
					1100	600	--	Converged to 300 psi at 10 msec, then diverged to 800 psi at FS_2.
Pentad	6	910	12	20	4000	100	6	
	6	910	12	40	4000	175	6	
	6	910	12	80	4000	155	5	
	6	910	12	160	4000	110	5	Pulse gun pressure leakage at 160 gr.
	6	1935	20	20	3600	250	3	
	6	1935	20	40	3600	250	4	
	6	1935	20	80	3600	400	5	
	6	1935	20	160	3600	630	4	
	6	2255	13	20	4000	150	3	
					375	260	17	
	6	2255	13	40	4000	200	3	
					375	480	50	
	6	2255	13	80	4000	750	13	
					375	1100	--	Converged to 540 psi in 15 msec, then diverged to 860 psi prior to the 160-gr pulse.
	6	2255	13	160	4000	750	14	All high-frequency oscillations damped.
					375	1000	--	Converged to 800 psi in 15 msec, then oscillated at constant amplitude until FS_2.
	12.5	2141	22	20	4100	800	8	
	12.5	2141	22	80	4100	1400	7	
	12.5	2141	22	160	4100	900	8	Pulse gun pressure leakage at 160 gr.
	26	1036	1	20	4000	380	14	
	26	1036	1	40	4000	630	14	
	26	1036	1	80	4000	465	12	Pulse gun pressure leakage at 160 gr.
	26	1515	2	20	4100	385	8	
	26	1515	2	40	4100	725	25	
	26	1515	2	80	4100	830	17	
	26	2415	19	20	4000	300	12	
					1100	200	8	
	26	2415	19	40	4000	540	13	
					1100	460	11	
	26	2415	19	80	4000	840	15	
					1100	650	10	
	26	2415	19	160	4000	1460	12	All tangential pressure oscillations damped.
					1100	850	12	All longitudinal oscillations damped.

(1) Time for pulse to decay to 5% of P_c.

TABLE 4

SUMMARY OF STABILITY BEHAVIOR

Injector Type	Chamber Length, in.	Chamber Pressure (Nominal)					
		1000 psia		1500 psia		2500 psia	
		Max Pulse Size, gr	Stability	Max Pulse Size, gr	Stability	Max Pulse Size, gr	Stability
Conventional	6	80	S(1)	-	-	20	1T
	12.5	-	-	-	-	40	1T
	26	20	1T(2)	-	-	20	1T
Coaxial	6	-	-	-	-	160	S
	12.5	-	-	-	-	160	S
	26	160	S	160	S	20	1L(3)
Pentad	6	160	S	-	-	160	S
	12.5	-	-	-	-	160	S
	26	80	S	80	S	160	S

NOTES: (1) S = Stable with respect to high-frequency modes
(2) 1T = First tangential mode (approximately 4000 cps)
(3) 1L = First longitudinal mode (approximately 1100 cps)

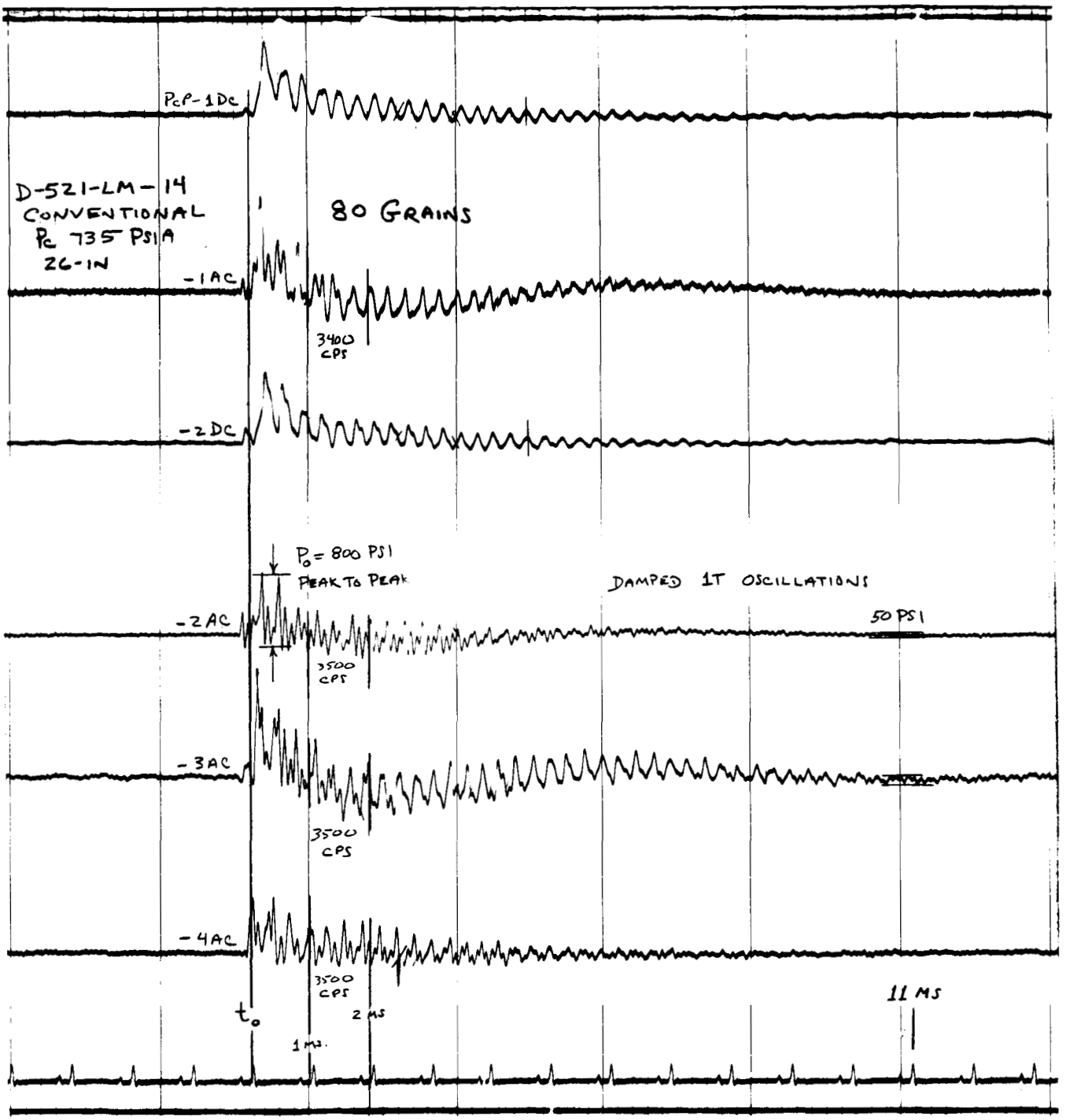

Oscillogram - D521-LM-14, Stable Run, Conventional Injector

Figure 20

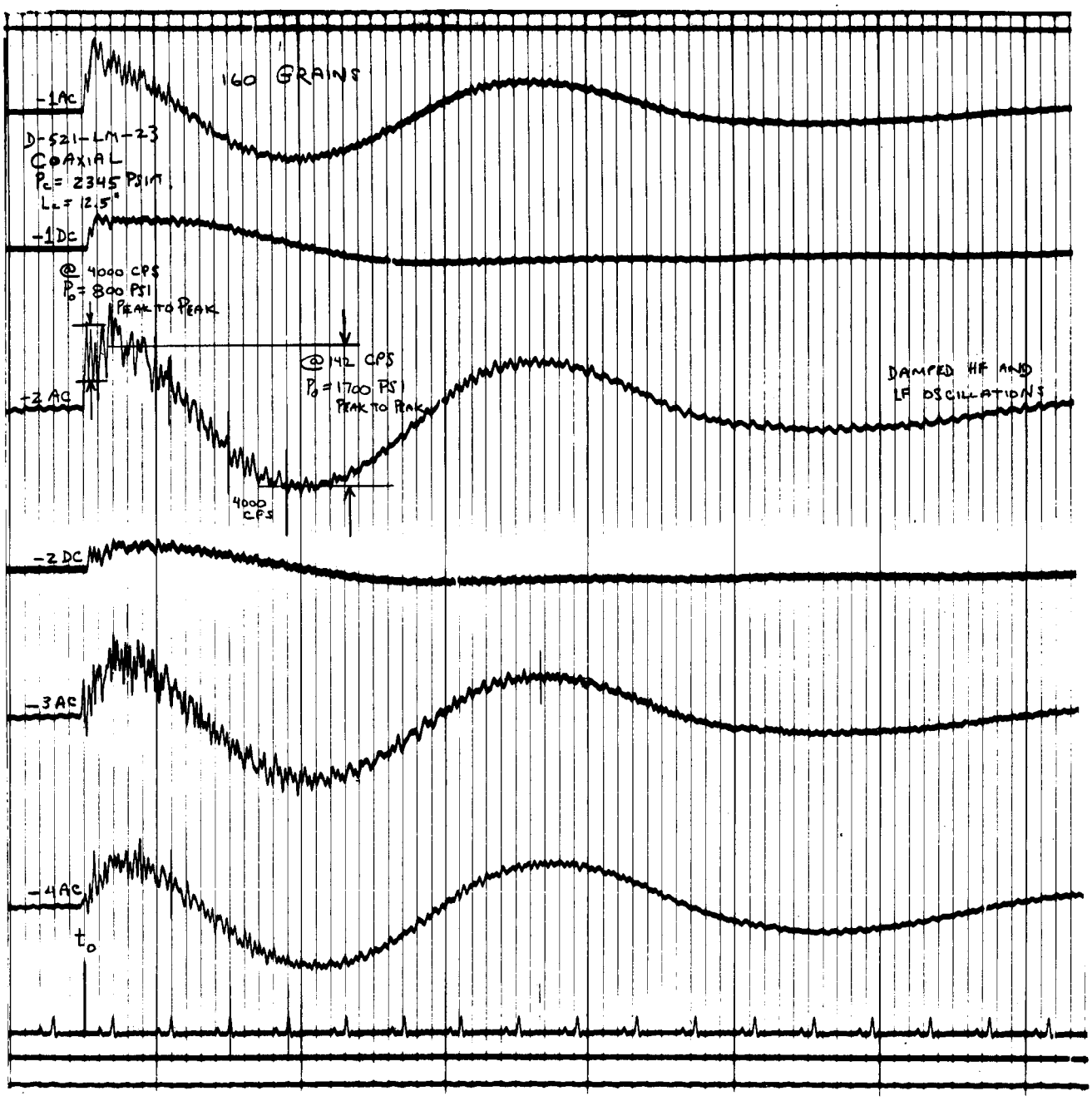

Oscillogram - D521-LM-23, Stable Run, Coaxial Injector

Figure 21

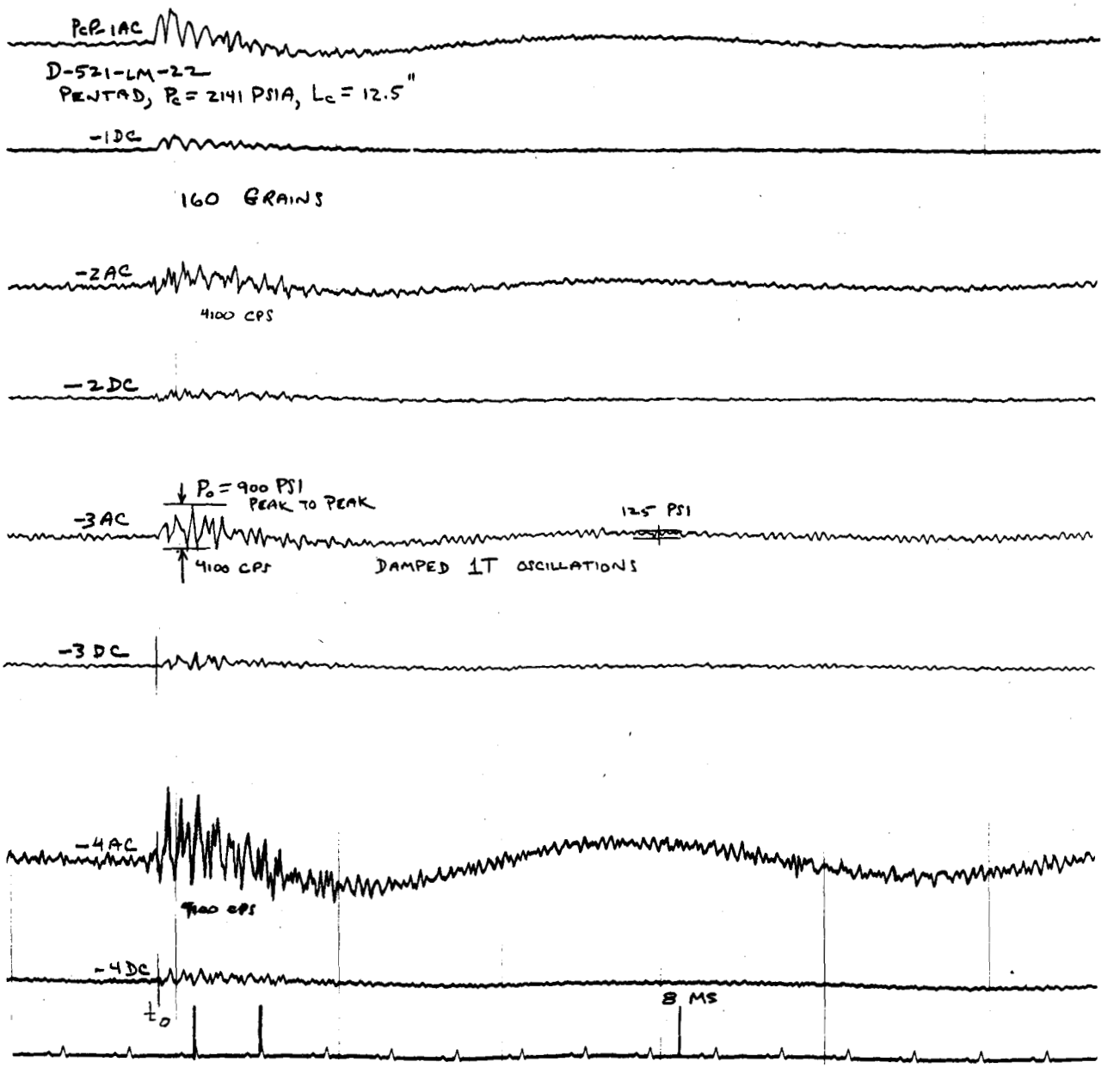

Oscillogram - D521-LM-22, Stable Run, Pentad Injector

Figure 22

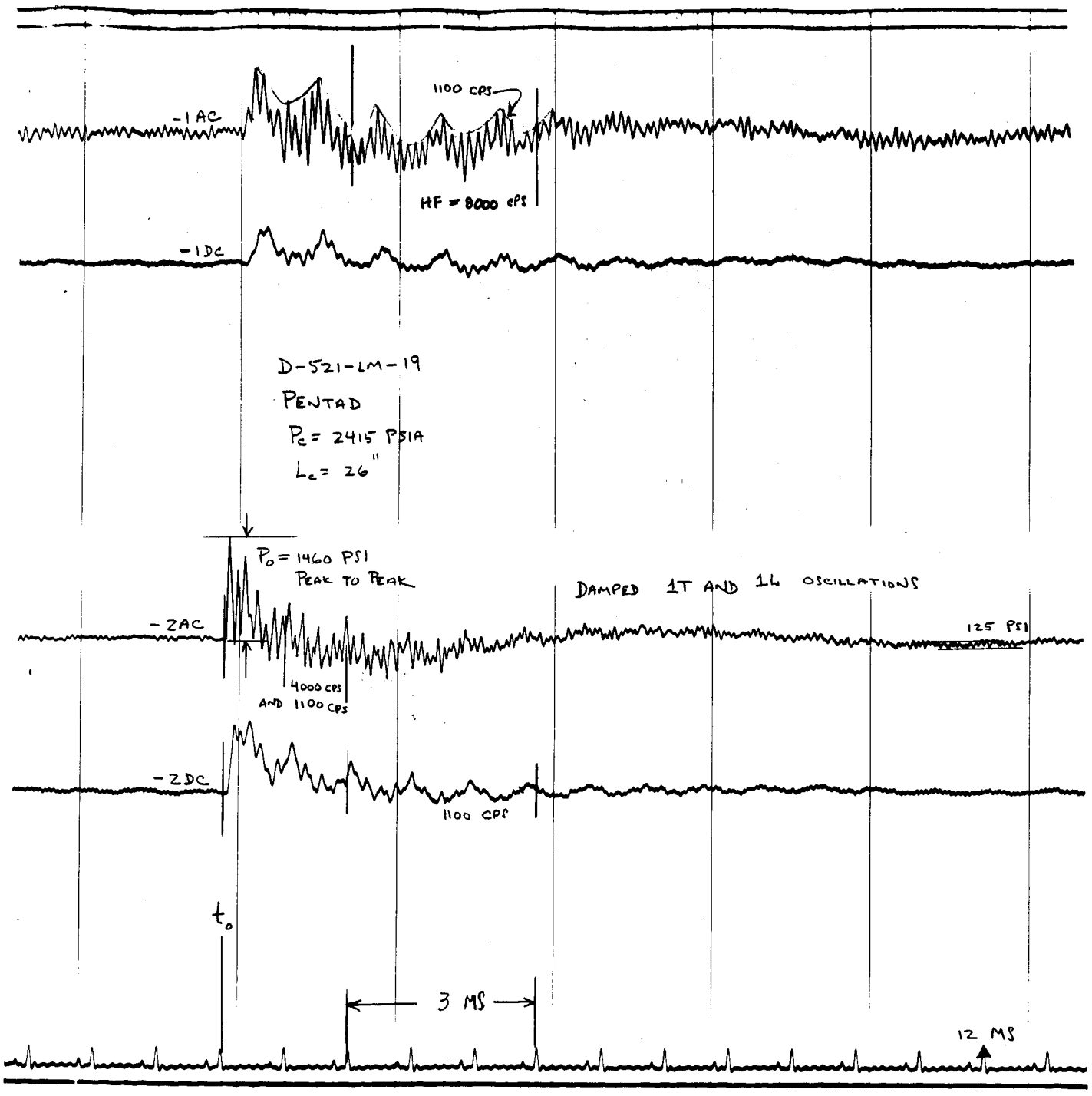

Oscillogram - D521-LM-19, Stable Run, Pentad Injector

Figure 23

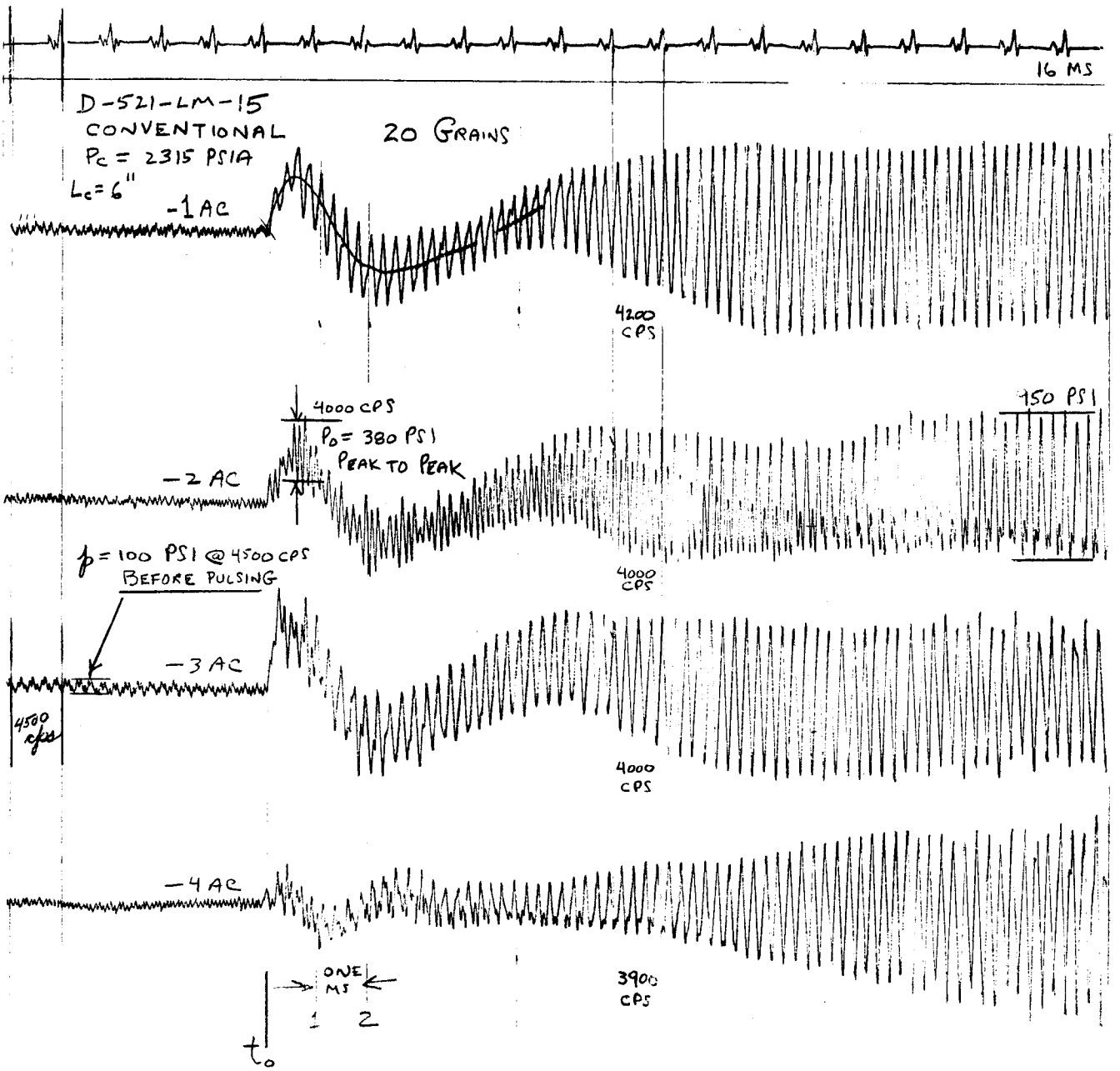

Oscillogram - D521-LM-15, Unstable Run, Conventional Injector (1T)

Figure 24

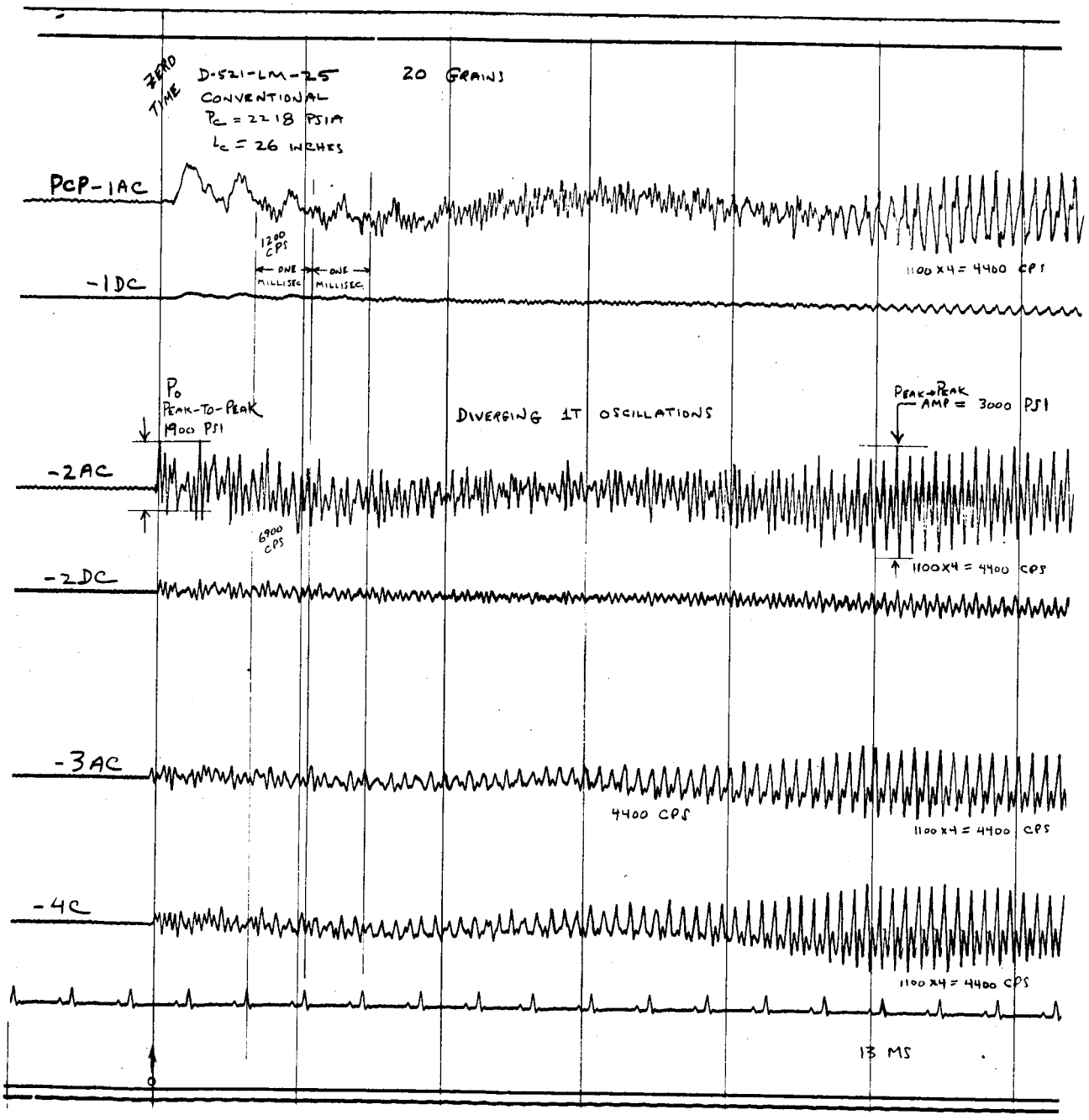

Oscillogram - D521-LM-25, Unstable Run, Conventional Injector (1T)

Figure 25

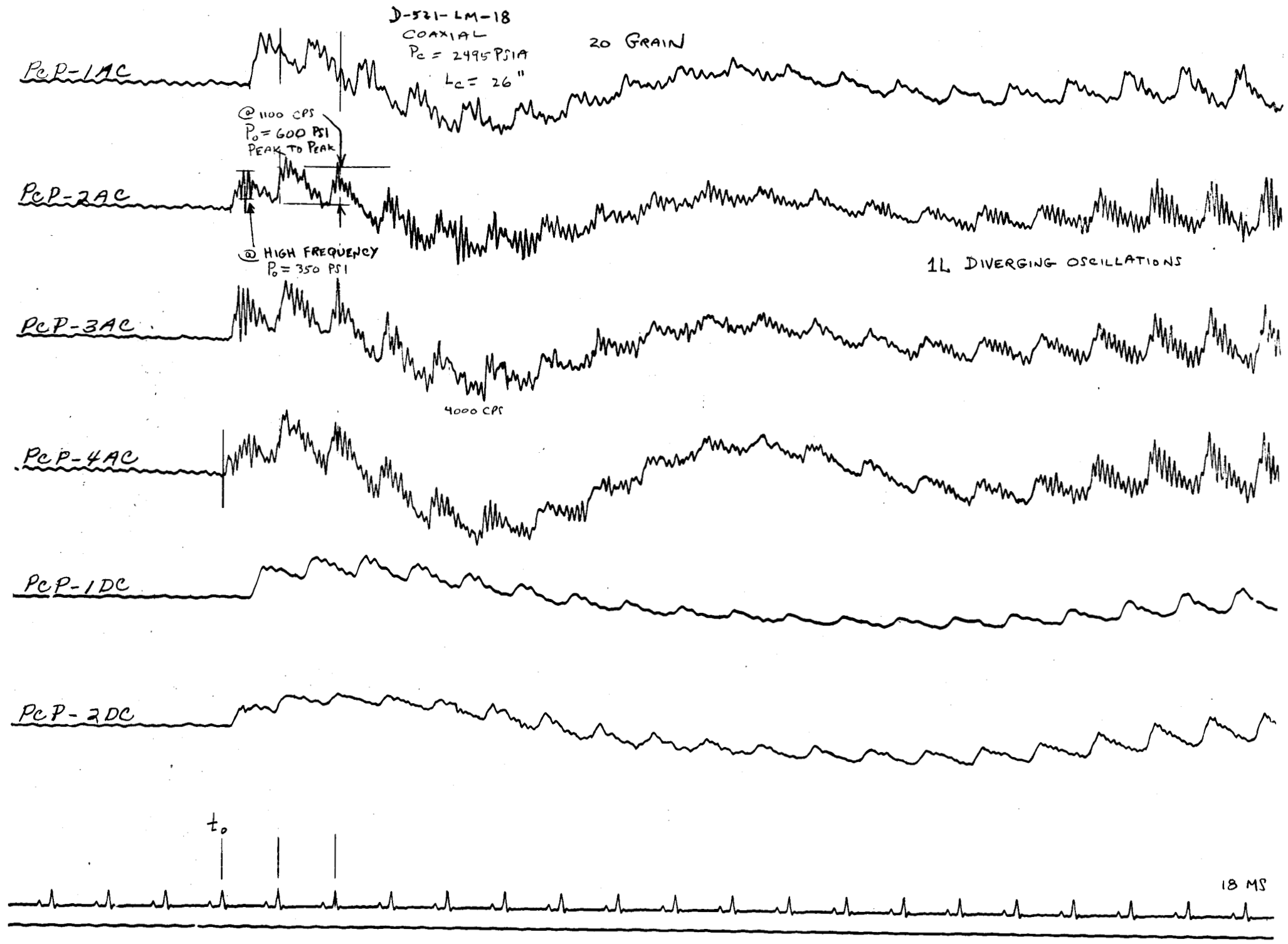

Oscillogram - D521-LM-18, Unstable Run, Coaxial Injector (1L)

Figure 26

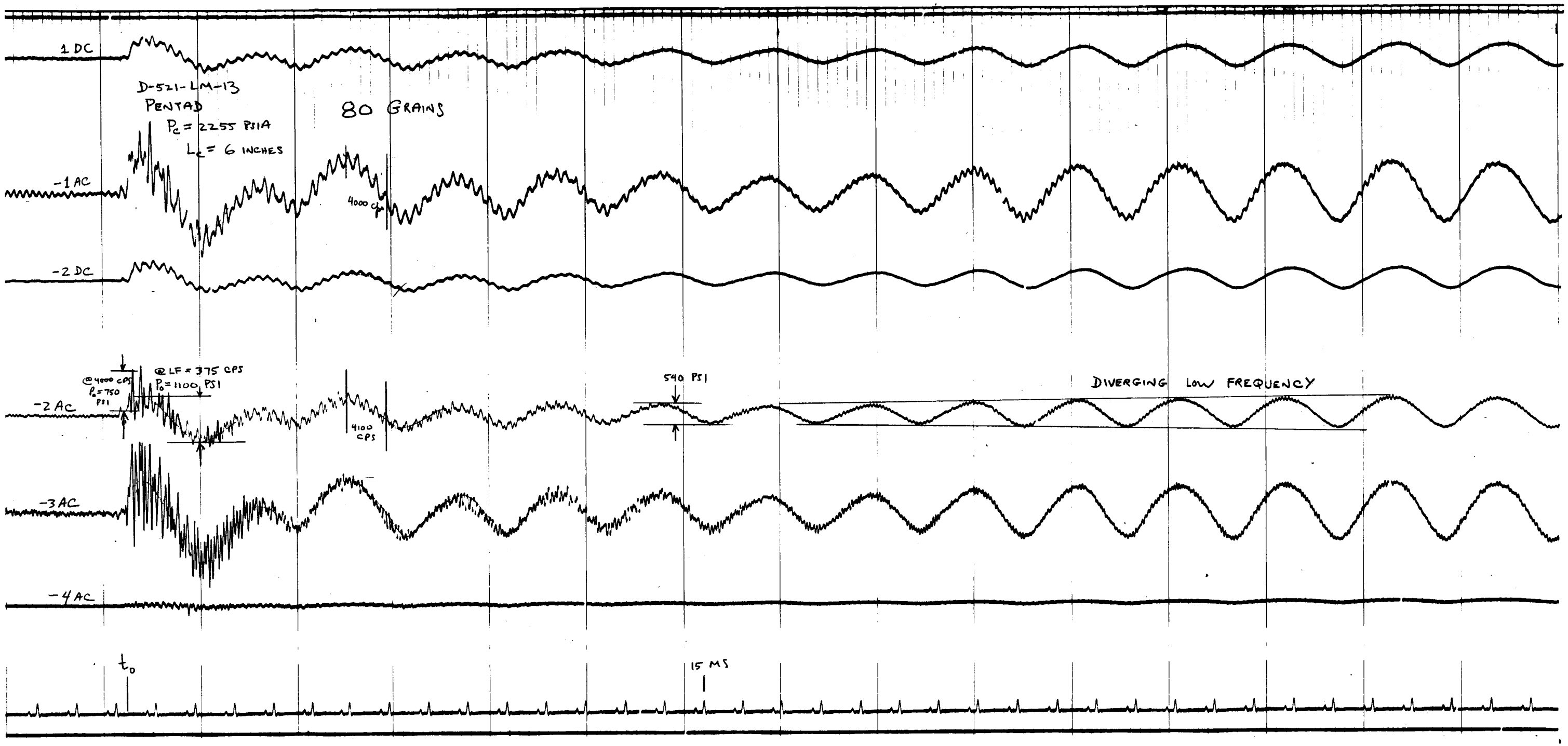

Oscillogram - D521-LM-13, Unstable Run, Pentad Injector (LF)

Figure 27

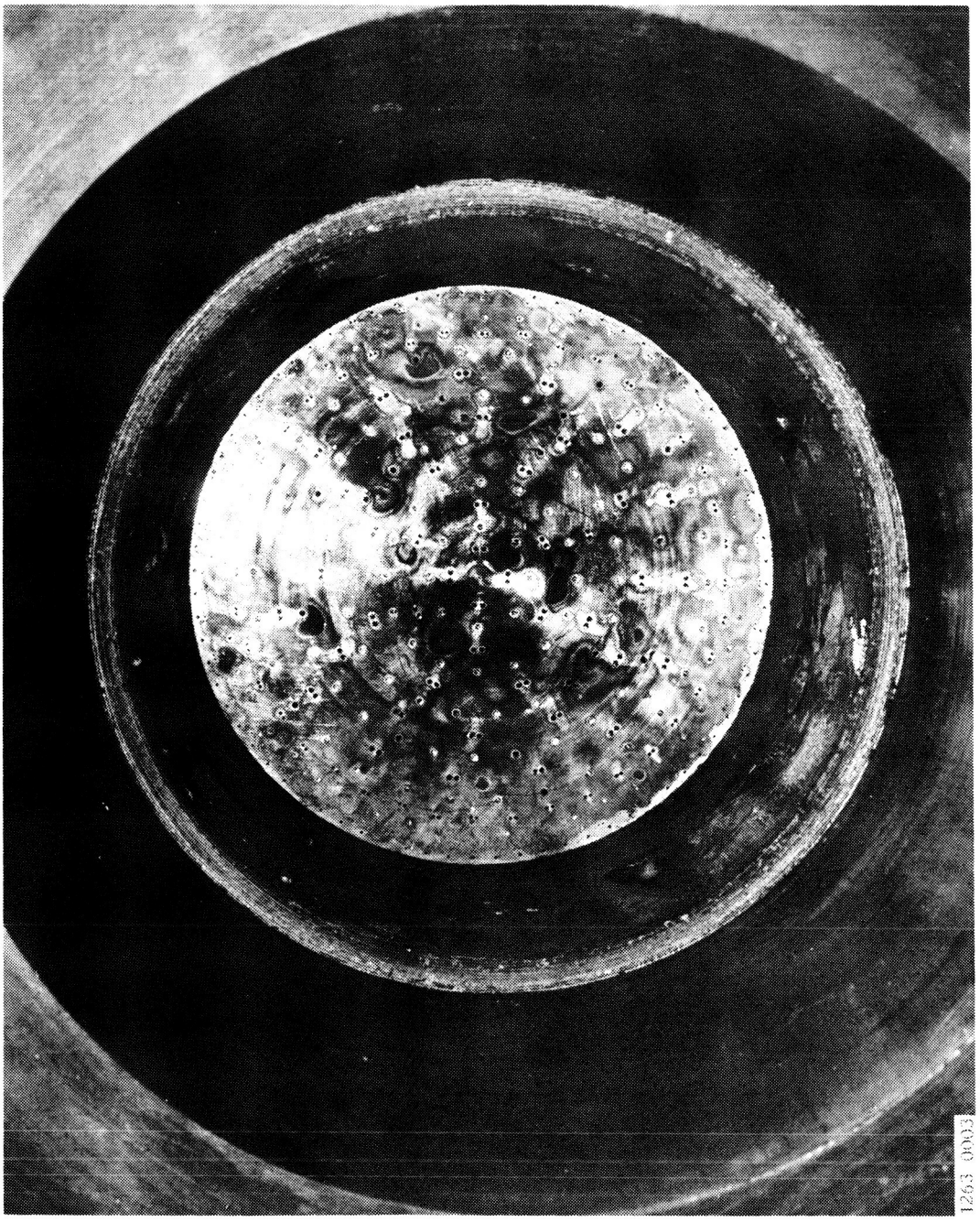

Conventional Injector After Test D521-LM-14

Figure 28

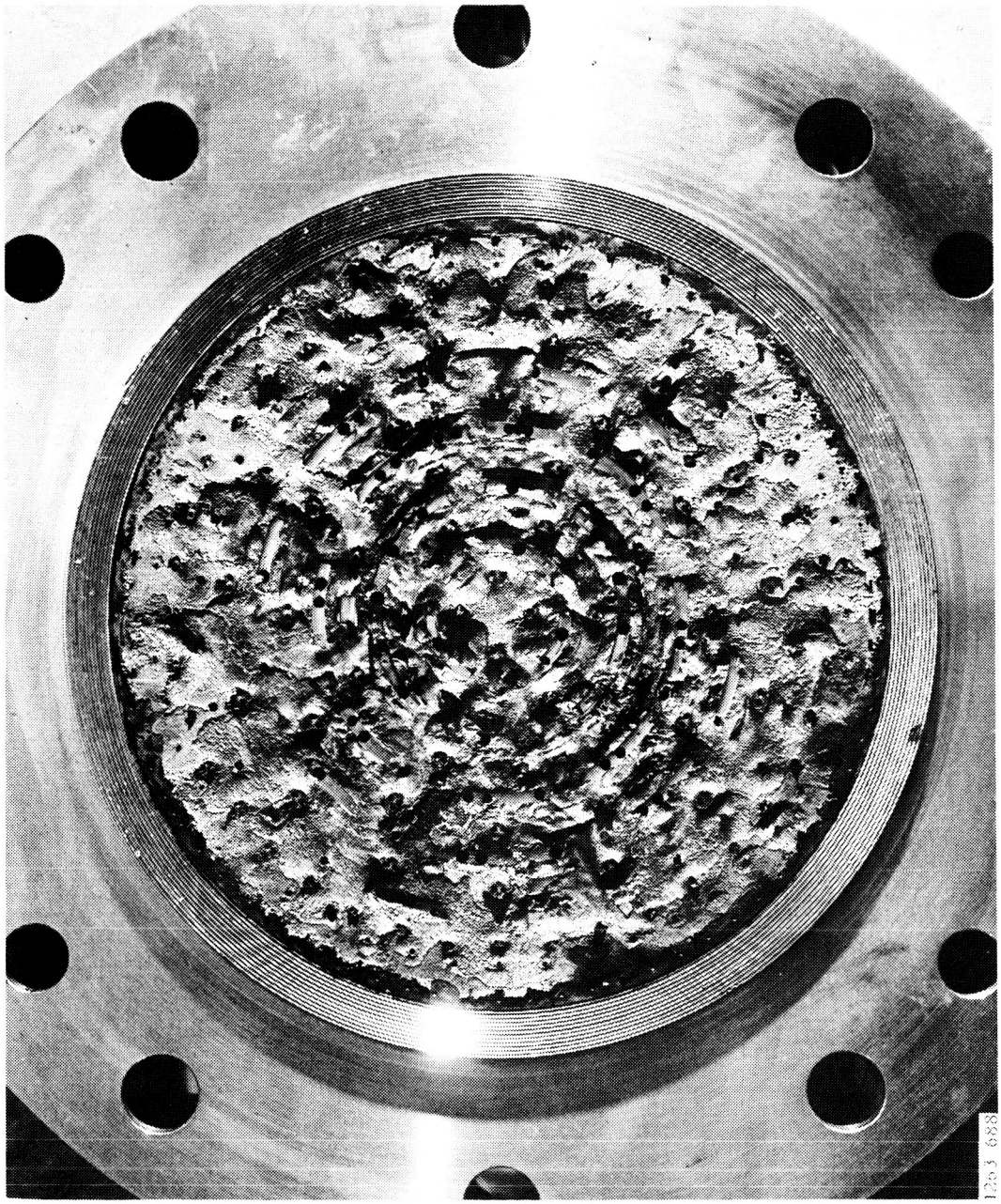

Damage to Conventional Injector After Test D521-LM-15

Figure 29

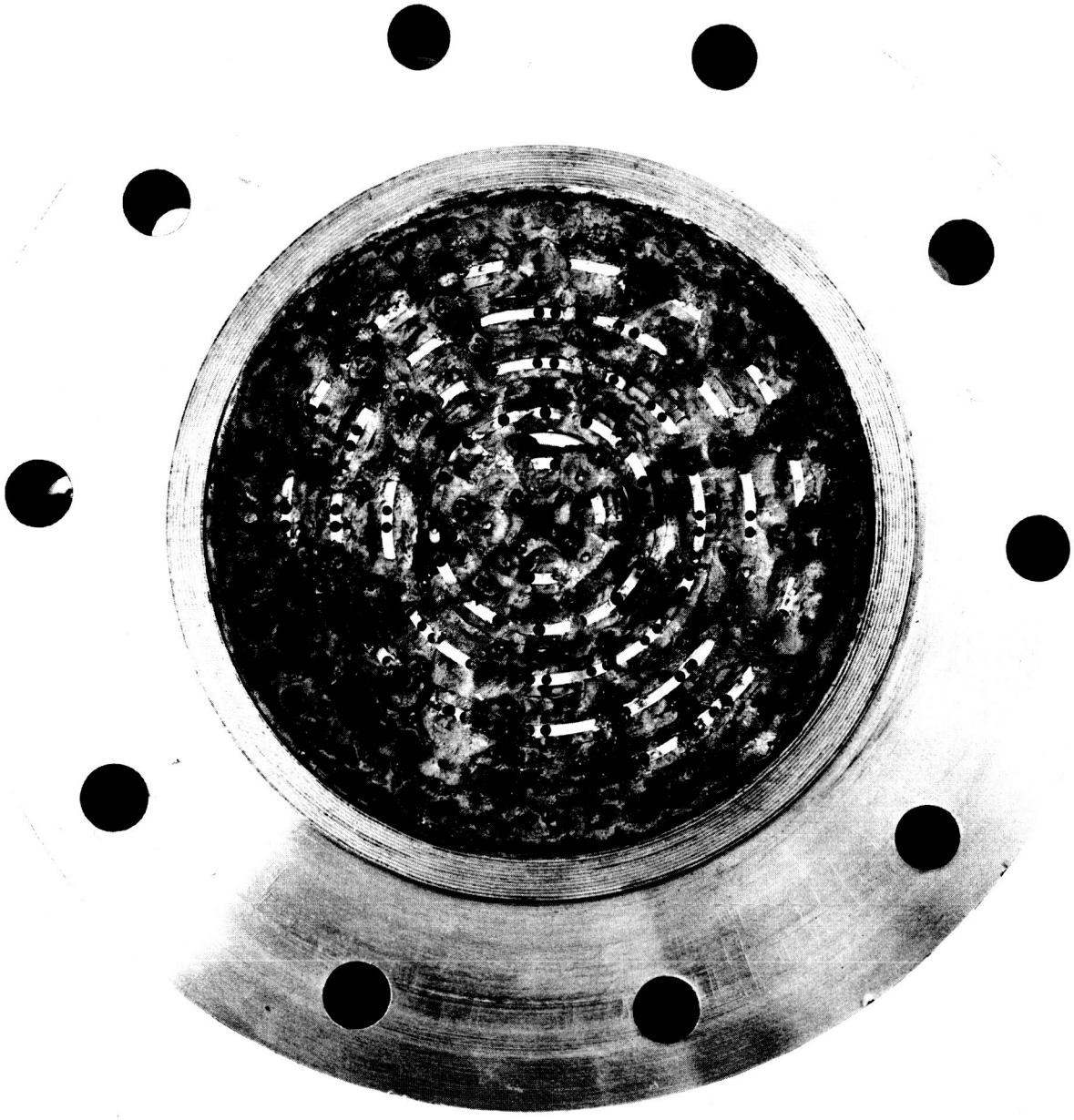

Damage to Conventional Injector After Test D521-LM-5

Figure 30

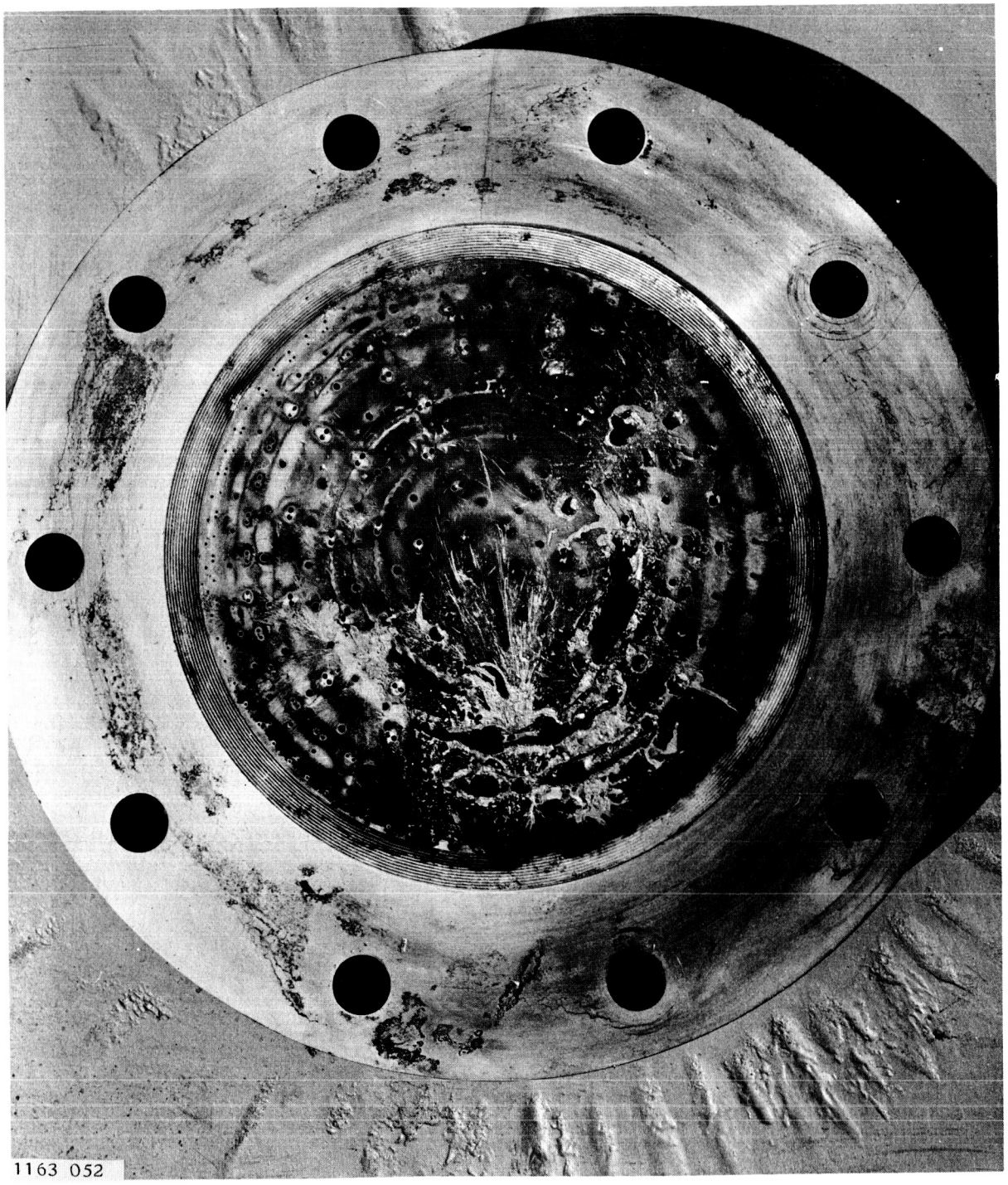

Damage to Conventional Injector After Test D521-LM-10

Figure 31

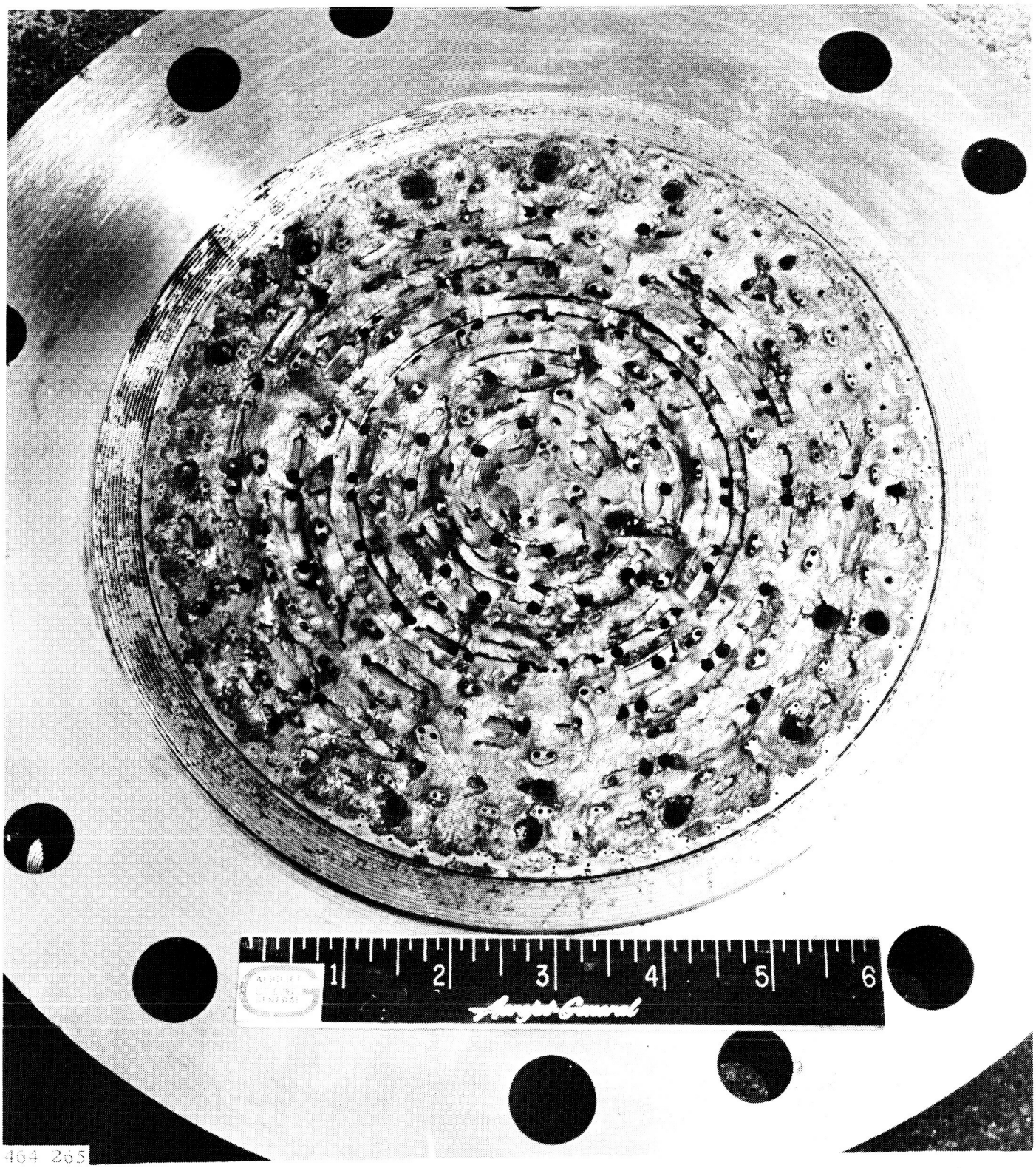

Damage to Conventional Injector After Test D521-LM-25

Figure 32

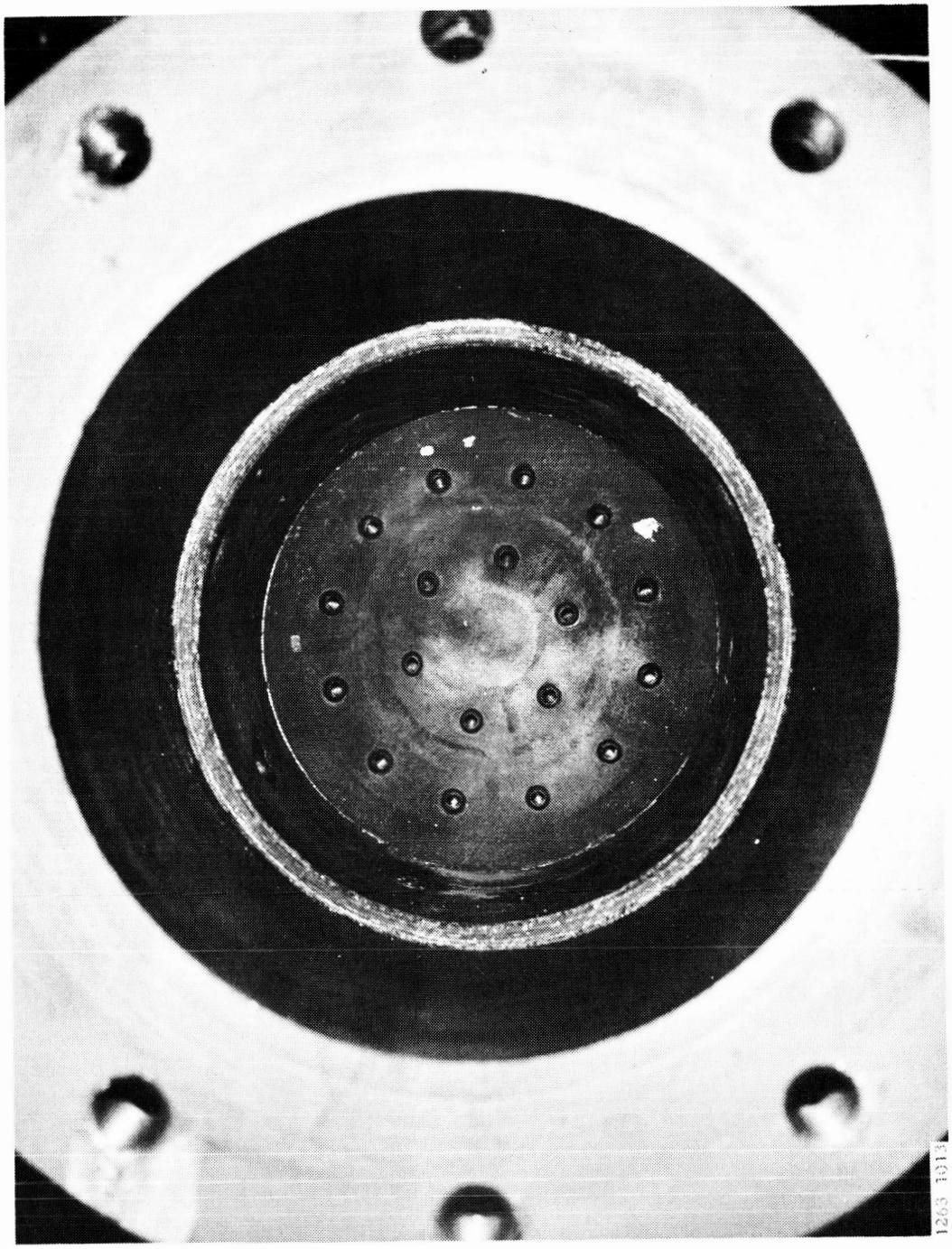

Coaxial Injector After Test D521-LM-17

Figure 33

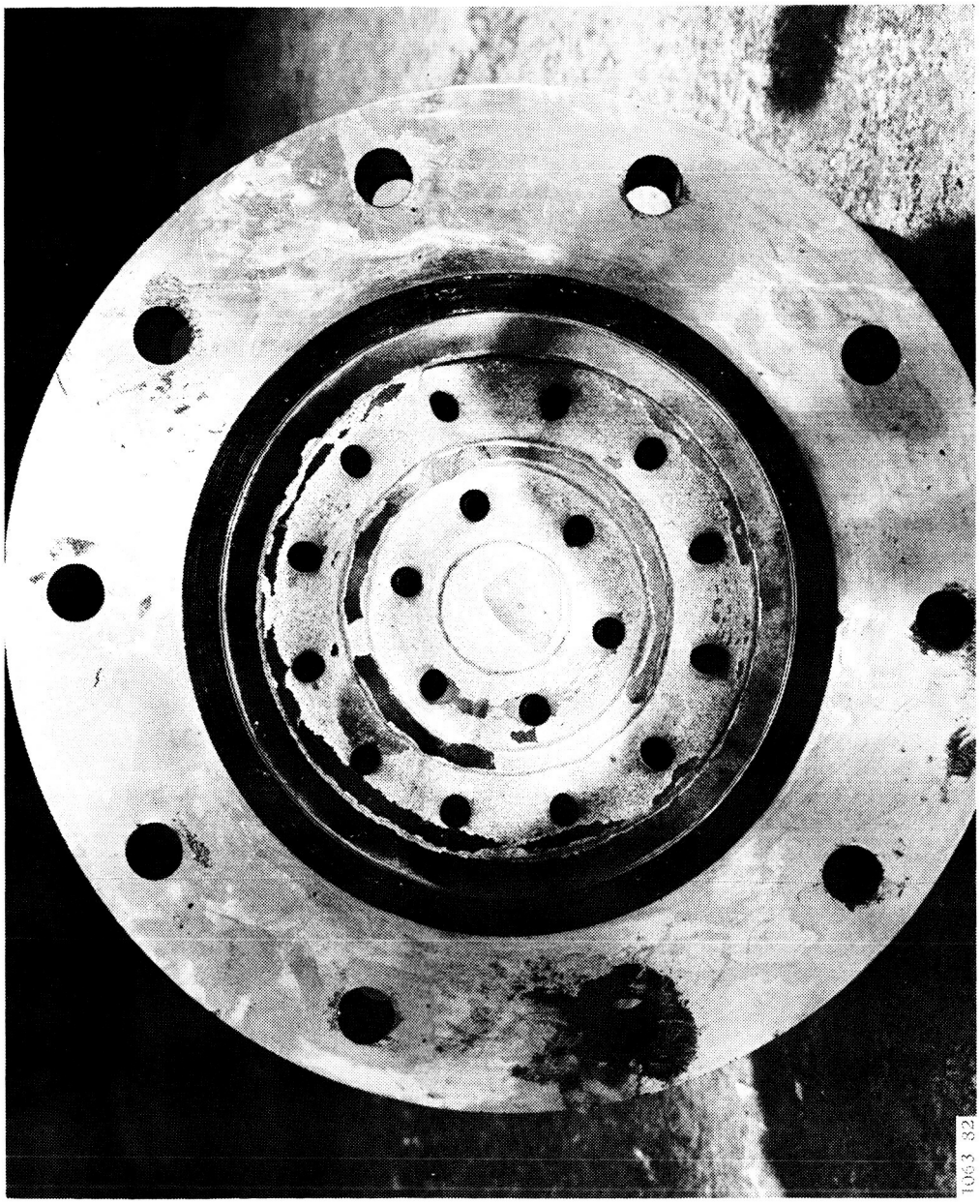

Damage to Coaxial Injector After Test D521-LM-8

Figure 34

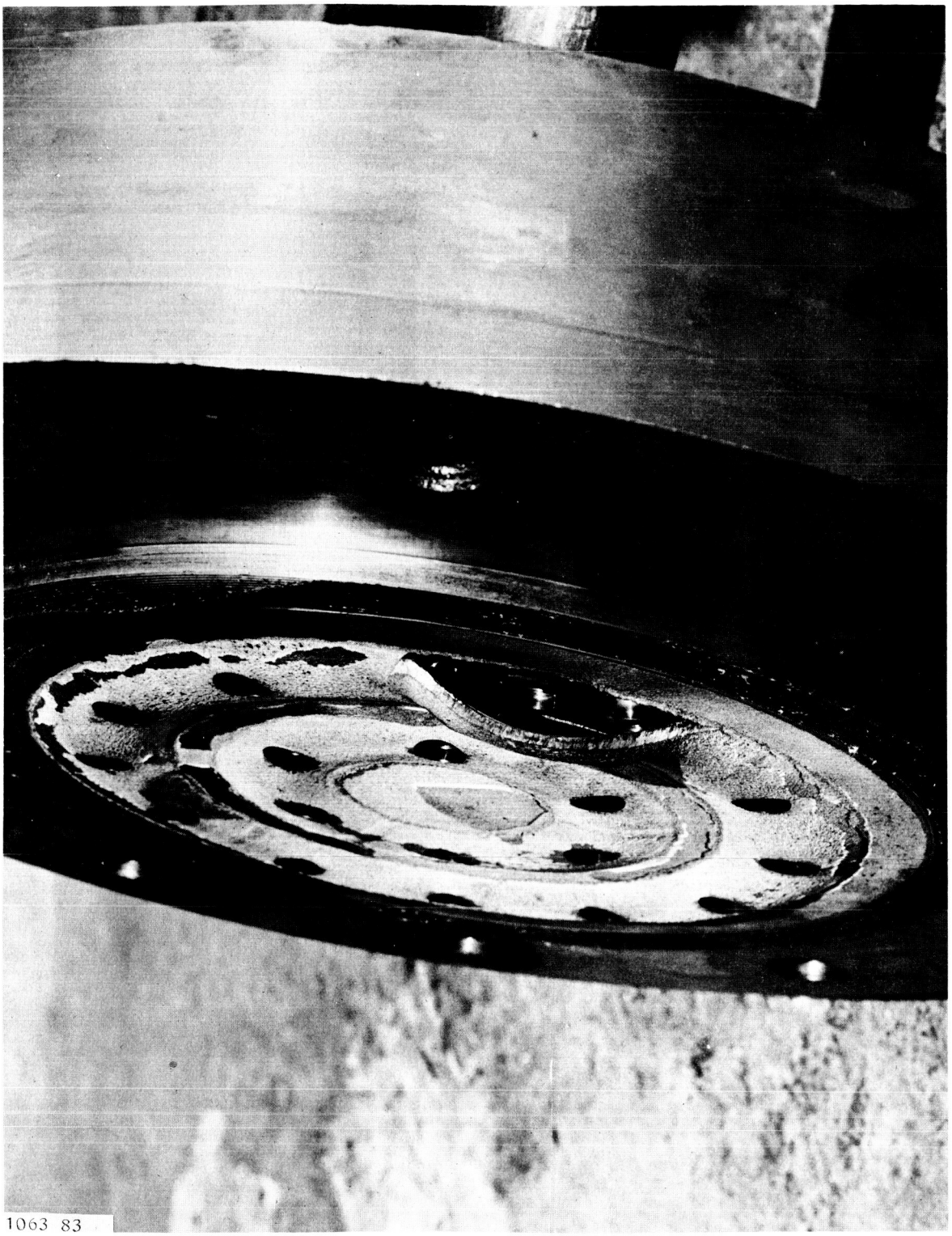

Damage to Coaxial Injector After Test D521-LM-8

Figure 35

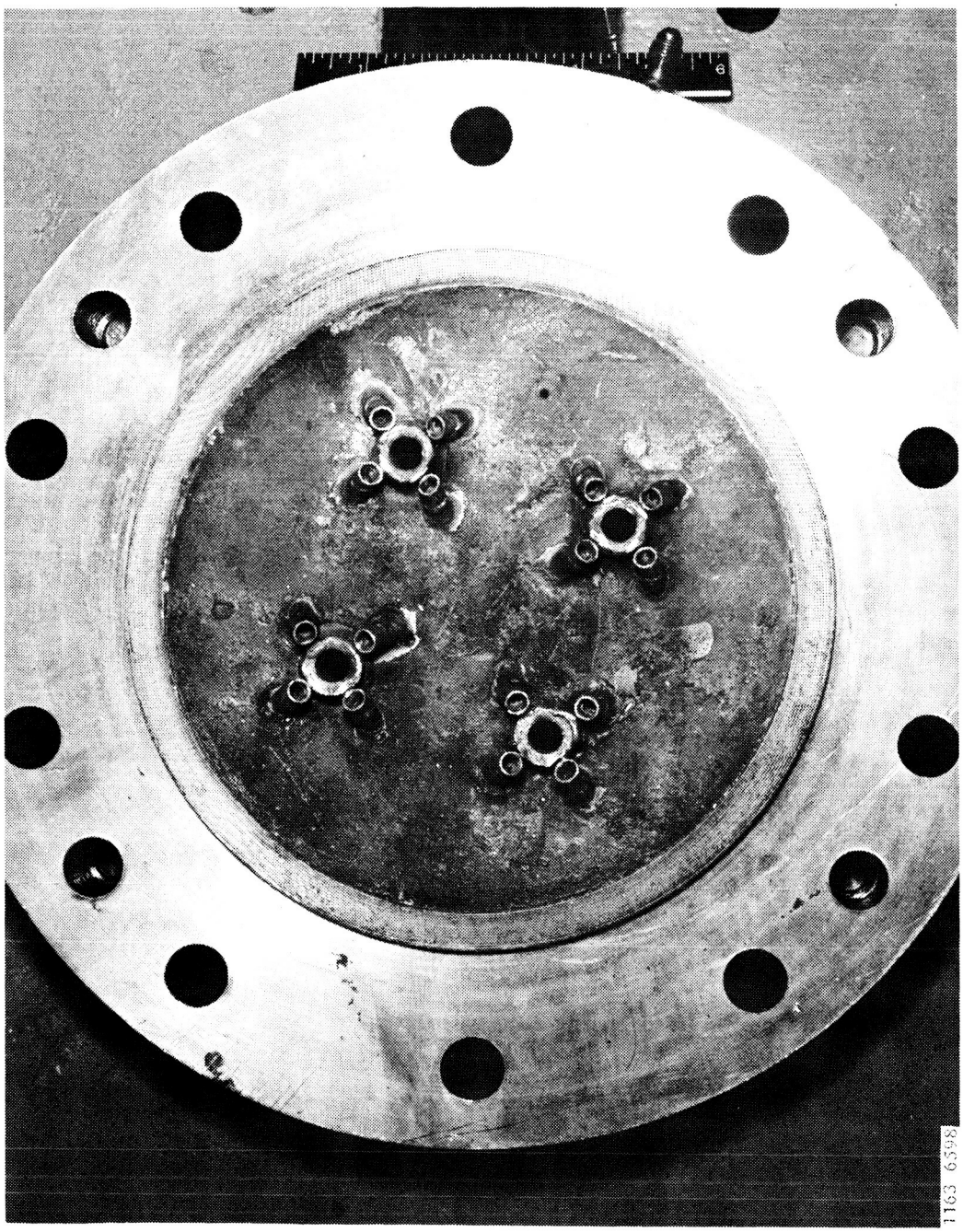

Pentad Injector After Test D521-LM-13

Figure 36

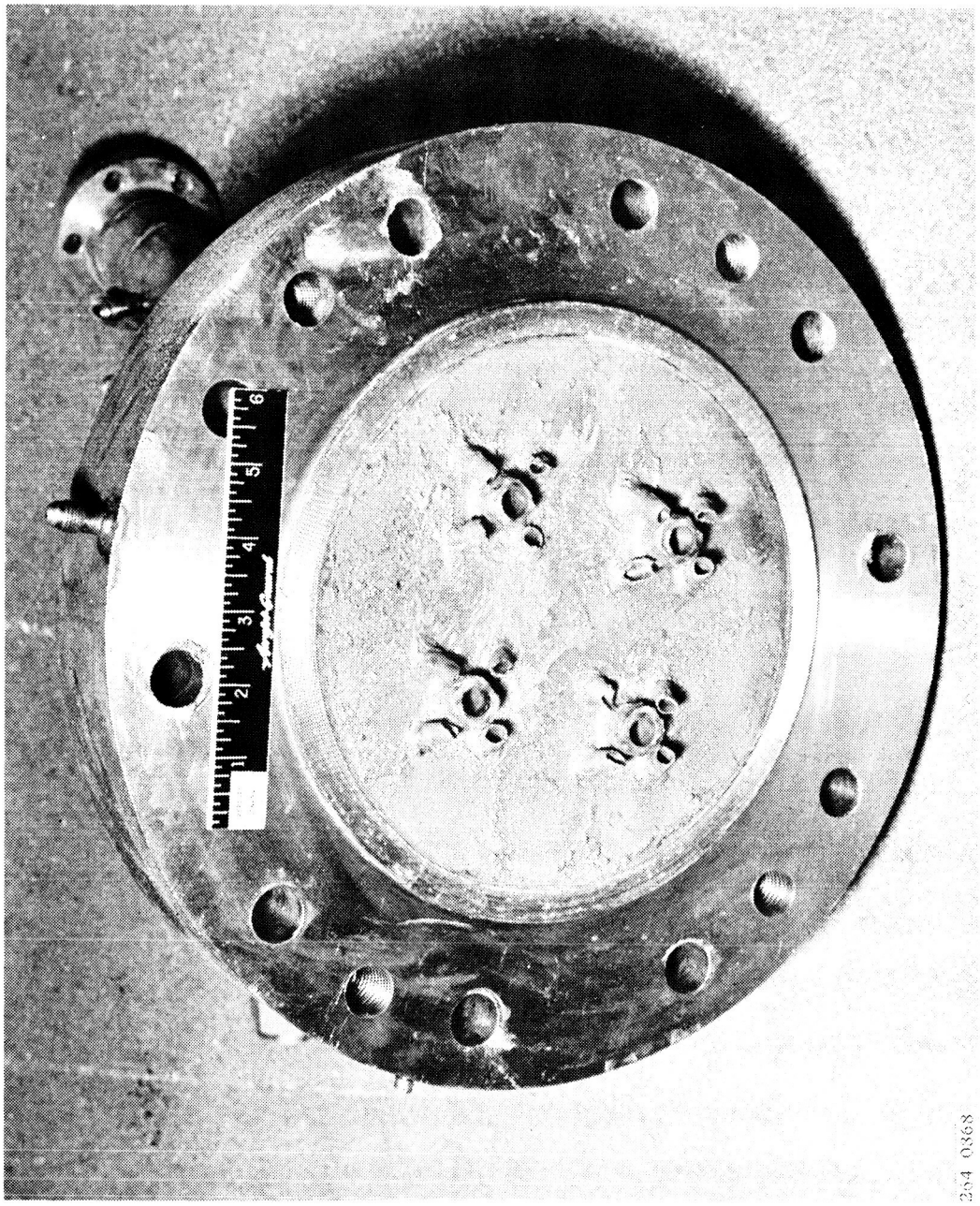

Damage to Pentad Injector After Test D521-LM-22

Figure 37

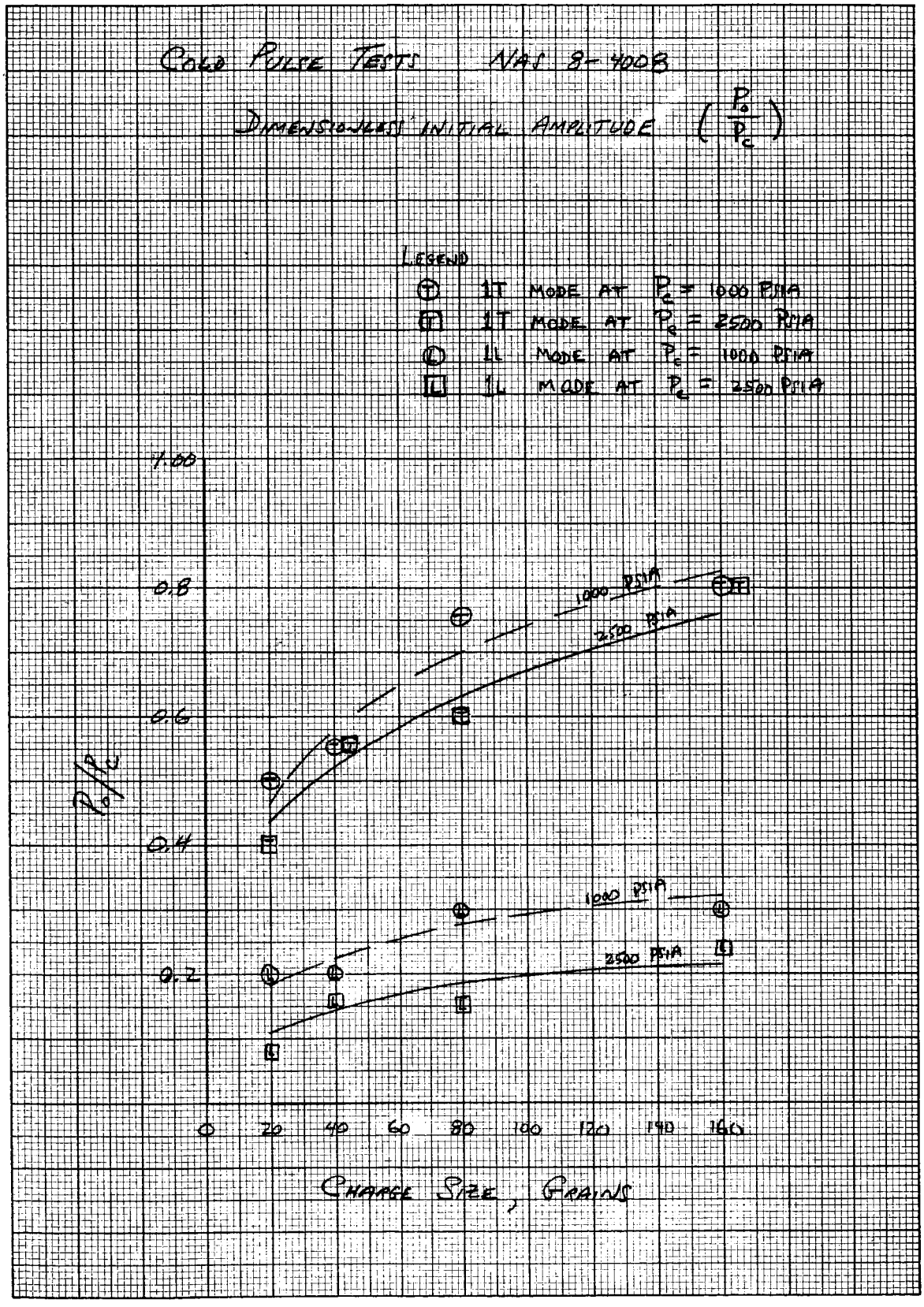

"Cold Pulse" Calibrations

Figure 38

IV, Accomplishments (cont.)

F. STABILITY PARAMETERS

Values of the stability parameters (the interaction index, η, and the sensitive time lag, τ) can be deduced by comparing the observed stability behavior for each test with the theoretical instability zones in the η, τ plane calculated by means of the Sensitive Time Lag Theory. At present, the treatment of nonlinear, or pulsed, instability is necessarily qualitative. Testing with fixed hardware also limits the precision of the stability parameter results.

The deduction of η, τ values is based upon the following principles: If a given mode is observed to occur spontaneously, the η, τ operating point must be inside of the corresponding instability zone (Figure 39). If a given mode is not observed, the point must be outside of the zone. However, if the given mode occurs as the result of a pulse, the η, τ points must lie outside of, but near to, the zone of instability. The distance of the η, τ point from the instability zone is proportional to the magnitude of the pulse causing the instability. In this regard, it is necessary to use the measured pressure perturbation rather than the size of the charge used.

Table 2 lists the pertinent stability data for the current program. The theoretical instability zones for the tangential and longitudinal modes are shown in Figures 40, 41, and 42. For the exhaust nozzle used, the calculations show little effect of chamber length on the tangential modes of instability.

Five of the six conventional injector tests were pulsed to instability in the first tangential mode. Since this was the only mode observed, the value of the sensitive time lag can be set only between the limits 0.08 and 0.12 msec. The lack of spontaneous instability implies that the interaction index is less than 1.1. The effect of chamber pressure is apparent because a pulse with a peak-to-peak amplitude of 16% of the mean chamber pressure triggered an instability at 2315 psia (Test D-521-LM-15), but pulses up to 109% did not result in instability

IV, F, Stability Parameters (cont.)

at 735 psia (Test D-521-LM-14). This result may also be caused by operation at off-design mixture ratio, since Crocco, Grey, and Harrje (Ref 2) report that η decreases and τ increases for mixture ratios different from design. For the conventional injector at 1000 psia (nominal), the values of η and τ may be estimated as

$$0.8 < \eta < 1.0$$
$$0.008 < \tau < 0.12 \text{ msec;}$$

and at 2500 psia (nominal)

$$0.9 < \eta < 1.1$$
$$0.08 < \tau < 0.12 \text{ msec.}$$

Two of the six coaxial injector tests showed high-frequency instability in the first longitudinal mode. These instabilities occurred only when using the 26-in.-length chamber. Both unstable tests occurred at the nominal 2500 psia level although their mixture ratios differed by 49%. Test D-521-LM-8 was performed at a mixture ratio of 3.2, whereas Test D-521-LM-18 was performed near the design mixture ratio point at 6.3. The corresponding tests performed with the 26-in.-length chamber at the nominal pressures of 1500 and 1000 psia showed progressively faster attenuation of the longitudinal pressure oscillations as the pressure level decreased. It was concluded that the coaxial injector was pressure-sensitive to the first longitudinal mode of instability at the 26-in.-chamber length. The tests performed at 2500 psia with the 12.5- and 6-in. chamber lengths were devoid of the longitudinal mode; therefore, the η, τ values estimated for the coaxial injector are

$$0.5 < \eta < 0.8$$
$$0.18 < \tau < 0.35 \text{ msec.}$$

No high frequency instability was observed with the pentad injector, even with pulses up to 65% of mean chamber pressure. At 2255 psia chamber pressure, a 65% pulse failed to produce a first tangential mode with the pentad ejector, although a 16% pulse produced a first tangential mode with the conventional

IV, F, Stability Parameters (cont.)

injector. This result implies there is a smaller η or larger τ, or both, for the pentad injector as compared with the conventional injector. This agrees with the trends shown in Figure 23. Approximate values for η and τ may be estimated as

$$0.5 < \eta < 0.8$$
$$0.07 < \tau < 0.18 \text{ msec.}$$

In general, the results of the present program are in agreement with trends observed previously and reported in Ref 5. Figure 43 shows the stability parameters (interaction index, η, and sensitive time lag, τ) correlated with injector element size (thrust-per-element) and chamber pressure. The basic trends shown by this correlation are that, for a given chamber pressure, the sensitive time lag increases and the interaction index decreases with increasing element size. For a given size of injector element, increasing the pressure results in an increase in the interaction index and a decrease in the sensitive time lag. Previous data did not show a significant effect for element type. The present results indicate that there is a definite influence of the type of injection pattern upon the stability parameters. Although it is not possible on the basis of the present data to make definitive statements about this effect, it appears that, for a given injector element size and chamber pressure, the progression of injector types from coaxial to conventional to pentad results in a decreasing sensitive time lag. Corresponding conclusions concerning the interaction index cannot be clearly drawn.

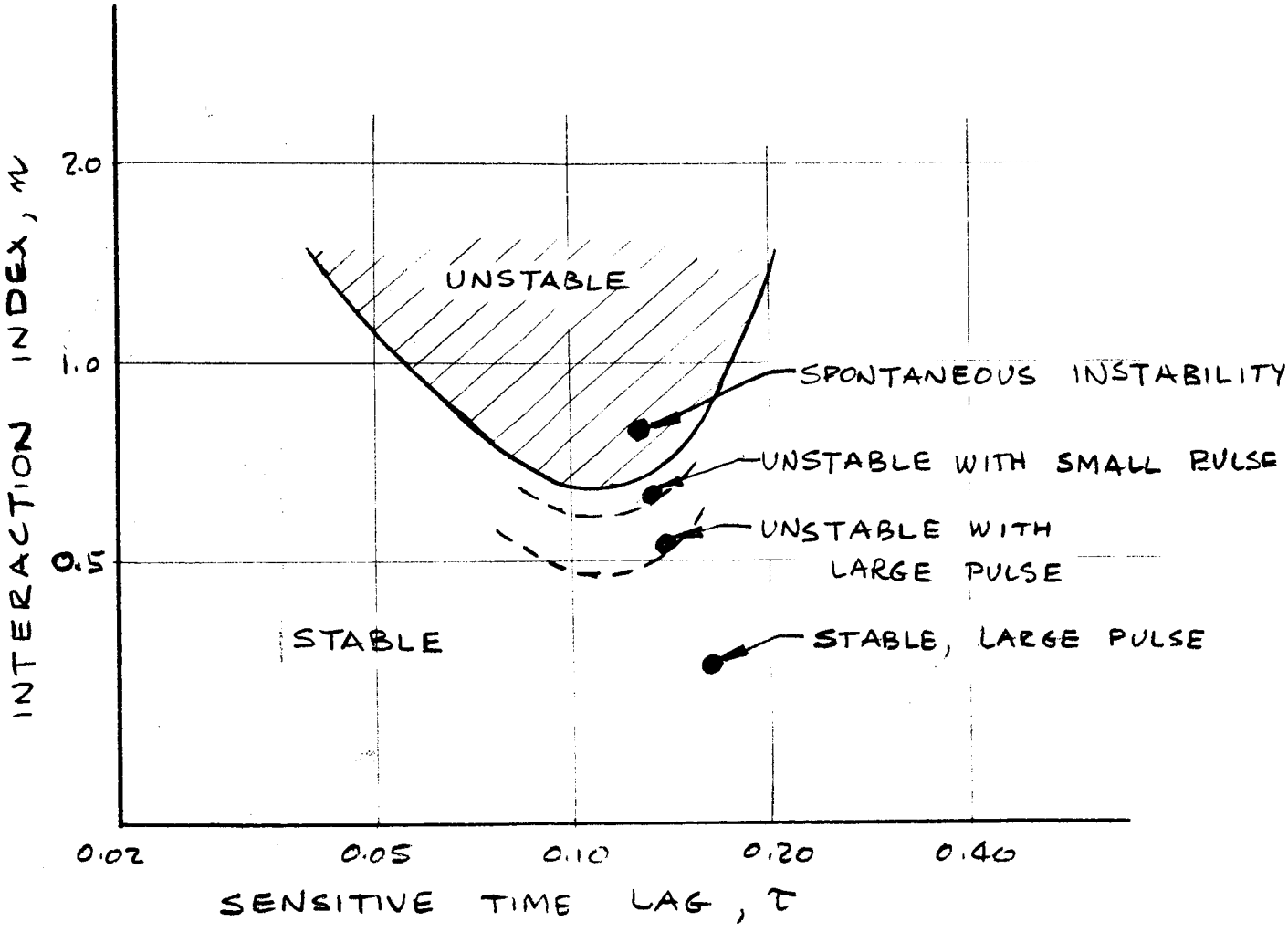

Typical Instability Zone for a Given Mode and Combustor Configuration

Figure 39

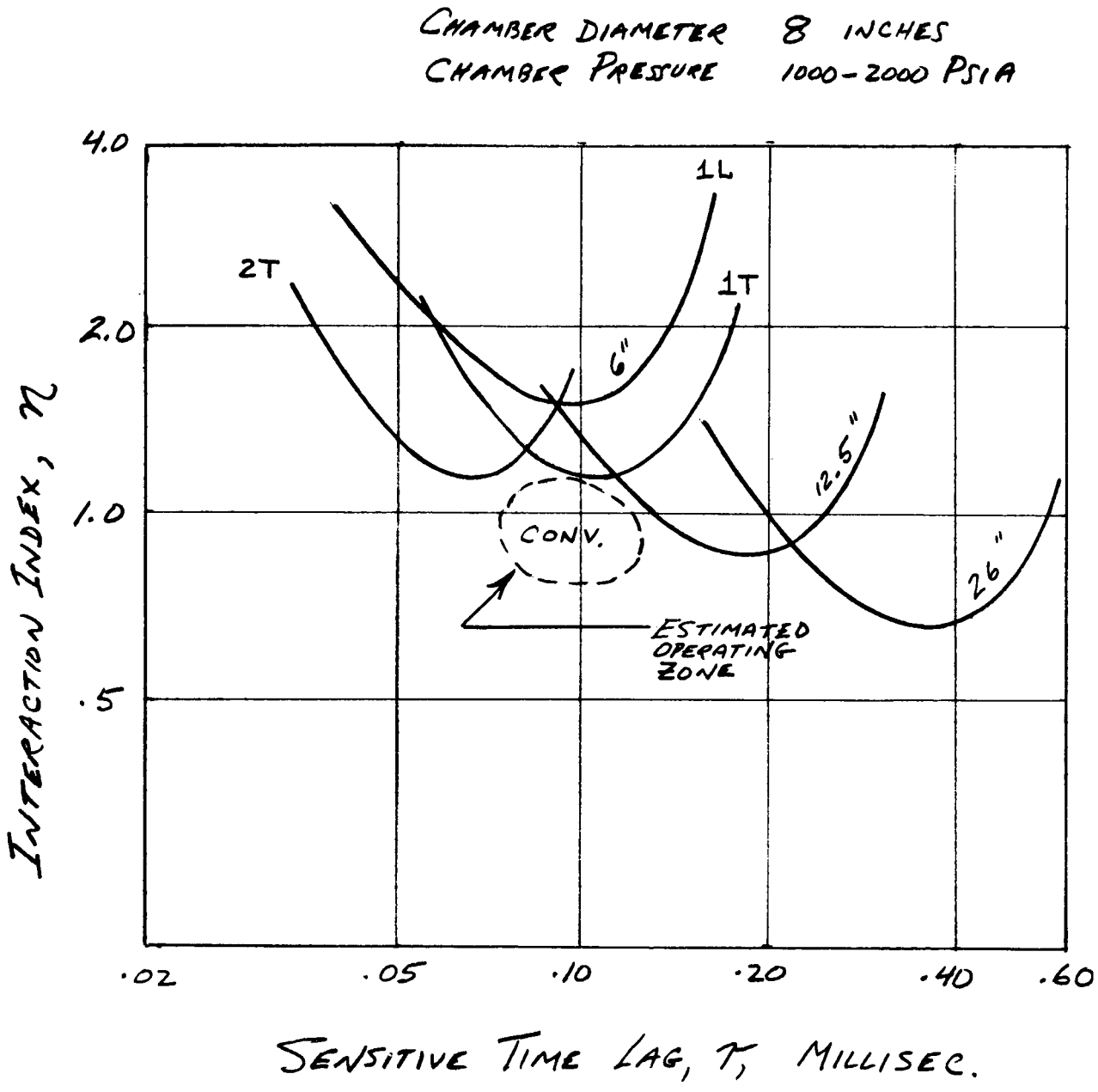

Instability Zones and Estimated Operating Point of Conventional Injector

Figure 40

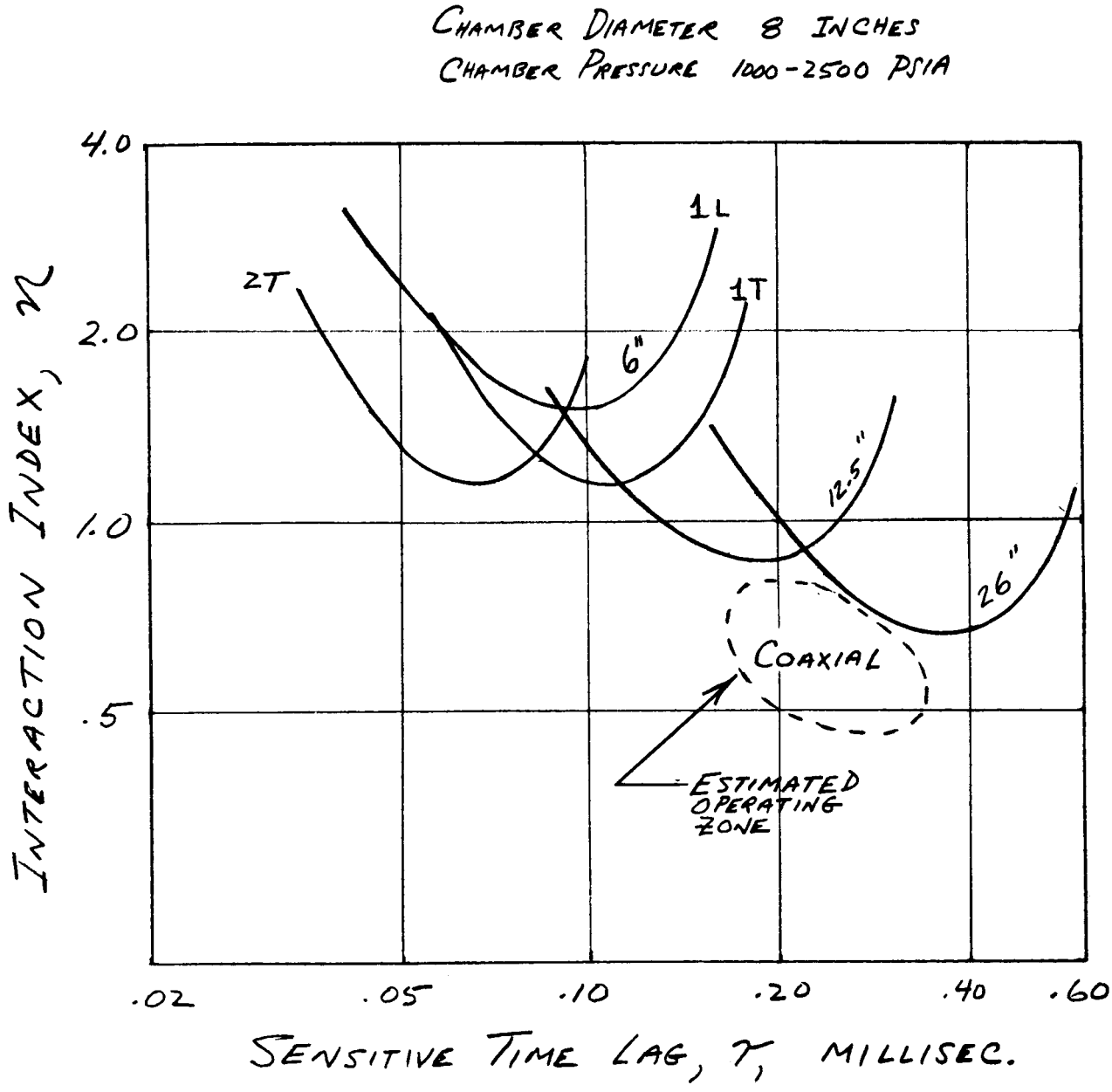

Instability Zones and Estimated Operating Point of Coaxial Injector

Figure 41

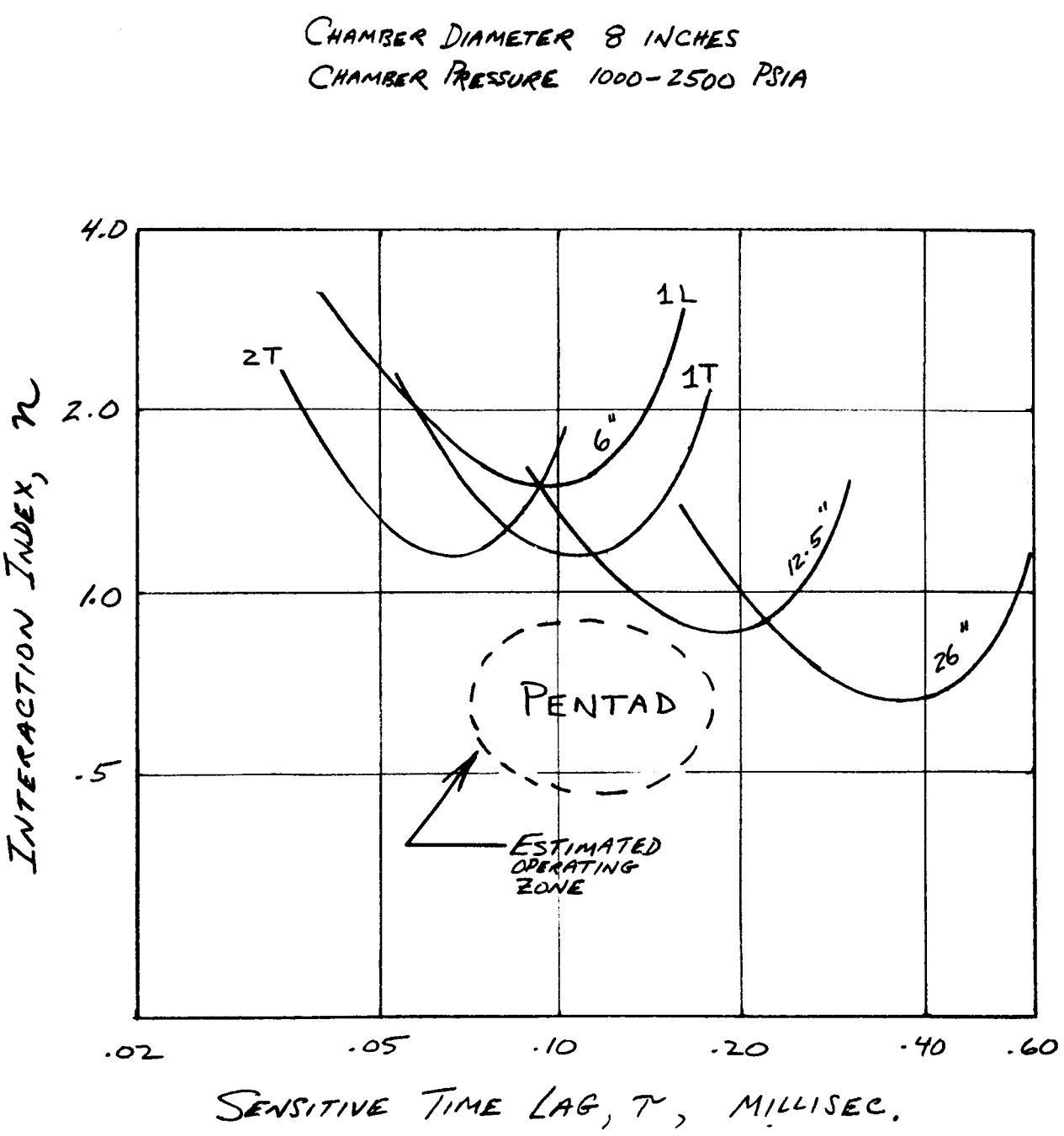

Instability Zones and Estimated Operating Point of Pentad Injector

Figure 42

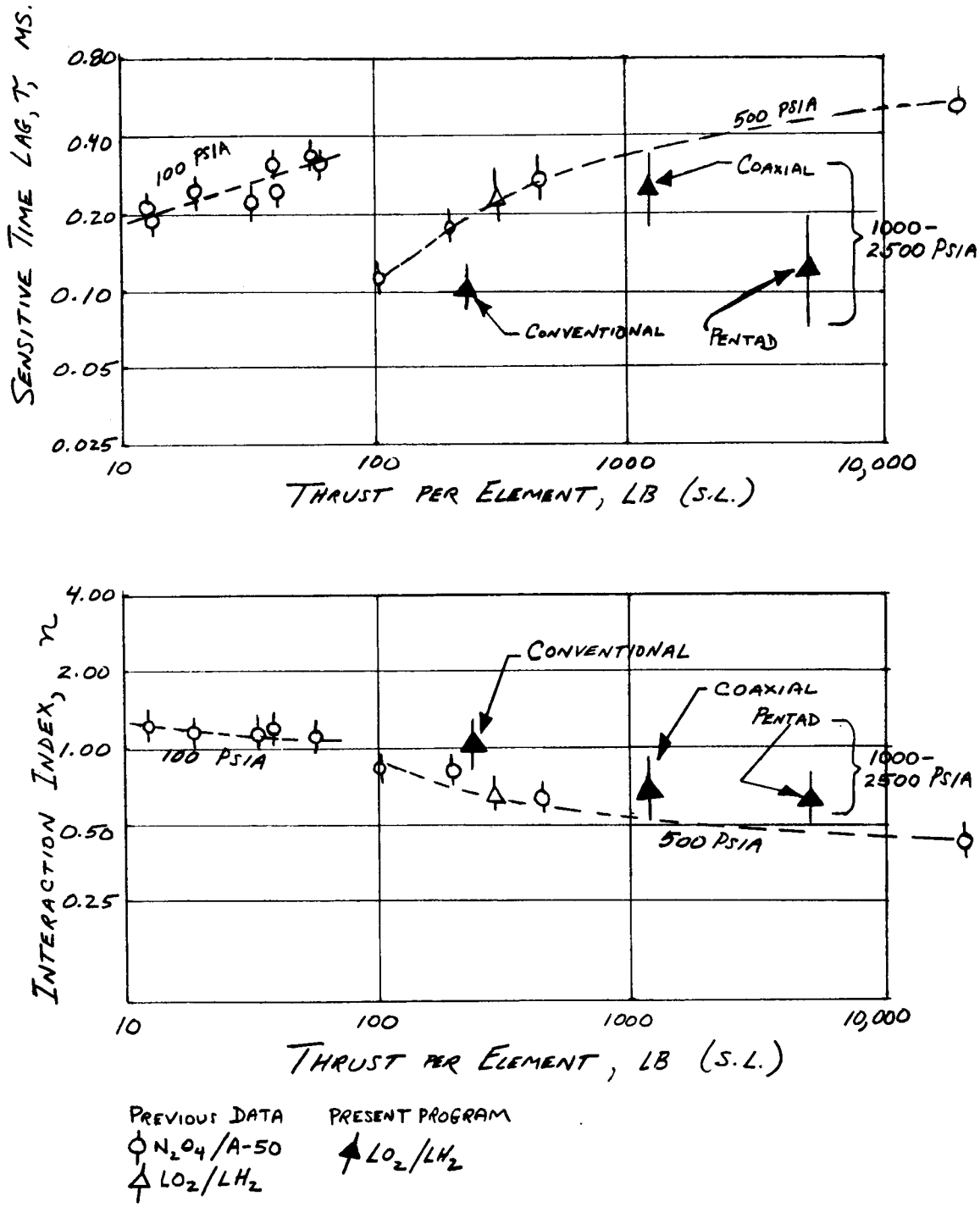

Correlation of Stability Parameters

Figure 43

IV. Accomplishments (cont.)

G. EXPERIMENTAL TEST PERFORMANCE

The most suitable method of determining rocket engine performance is that of determining the characteristic velocity, c*. From the definition

$$c^* = P_c A_t \frac{g}{\dot{w}},$$

it is evident that this criterion is independent of thrust level, and therefore, back pressure and area ratio. The characteristic velocity is essentially a measure of the success of conversion of chemical energy. From an experimental standpoint, measurement of the characteristic velocity has the advantage that it is possible to measure accurately all the variables appearing in the definition.

In this program, the performance for each test was taken just before the first pulse gun was fired. As shown in Figure 44, the average test duration was 0.55 sec from 90% P_c to 90% P_c; the first pulse was fired at 0.14 sec following the attainment of 90% of chamber pressure. By using Potter flow meters to measure the propellant flow and Wianko pressure transducers to measure chamber pressure, the accuracy of the performance for each test is very good even through this was not a main requirement of the program.

A summary of all tests is shown in Table 1. This summary includes characteristic chamber length, L*, ratio of chamber area to throat area, A_c/A_t, chamber pressure, flow rate, propellant temperature, thrust, percent of theoretical c*, pulse charges used, duration of tests, and remarks. Short test durations were used to prevent excessive hardware damage since the chambers were of the uncooled workhorse type.

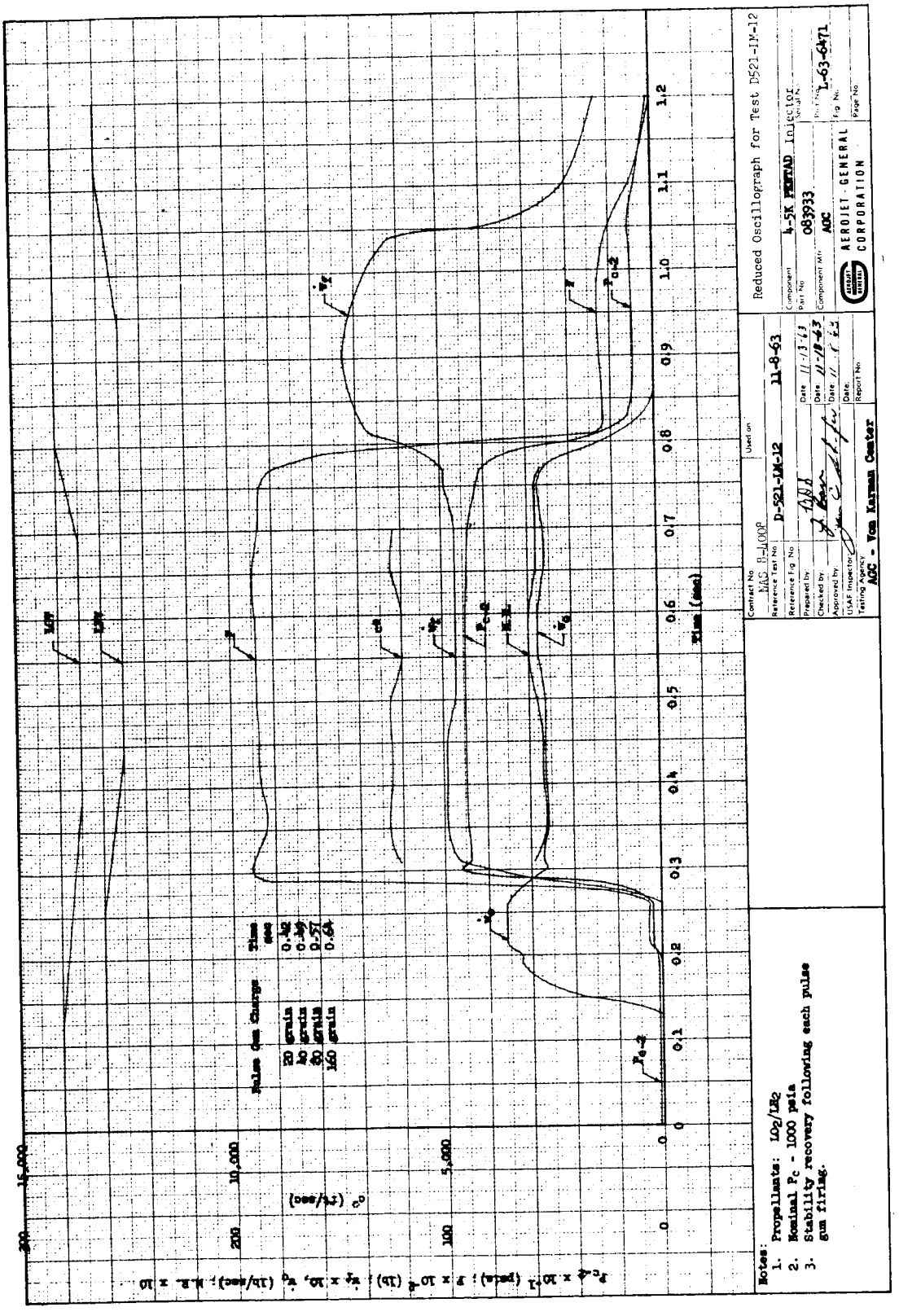

Reduced Oscillograph for Test D521-LM-12

Figure 44

IV, Accomplishments (cont.)

H. PROBLEM AREAS

Some difficulty was experienced during this test program in maintaining the proper engine mixture ratio. This problem was a result of the test stand pressurization system not functioning properly at all times. This condition was improved during the latter part of the program by reducing the pressure drop between the high-pressure nitrogen tank and the oxygen run tank. Also, the liquid hydrogen temperature would change if there was a delay in testing following filling the tank and pressurization cycle. The temperature problem could only be corrected by reducing the test countdown to a minimum.

Hardware damage was mainly restricted to injector face erosion and minor nozzle erosion. Test D-521-LM-4 resulted in a failure when the injector-chamber flange gasket failed to seal; the hot gases sheared the flange bolts. Severe erosion was sustained by the injector and chamber flanges. Damage to the injector is shown in Figure 45. This condition was corrected by changing the sealing joint.

The conventional injector was consistently damaged during most tests as the result of instability induced by pulse changes. Figure 32 shows typical damage incurred by this injector.

The coaxial injector was damaged during only one test of this series. Following this test, corrective measures were taken by increasing the pressure drop across the injector with an orifice in the injector manifold; this prevented any further injector damage. Injector damage following Test D-521-LM-8 is shown in Figures 34 and 35.

The pentad injector was the least damaged of the three types tested. Only minor erosion of the element tubes was sustained. A typical condition of the injector following several tests is presented in Figure 36.

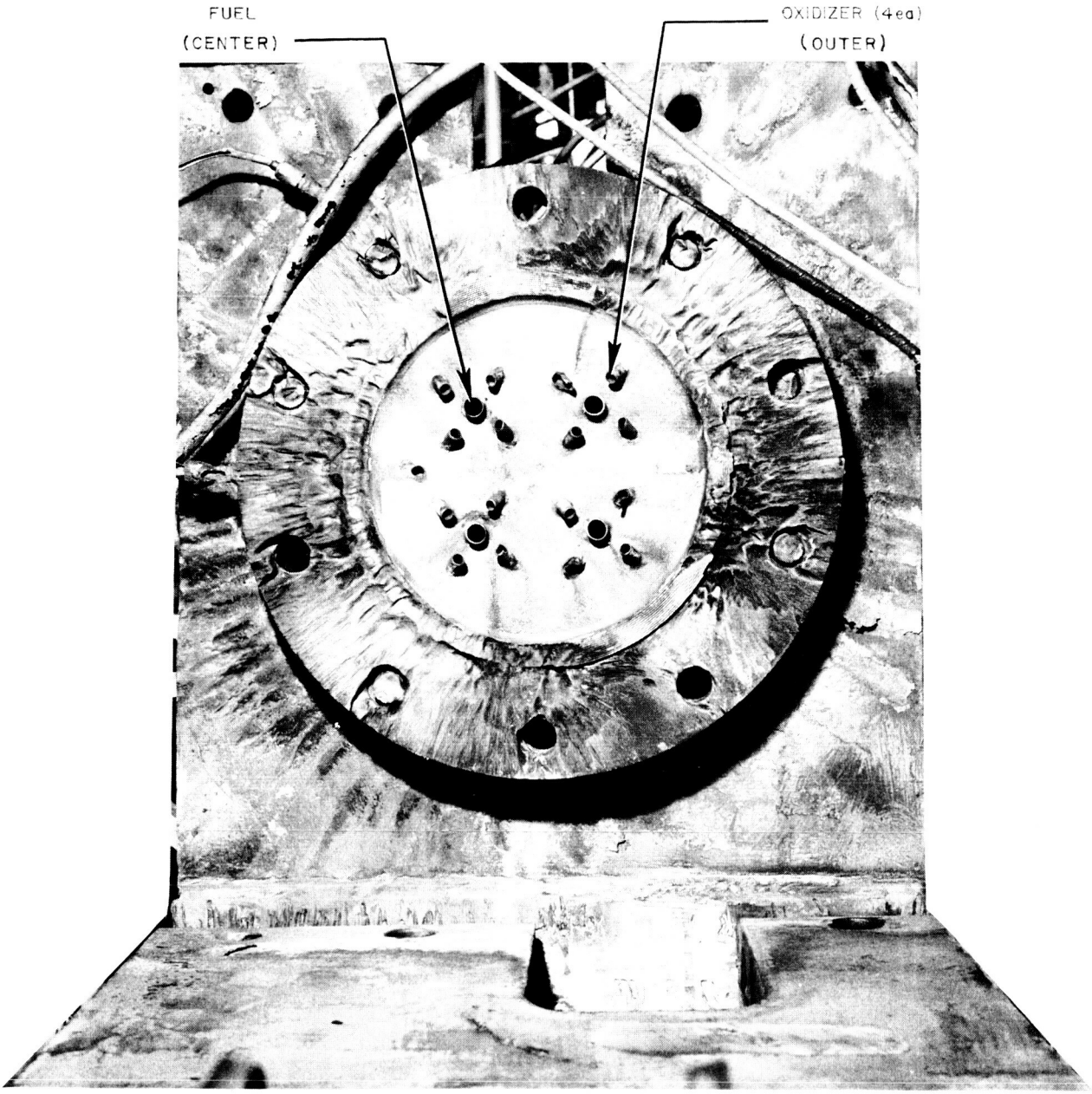

Pentad Injector Damage After Test D521-LM-4

Figure 45

V. NONLINEAR EXTENSION OF SENSITIVE TIME-LAG THEORY

A. INTRODUCTION

The Sensitive Time-Lag Theory of high-frequency instability has been shown to be an effective tool for the systematic correlation of experimental combustion-stability results[(1-5)*]. However, it has certain drawbacks, one of which is its incapacity to treat large amplitude, shock-type disturbances. As presently developed, the theory is based on the classical analysis of the stability of small perturbations from a mean condition. The nonsteady combustion process is represented by three parameters: (1) a characteristic time of the combustion process, referred to as the "sensitive time lag," τ ; (2) a "pressure interaction index," n, which measures the magnitude of the response of the combustion process to a pressure disturbance; and (3) a "velocity interaction index," $\underline{\ell}$, which measures the combustion response to a transverse gas velocity perturbation.

Physically, the sensitive time lag is that fraction of the time between the injection and conversion to combustion products of an elemental mass of propellants during which the combustion process rates are most sensitive to changes in the thermodynamic state of the gases filling the chamber. The pressure index, n, is somewhat akin to the effective order of a chemical reaction. It should be noted that the velocity index, $\underline{\ell}$, is vectorial; in general, it is most convenient to deal with the components, ℓ_r , and ℓ_θ , in the radial and tangential directions, respectively.

Such a small perturbation analysis is useful for studying "spontaneous" instability, which results from the selective amplification of one frequency component contained in the ever-present combustion "noise." Nonlinear, or pulse-triggered instability, can be discussed only qualitatively within the framework of a linear theory. However, certain extensions can be made to the Sensitive

*Superscript numbers in parentheses refer to the List of References found at the end of this report.

V, A, Introduction (cont.)

Time-Lag theory to enable it to be applied to at least some of the types of non-linearly initiated oscillatory combustion.

Nonlinearities in the oscillatory flow in a liquid rocket thrust chamber derive from two sources: (1) the fluid mechanical behavior of the gases filling the combustion chamber, and (2) the dynamics of the combustion process. In general, oscillation amplitudes below about 20% of the mean chamber pressure permit linearization of the fluid mechanical equations. However, significant non-linear behavior of the combustion process can occur even for such perturbations. It is the purpose of the present analysis to investigate nonlinear instabilities of moderate amplitude by assuming that the combustion process is the only nonlinear element in the entire rocket system. In order to insert the nonlinear combustion dynamic behavior into the framework of the Sensitive Time Lag theory, the "describing function" method of equivalent linearization[6] will be employed, as discussed in the sections following.

B. GOVERNING EQUATIONS

The present analysis will closely parallel the procedures followed in previous discussions of the Sensitive Time Lag Theory[1 to 4]. In unsteady conditions, the form of each time-varying property is taken to be the sum of the steady state, or mean, value and a time varying quantity. Thus, the chamber pressure is written

$$p(t) = \bar{p} + \tilde{p}(t) \qquad \text{(Eq 1)}$$

The steady state solution of the equations of flow in a rocket combustion chamber is found to be[3]

$$\bar{p} = \bar{\rho} = \bar{T} = 1$$

$$\bar{u} = \int_0^z \bar{\phi}\, dz' \quad \text{or} \quad \bar{\phi} = \frac{d\bar{u}}{dz} \qquad \text{(Eq 2)}$$

$$\bar{\rho}_L \bar{u}_L = \bar{u}_e - u$$

V, B, Governing Equations (cont.)

where the pressure, p, density, ρ, and temperature, T, have been nondimensionalized by dividing by the corresponding values at the injector face; the gas velocity, u, and the liquid velocity, u_L, are nondimensionalized by the stagnation sound velocity of the combustion products; ϕ is the dimensionless mass burning rate per unit volume; and ρ_L represents the total mass of liquid droplets per unit volume. The axial coordinate, z, is taken as the ratio of the distance downstream from the injector face to the radius of the (cylindrical) combustion chamber. The exhaust nozzle entrance (combustion chamber exit) station is denoted by the subscript, e. It is assumed that the flow in the combustor is adiabatic, inviscid, and with negligible heat conduction, and that combustion is complete at the chamber exit.

The linearized, partial differential equation for the perturbation $\tilde{p}$ takes the form of the inhomogeneous wave equation,

$$\frac{\partial^2 \tilde{p}}{\partial t^2} = \nabla^2 \tilde{p} + \tilde{Q}(\tilde{p}[t]) - \tilde{\mathcal{D}}(\tilde{p}[t]) \qquad \text{(Eq 3)}$$

where $\tilde{Q}$ represents the combustion effects and $\tilde{\mathcal{D}}$, the damping effects. ∇^2 is the Laplacian operator, $\frac{\partial^2}{\partial x^2} + \frac{\partial^2}{\partial y^2} + \frac{\partial^2}{\partial z^2}$.

Equation 3 can be solved by writing the perturbation $\tilde{p}$ in the form of a series with harmonic time dependence:

$$\tilde{p} = e^{st}(p_0 + p_1 + \cdots) \qquad \text{(Eq 4)}$$

where $s = \lambda + i\omega$, and it is assumed that $p_1^2 << p_0^2$ and $\bar{u}_e^2 << 1$, so that $\bar{u}_e p_1 << p_0$.

V, B, Governing Equations (cont.)

The zeroth-order perturbation solution, p_0 , does not involve the combustion or damping effects. Therefore, it is identical to that obtained in previous analyses. The homogeneous equation, derived from Eq 3

$$\nabla^2 p_0 - s^2 p_0 = 0 \qquad \text{(Eq 5)}$$

has the solution

$$p_0 = P_{00} \left[1 + (s^2 + s_{\nu\eta}^2) \frac{z^2}{2} \right] \Psi_{\nu\eta}(r)\, \Theta_\nu(\theta) \qquad \text{(Eq 6a)}$$

with

$$\Psi_{\nu\eta}(r) = J_\nu(s_{\nu\eta} r)$$

and

$$\Theta_\nu(\theta) = \begin{cases} \cos \nu\theta & \text{(standing mode)} \\ e^{-i\nu\theta} & \text{(spinning mode)} \end{cases}$$

J_ν is the Bessel function of the first kind of order ν , and $s_{\nu\eta}$ is a constant that depends on the mode of oscillation under consideration. Typical values of $s_{\nu\eta}$ are given in the following table:

Mode	ν	η	$s_{\nu\eta}$
Longitudinal	0	1	0
First tangential	1	1	1.84129
Second tangential	2	1	3.0543
First radial	0	2	3.8317
Second radial	0	3	7.0156
First combined	1	2	5.3313

V, B, Governing Equations (cont.)

For purely transverse modes, $s^2 + s_{\nu\eta}^2$ is of the order of magnitude of the dimensionless gas velocity $\bar{u}_e$. In the following development, this order of magnitude relationship will be denoted by the abbreviation $s^2 + s_{\nu\eta}^2 = O(\bar{u}_e)$.

The other zeroth-order perturbation quantities are given by the following expressions:

density,

$$\rho_0 = \frac{1}{\gamma} P_{00} \left[1 + (s^2 + s_{\nu\eta}^2) \frac{z^2}{2} \right] \Psi_{\nu\eta} \Theta_\nu \qquad \text{(Eq 6b)}$$

axial velocity,

$$u_0 = -\frac{1}{\gamma s} P_{00} (s^2 + s_{\nu\eta}^2) z \Psi_{\nu\eta} \Theta_\nu \qquad \text{(Eq 6c)}$$

radial velocity,

$$v_0 = -\frac{1}{\gamma s} P_{00} \left[1 + (s^2 + s_{\nu\eta}^2) \frac{z^2}{2} \right] \frac{d\Psi_{\nu\eta}}{dr} \Theta_\nu \qquad \text{(Eq 6d)}$$

tangential velocity,

$$w_0 = -\frac{1}{\gamma s} P_{00} \left[1 + (s^2 + s_{\nu\eta}^2) \frac{z^2}{2} \right] \frac{\Psi_{\nu\eta}}{r} \frac{d\Theta_\nu}{d\theta} \qquad \text{(Eq 6e)}$$

The first-order perturbation equation is

$$\nabla^2 p_1 - s^2 p_1 = \mathcal{D}_0(p_0) - Q_0(p_0, v_0, w_0) \qquad \text{(Eq 7)}$$

V, B, Governing Equations (cont.)

where the damping term, $\mathcal{D}_0$, is the same as that used in the linear theory, namely

$$\mathcal{D}_0 = \left[k' \bar{\rho}_L + (\gamma + 1) \frac{d\bar{u}}{dz} \right] s \, p_0 \qquad \text{(Eq 8)}$$

The factor k' is a dynamic droplet-gas momentum interchange coefficient.(3)

C. COMBUSTION TERM

In the linear theory of transverse mode instability, with velocity effects(4), the combustion term was found to take the form of a sum,

$$Q_0 = \gamma s \frac{d\bar{u}}{dz} \left[\mathcal{P} p_0 + \mathcal{R} v_0 + \mathcal{J} w_0 \right] \qquad \text{(Eq 9)}$$

with

$$\mathcal{P} = n \left(1 - e^{-i\omega\tau}\right)$$

$$\mathcal{R} = l_r \left(1 - e^{-i\omega\tau}\right)$$

$$\mathcal{J} = l_\theta \left(1 - e^{-i\omega\tau}\right)$$

When a sinusoidal signal is put into a nonlinear element, the output will, in general, not be sinusoidal. A Fourier analysis of the output will reveal many frequency components, among which is one, the fundamental, which corresponds to the frequency of the sinusoidal input signal. A ratio can be constructed that is similar to the linear transfer function, the ratio of the output (fundamental component, $\mathcal{O}_f$) to the input ($\mathcal{I}$) amplitudes, which are complex numbers in this analysis and include phase as well as magnitude of the perturbations. This ratio can be written as

V, C, Combustion Term (cont.)

$$\frac{\theta_f}{\alpha} = f \cdot (T.F.)_L \qquad \text{(Eq 10)}$$

where $(T.F.)_L$ is the transfer function of the element if it were linear, and f is the so-called "describing function."

Thus, in the present analysis, nonlinear effects will be introduced by using three describing functions, i.e.,

$$Q_o = \gamma s \frac{d\bar{u}}{dz} \left[f_p \mathcal{P} p_o + f_r \mathcal{R} v_o + f_\theta \mathcal{J} w_o \right] \qquad \text{(Eq 11)}$$

where $\mathcal{P}$, $\mathcal{R}$, and $\mathcal{J}$ retain their definitions as given above for the linear case, and interactions between pressure and velocity effects are neglected.

The form of the describing function depends on the nature of the nonlinearity under consideration. In some cases the nonlinear effects enter only after some amplitude has been exceeded; in others, nonlinear effects are important only below a certain amplitude. Therefore, the describing function can very often be expressed as a function of the ratio of actual input (say, v_o) to a reference value (v_R). Calculations of describing functions for many types of nonlinearity, including step, deadband, saturation, and power law types, are available in the literature of servo-control systems.

V, Nonlinear Extension of Sensitive Time Lag Theory (cont.)

D. FIRST-ORDER SOLUTION

The first-order perturbation equation becomes, in combining Eq 7 and 11,

$$\nabla^2 p_1 - s^2 p_1 = \left[k' \bar{\rho}_L + (\gamma+1) \frac{d\bar{u}}{dz} \right] s\, p_0$$
$$- \gamma s \frac{d\bar{u}}{dz} \left[f_p(p_0)\, \mathcal{P}\, p_0 + f_r(v_0)\, \mathcal{R}\, v_0 + f_\theta(w_0)\, \mathcal{J}\, w_0 \right] \qquad \text{(Eq 12)}$$

The solution is obtained, as in the linear case, by superposition letting

$$p_1 = p_A + p_B + p_C + p_D \qquad \text{(Eq 13)}$$

These "partial solutions," $p_A, \ldots, p_D$, satisfy the following equations:

$$\nabla^2 p_A - s^2 p_A = -\gamma s \frac{d\bar{u}}{dz} f_p(p_0)\, \mathcal{P}\, p_0 \qquad \text{(Eq 14a)}$$

$$\nabla^2 p_B - s^2 p_B = -\gamma s \frac{d\bar{u}}{dz} f_r(v_0)\, \mathcal{R}\, v_0 \qquad \text{(Eq 14b)}$$

$$\nabla^2 p_C - s^2 p_C = -\gamma s \frac{d\bar{u}}{dz} f_\theta(w_0)\, \mathcal{J}\, w_0 \qquad \text{(Eq 14c)}$$

and

$$\nabla^2 p_D - s^2 p_D = \left[k' \bar{\rho}_L + (\gamma+1) \frac{d\bar{u}}{dz} \right] s\, p_0 \qquad \text{(Eq 14d)}$$

Equation 14d is unchanged from the linear case; it has the solution

$$p_D = P_D(z)\, \Psi_{\nu\eta}(r)\, \Theta_\nu(\theta) \qquad \text{(Eq 15a)}$$

V, D, First-Order Solution (cont.)

with

$$\frac{P_D(z)}{P_{00}} = s\int_0^z dz' \int_0^{z'} k'\bar{\rho}_i\, dz'' + (\gamma+1)\, s\int_0^z \bar{u}\, dz' + K_D \qquad \text{(Eq 15b)}$$

where

$$K_D = \frac{P_D(0)}{P_{00}}$$

Substituting Eq 6a into 14a and neglecting higher-order terms yields the equation for p_A :

$$\nabla^2 p_A - s^2 p_A = -\gamma s \mathcal{P} \frac{d\bar{u}}{dz} f_p P_{00} \Psi_{\nu\eta} \Theta_\nu \qquad \text{(Eq 16)}$$

The solution of Eq 16 is obtained by expanding in transverse eigenfunctions, which are the solutions of the zeroth order, homogeneous equation, viz.,

$$\Psi_{pq}(r) = J_p(s_{pq} r) \;;\quad \Theta_p = \cos p\theta \text{ or } e^{-ip\theta} \;;\quad p = 0, 1, 2, \cdots \;;\quad q = 1, 2, 3, \cdots$$

That is, let

$$p_A = \sum_{p=0}^{\infty} \sum_{q=1}^{\infty} A_{pq} P_{pq}(z) \Psi_{pq}(r) \Theta_p(\theta) \qquad \text{(Eq 17a)}$$

and

$$f_p \Psi_{\nu\eta} \Theta_\nu = \sum_{p=0}^{\infty} \sum_{q=0}^{\infty} A_{pq} \Psi_{pq}(r) \Theta_p(\theta) \qquad \text{(Eq 17b)}$$

V, D, First-Order Solution (cont.)

Then, the functions, $P_{pq}(z)$, are given by the ordinary differential equation

$$\frac{d^2 P_{pq}}{dz^2} - (s^2 + s_{pq}^2) P_{pq} = -\gamma s \mathcal{P} \frac{d\bar{u}}{dz} P_{00} \qquad \text{(Eq 18)}$$

and the expansion coefficients, A_{pq}, by

$$A_{pq} = \frac{\int_0^1 \int_0^{2\pi} f_p(r,\theta) \Psi_{\nu\eta} \Psi_{pq} \Theta_\nu \Theta_p^* \, r dr d\theta}{\int_0^1 \int_0^{2\pi} \Psi_{pq}^2 \Theta_p \Theta_p^* \, r dr d\theta} \qquad \text{(Eq 19a)}$$

where Θ_p^* is the complex conjugate of Θ_p.

For $p = \nu$, $q = \eta$, Eq 18 has the solution

$$\frac{P_{A\nu\eta}}{P_{00}} = -\gamma s \mathcal{P} \int_0^z \bar{u}(z') dz' + K_{A\nu\eta} \qquad \text{(Eq 20a)}$$

All other terms in the expansion, i.e., $p \neq \nu$ and $q \neq \eta$, are given by

$$\frac{P_{Apq}}{P_{00}} = -\gamma s \mathcal{P} \int_0^z \frac{d\bar{u}}{dz} \frac{\sinh \sqrt{s_{pq}^2 - s_{\nu\eta}^2}(z - z')}{\sqrt{s_{pq}^2 - s_{\nu\eta}^2}} dz' + K_{Apq} \cosh \sqrt{s_{pq}^2 - s_{\nu\eta}^2}\, z \qquad \text{(Eq 20b)}$$

V, D, First-Order Solution (cont.)

The solution for p_B and p_C are of the same form, with the expansion coefficients given by

$$B_{pq} = \frac{\int_0^1 \int_0^{2\pi} f_r(r,\theta) \frac{d\Psi_{\nu\eta}}{dr} \Psi_{pq} \Theta_\nu \Theta_p^* \, r\,dr\,d\theta}{\int_0^1 \int_0^{2\pi} \Psi_{pq}^2 \Theta_p \Theta_p^* \, r\,dr\,d\theta} \qquad \text{(Eq 19b)}$$

$$C_{pq} = \frac{\int_0^1 \int_0^{2\pi} f_\theta(r,\theta) \frac{1}{r} \Psi_{\nu\eta} \Psi_{pq} \frac{d\Theta_\nu}{d\theta} \Theta_p^* \, r\,dr\,d\theta}{\int_0^1 \int_0^{2\pi} \Psi_{pq}^2 \Theta_p \Theta_p^* \, r\,dr\,d\theta} \qquad \text{(Eq 19c)}$$

The first-order solution can then be written as

$$p_1 = P_{1\nu\eta} \Psi_{\nu\eta} \Theta_\nu + \sum_{p=0}^{\infty} \sum_{q=1}^{\infty} P_{1pq} \Psi_{pq} \Theta_p \qquad \text{(Eq 21)}$$

where

$$P_{1\nu\eta} = A_{\nu\eta} P_{A\nu\eta} + B_{\nu\eta} P_{B\nu\eta} + C_{\nu\eta} + P_{C\nu\eta} + P_D$$

$$P_{1pq} = A_{pq} P_{Apq} + B_{pq} P_{Bpq} + C_{pq} P_{Cpq}$$

This result is the same as that obtained in the linear analysis, except that the expansion coefficients, A_{pq}, B_{pq}, and C_{pq}, are now functions of the amplitude, P_{oo}, as well as of the nature of the particular type of nonlinearity under consideration. That is, all of the nonlinear behavior of the combustion process has been absorbed into the expansion coefficients.

V, Nonlinear Extension of Sensitive Time Lag Theory (cont.)

E. CHARACTERISTIC EQUATION: STABILITY CRITERIA

Since the forms of the perturbation solutions are unchanged from the linear case, the characteristic equation for neutral oscillations ($s = i\omega$) also remains the same, i.e.,

$$A_{\nu\eta}\,\mathcal{P} + i\,\frac{B_{\nu\eta}}{\gamma\omega}\,\mathcal{R} + i\,\frac{C_{\nu\eta}}{\gamma\omega}\,\mathcal{J} = h = \frac{\gamma+1}{\gamma} + \frac{h_2}{h_1} \qquad \text{(Eq 22)}$$

where

$$h_1 = \gamma\bar{u}_e - i\gamma s_{\nu\eta}\,\mathcal{E}\int_0^{z_e}\bar{u}\,dz$$

$$h_2 = \int_0^{z_e} k'\bar{\rho}_L + i\,s_{\nu\eta}\,z_e\left(f - \frac{1}{f}\right) \qquad \text{(Eq 23a)}$$

$$-\,\mathcal{E}\left[\frac{1}{f} - \frac{s_{\nu\eta}^2 z_e^2}{2}\left(f - \frac{1}{f}\right) + i\,s_{\nu\eta}\int_0^{z_e} dz \int_0^{z} k'\bar{\rho}_L\,dz'\right] \qquad \text{(Eq 23b)}$$

In Eq 23a and 23b, $\mathcal{E} = \mathcal{E}_r + i\mathcal{E}_i$ is the complex nozzle admittance, and $f = \omega/s_{\nu\eta}$ is a reduced frequency. For purely transverse modes, the reduced frequency takes on values near unity.

The characteristic Eq 22 exhibits the balance that exists at a stability limit. In order to maintain neutral oscillations, the energy supplied by the combustion process, represented by the left side of Eq 21, must be completely absorbed by the fluid mechanical processes that are represented by the function h on the right side. If more than sufficient energy is supplied, the oscillation amplitude will grow. Such an oscillation is unstable. Stable operation results in the case that the energy release is insufficient to balance the energy absorbed by the oscillation. The fact that the characteristic equation is complex implies that there is a phase condition, as well as the amplitude

V, E, Characteristic Equation: Stability Criteria (cont.)

condition, relating the oscillating rates of energy release and energy absorption for stability.

Equation 22 can be rewritten in the form

$$n(1-e^{-i\omega\tau}) = \frac{h}{A_{\nu\eta} + i\left(\frac{B_{\nu\eta}}{\gamma\omega}\right)\frac{\ell_r}{n} + i\left(\frac{C_{\nu\eta}}{\gamma\omega}\right)\frac{\ell_\theta}{n}} \qquad \text{(Eq 24)}$$

From this (complex) equation, the values of the pressure index, n , and sensitive time lag, τ , can be obtained as functions of the other parameters in Eq 24, i.e.,

$$n = n\left(\omega, \frac{\ell_r}{n}, \frac{\ell_\theta}{n}, A_{\nu\eta}, B_{\nu\eta}, C_{\nu\eta}, s_{\nu\eta}, \bar{u}_e, \mathcal{E}, \gamma\right)$$

$$\tau = \tau\left(\omega, \frac{\ell_r}{n}, \frac{\ell_\theta}{n}, A_{\nu\eta}, B_{\nu\eta}, C_{\nu\eta}, s_{\nu\eta}, \bar{u}_e, \mathcal{E}, \gamma\right)$$

These are the values obtained at the boundary between stable and unstable operation. The inclusion of nonlinear combustion effects in the coefficients $A_{\nu\eta}$, $B_{\nu\eta}$, and $C_{\nu\eta}$, allows the investigation of the effect of wave amplitude on the criteria for combustion stability.

F. COMPUTER PROGRAM

A digital computer program is being written to carry out the necessary calculations. The computational procedure involves the following steps:

1. Input the combustion chamber geometry, including the subsonic portion of the exhaust nozzle; the injection distribution $\mu(r, \theta)$, if nonuniform; the mode, and frequency of oscillation ω ; the functional characteristics of the nonlinear combustion response; and the amplitude level P_{oo} of the oscillation.

V, F, Computer Program (cont.)

2. Compute the pressure and velocity amplitude distributions, $p_o\ (P_{oo}, r, \theta)$, $v_o(P_{oo}, r, \theta)$, $w_o\ (P_{oo}, r, \theta)$.

3. Compute the describing functions for the combustion response, $f_p(r,\theta)$, $f_r(r,\theta)$, $f_\theta(r,\theta)$ using the pressure and velocity amplitudes calculated in Step 2.

4. Compute the combustion coefficients $A_{\nu\eta}(\mu, f_p)$, $B_{\nu\eta}(\mu, f_r)$ $C_{\nu\eta}(\mu, f_\theta)$ which enter the characteristic equation.

5. Compute the nozzle admittance coefficients $\mathcal{E}_r(\omega)$, $\mathcal{E}_i(\omega)$ for the mode, frequency, and subsonic nozzle contour under consideration.

6. Solve the characteristic equation for the value of the interaction index, n, and sensitive time lag, τ, corresponding to neutral oscillations at the frequency under consideration.

7. Repeat above steps for each frequency; then plot n vs τ.

8. Repeat Steps 1 through 7 for each amplitude level.

The flow diagram for the computer program is illustrated in Figure 46.

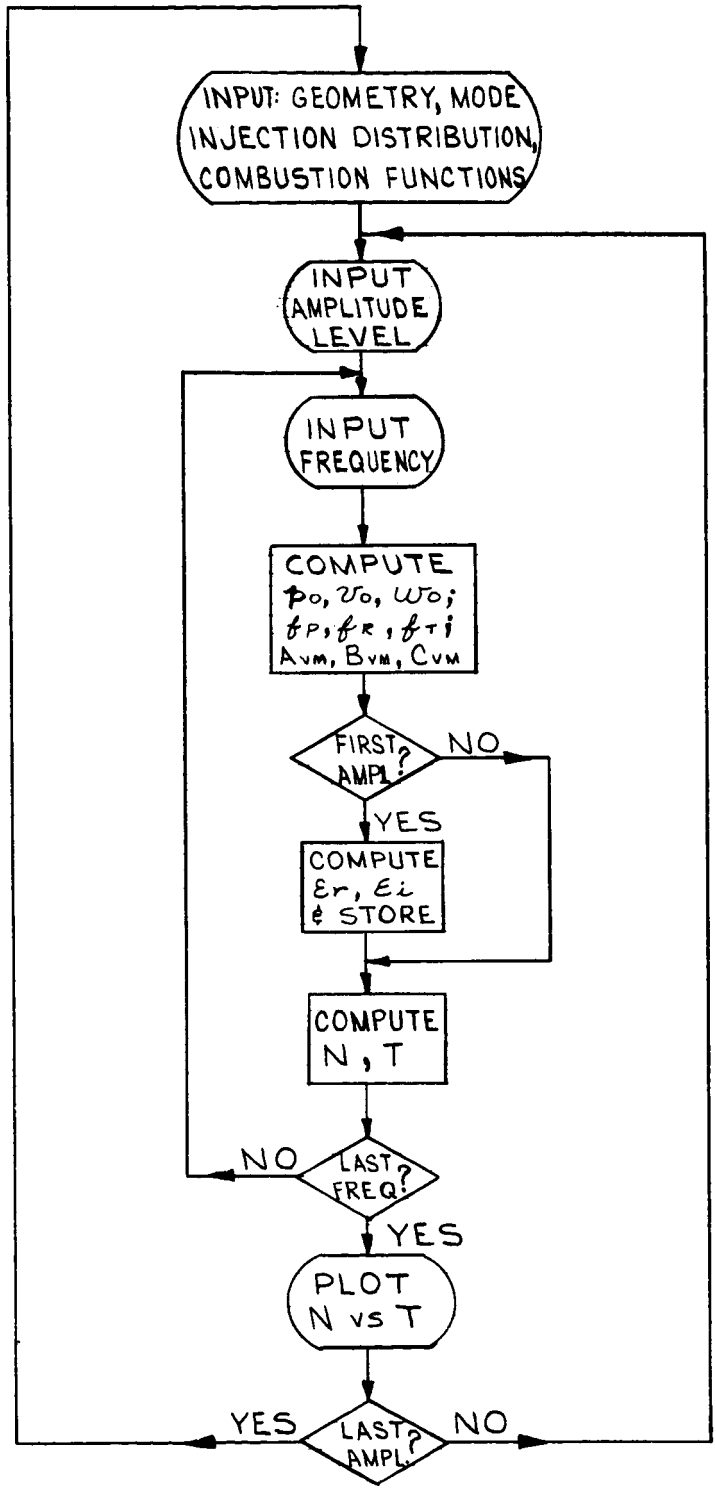

Computer Program Flow Diagram

Figure 46

VI. RECOMMENDATIONS

This exploratory study showed a general trend of increasing combustion sensitivity and decreasing combustion time lag with increasing chamber pressure. However, no qualitatively different effects were observed to accompany high pressure operation. Differences between injector types appeared in the test results. To provide the designer with sufficient information, additional dynamic testing and analysis will be required. Further testing should be undertaken in larger diameter chambers so that higher modes of transverse instability can be excited. Investigations of the effects of injector type and size must be systematized to provide a clear understanding of the dynamic combustion process as well as useful design data.

REFERENCES

1. Crocco, L., and Cheng, S. I., "Theory of Combustion Instability in Liquid Propellant Rocket Motors," AGARDograph No. 8, Butterworth's Scientific Publications, Ltd., London, 1956.

2. Crocco, L., Grey, J., and Harrje, D. T., "Theory of Liquid Propellant Rocket Instability of its Experimental Verification," ARS Journal, Vol 30, No. 2, February 1960.

3. Crocco, L., Harrje, D. T., and Reardon, F. H., "Transverse Combustion Instability in Liquid Propellant Rocket Motors," ARS Journal, Vol 32, No. 3, March 1962.

4. Reardon. F. H., Crocco, L., and Harrje, D. T., "Velocity Effects in Transverse Mode Liquid Propellant Rocket Combustion Instability," to be published in AIAA Journal.

5. Reardon, F. H., and Finden, L. E., "The Application of the Sensitive Time-Lag Theory to Combustion Instability in Titan II Development," presented at the Fourth JANAF-NASA-ARPA Liquid Propulsion Meeting, 4 to 6 November 1962.

6. Chestnut, H., and Mayer, R. W., Servomechanisms and Regulating System Design, Vol II, John Wiley and Sons, Inc., New York, 1955.